2009

The role of inflammation in diet-induced insulin resistance

Lindsey Ann Alexander
The University of Toledo

A Dissertation

Entitled

The Role of Inflammation in Diet-Induced Insulin Resistance

By

Lindsey Ann Alexander

Submitted as partial fulfillment of the requirements for

The Doctor of Philosophy in Medicinal Chemistry

_____
Advisor: Marcia F. McInerney, Ph.D

_____
Katherine A. Wall, Ph.D

_____
Hermann von Grafenstein, Ph.D

_____
Z. Kevin Pan, Ph.D

_____
College of Graduate Studies

The University of Toledo
December 2009

An Abstract of

The Role of Inflammation in Diet-Induced Insulin Resistance

By

Lindsey Ann Alexander

Submitted as partial fulfillment of the requirements for

The Doctoral of Philosophy in Medicinal Chemistry

The University of Toledo

December 2009

Type 2 diabetes (T2D) is a disease of cellular insulin resistance and a dysfunction of pancreatic beta cells resulting in aberrations of carbohydrate and lipid metabolism and a loss of tight control of blood glucose levels. Prior to the diagnosis of overt T2D, patients are often grouped into a diagnosis of the metabolic syndrome, a collection of related biochemical and anthropometric features including impaired glucose tolerance, central or visceral obesity, hypertension, and dyslipidemia. Research has implicated inflammation as a contributor to insulin resistance and the development of type 2 diabetes. The aim of this project is to investigate the role of inflammatory cells, particularly macrophages, and cytokines of the innate immune system, in the development and progression of the metabolic syndrome.

It is now accepted that metabolic syndrome and T2D have an underlying component of sub-acute, chronic inflammation. Obese and T2D humans and mice both have elevated serum levels of pro-inflammatory cytokines and these cytokines have been

linked directly to insulin resistance through effects on key molecules involved in insulin signaling and glucose uptake into cells. A thorough examination of the effects of diet, particularly high fat and Western (high fat and high carbohydrate/sugar) diets in mouse models of insulin resistance, compared to the same mice fed regular chow, should yield further understanding of the development and pathogenesis of obesity and T2D. These mouse strains have alterations in the CEACAM1 gene, which is a key mediator of hepatic insulin clearance and suffer from insulin resistance, mainly caused by prolonged insulin circulation due to a decrease in insulin clearance in the liver. High fat and Western diets are associated with weight gain, visceral adiposity, and liver mass increase. The relationship of insulin resistance to inflammatory markers from immune macrophages and T cells found within adipose tissue of special diet fed mice with modified expression of CEACAM1 was investigated.

Type 1 diabetes differs from T2D in its etiology, but long-term, both diseases have the same detrimental effects and associated complications. Type 1 diabetes is due to an autoimmune destruction of the insulin producing beta cells of the pancreatic islets. With both diseases, the cells can no longer effectively use glucose resulting in hyperglycemia and hyperglycemia-related complications. The role of hyperglycemia on bone marrow-derived macrophages from type 1 diabetic mice was investigated independently from the type 2 diabetes experiments described above. Specifically, bone marrow-derived macrophages in both basal and stimulated states were examined for hyperglycemia-induced deviations in TLR2 expression, signal transduction and inflammatory tumor necrosis factor alpha in comparison to normoglycemic culture conditions.

Acknowledgments

I would like to thank the people in my life who are unfamiliar with the path of the scientist for their patience and support. Tim, my fiancée, is my steadfast rock who rolls with the punches and lets me do "my own thing" career-wise. He understands the importance and investment of my college education. He is also baffled by the fact that the next step in my path, a postdoctoral fellowship, is still not a final job. Thanks to my parents for trying their best to be patient, they just want me to get done and enter the real world and have been asking for the past three years when I am going to graduate. I am grateful for the wonderful students of the Medicinal Chemistry Department and other University of Toledo departments, who have shared their journey with me and have been good friends during my time here in Toledo. I am grateful to my old friends for keeping my spirits high with visits, e-mails and phone calls and reminding me that I will be the first doctor of the bunch. I feel my education has been enriched exponentially by being able to spend so much one-on-one time with the faculty of the University of Toledo. I thank you for all the time, help, and wisdom you have shared with me and above all, treated the graduate students here like intelligent individuals that are the future of science. Mostly, I am happily indebted to the people I have worked closest with in the lab, Mike, Nirdesh, Brandon, and Dr. Marcia McInerney. They have all taught me different important values and skills, and have shared a part of their lives while working with me. Dr. McInerney, truly a one-in-million woman, has been a shining example of how to fill every role you are given with pride, honor, and grace. She has been more than just a professional mentor to me; as a wonderful example of how to live one's life well.

Table of Contents

Abstract……....ii

Acknowledgments……..iv

Table of Contents…….……v

List of Figures and Tables……....viii

Chapter 1: Introduction

1.1 Metabolic disease and inflammation…….....1

1.2 Insulin action, secretion by pancreas, and liver clearance mediated by CEACAM1....2

1.3 High fat and Western diets…….3

1.4 Development and phenotyping of L-SACC

(liver-specific serine to alanine Ceacam1) mice……5

1.5 Development and phenotyping of CEACAM1 knock-out mice……...6

1.6 Inflammation and insulin resistance……..7

1.7 Cytokines, adipocytokines, and chemokines implicated in insulin resistance…….11

1.8 Free fatty acids as TLR2/1 and TLR4 ligands…….14

1.9 Insulin resistance and nonalcoholic fatty liver disease……16

1.10 Type 1 Diabetes and effects of diabetic hyperglycemia……16

Chapter 2: Research Design and Methods

2.1 Mice…….……...….18

2.2 Special diets for metabolic syndrome experiments…….20

2.3 Anthropometric characterization and blood glucose levels…….20

2.4 Adipose tissue separation…….20

2.5 Magnetic separation of adipose tissue macrophages and T cells from SVC……...21

2.6 Flow cytometry……22

2.7 Tissue histology ……..23

2.8 RNA isolation and real time-PCR analysis…….…….23

2.9 Adipose lipid fraction fatty acid analysis…….……25

2.10 Fatty acid treatment of RAWblue cells……..25

2.11 Isolation and treatment of bone marrow-derived macrophages…….26

2.12 ELISA…….…...27

2.13 Western blot analysis of cytoplasmic and nuclear extracts……...27

2.14 Statistical analysis……..29

Chapter 3: Diet-induced metabolic syndrome results

3.1 L-SACC and Cc1$^{-/-}$ mice have increased weight gain, visceral adiposity, and liver mass compared to wild type mice following special diet feeding……30

3.2 HF and HF/HC diets cause liver steatosis and leukocyte infiltration which is worsened in L-SACC and Cc1$^{-/-}$ strains……..…….....38

3.3 HF and HF/HC diets induce adipose tissue leukocyte infiltration……...40

3.4 rt-PCR analysis of dysregulated macrophage receptor, cytokine, and chemokine expression in adipose tissue…….44

3.5 Adipose tissue separation into distinct cellular fractions shows differential cytokine contribution……49

3.6 Pancreatic abnormalities of HF and HF/HC fed Cc1$^{-/-}$ mice including immune cell infiltration and lipid deposits……..……59

3.7 You are what you eat; adipose tissue from mice fed HF/HC diets have greater saturated fat content than RD-fed mice……..……..63

3.8 Fatty acid stimulation of TLR on RAWblue reporter macrophage line……..65

Chapter 4: Type 1 diabetes hyperglycemia results

4.1 Hyperglycemic effects on inflammatory responses of Type 1 diabetic macrophages……...67

Chapter 5: Discussion

5.1 Diet-induced metabolic syndrome inflammation…….....75

5.2 Type 1 diabetes and hyperglycemic effects…….84

Chapter 6: References……88

List of Figures

Figure 1: Reduction in murine liver CEACAM1 mRNA by HF and HF/HC diets.....4

Figure 2: Proposed model for adipose tissue macrophage polarization and function in adipose tissue from lean to obese……..9

Figure 3: Structure of Lipid A……..14

Figure 4: TLR2 / TLR1 binding pocket with Pam_3CSK_4…….14

Figure 5: Anthropometric data from two month special diet fed L-SACC and $Cc1^{-/-}$ mice……..31

Figure 6: Anthropometric data from three month special diet fed L-SACC and $Cc1^{-/-}$ mice……..34

Figure 7: Anthropometric data from four month special diet fed L-SACC mice……35

Figure 8: Large fat-speckled mouse liver……..…….…….36

Figure 9: Comparison of visceral adiposity to liver mass of WT and $Cc1^{-/-}$ male mice……...37

Figure 10: Histological analysis of special diet fed L-SACC and $Cc1^{-/-}$ livers……..39

Figure 11: Histological analysis of WT and $Cc1^{-/-}$ adipose tissue following three month special diet feeding……..…….....42

Figure 12: Histological analysis of WT and L-SACC adipose tissue following four month special diet feeding…….……....43

Figure 13: Real-time PCR analysis of cellular markers and cytokines from three month special diet fed $Cc1^{-/-}$ male adipose tissue……46

Figure 14: Real-time PCR analysis of cellular markers and cytokines from

two month special diet fed $Cc1^{-/-}$ male adipose tissue…….…….48

Figure 15: Differential expression of IL-6 and IL-10 cytokine from separated adipocytes and stromal vascular cell populations…….……50

Figure 16: Purity analysis of separated adipose floating cell fraction by rt-PCR for adiponectin and macrophage marker F4/80……52

Figure 17: Magnetic separation of $F4/80^{+}$ macrophages from stromal vascular cell population…….……..53

Figure 18: Cell marker and cytokine expression from adipocytes before and after tissue culture……...……..55

Figure 19: TLR2 and cytokine expression from stromal vascular cells before and after adipose tissue macrophage purification…….……...56

Figure 20: FACS analysis of T cells from the stromal vascular cell population from male WT and $Cc1^{-/-}$ mice fed special diets for three months……58

Figure 21: Pancreatic insulitis associated with diet-induced insulin resistance…….60

Figure 22: Real-time PCR analysis of infiltration markers in pancreata from male $Cc1^{-/-}$ fed special diets for 3 months…….……....61

Figure 23: Anomalous lipid deposits in the pancreata of special diet fed L-SACC and $Cc1^{-/-}$ mice……...63

Figure 24: Gas chromatography fatty acid composition analysis of adipose lipid…….64

Figure 25: Stimulatory effect of free fatty acids on TLR of RAWblue macrophage reporter line…….....65

Type 1 Diabetes Results

Figure 26: Real time-PCR analysis of TLR2 expression from type 1 diabetic macrophages…….68

Figure 27: Flow cytometry analysis of TLR2 on cell surface……70

Figure 28: Signal transduction investigation……..72

Figure 29: Real time-PCR analysis of BM-MΦ stimulation in hyperglycemic and normoglycemic conditions with two strains of LPS……..…74

Figure 30: Comparison of anomalous WAT to BAT…….78

Chapter 1

Introduction

1.1 Metabolic disease and inflammation:

It has long been known that metabolism and immunity are connected, and extreme alterations in either directly affect the other system (3). Undernutrition is associated with immunodeficiency, and in modern times, when overnutrition is so prevalent in Westernized societies, improper immune stimulation related to nutrient and metabolic excess plays a key role in the development of metabolic diseases, such as type 2 diabetes (T2D) (3, 4). Energy usage is carefully modulated during the mounting of an inflammatory or immune response and during times of starvation (4). And so it should not be surprising that the organs that are key in energy storage such as the liver and adipose are organized with immune cells in proximity to metabolic cells (4). The metabolic syndrome which is characterized by insulin resistance, central or visceral obesity, and dyslipidemia, often progresses to T2D. Inflammatory cytokines and free fatty acids can block the functioning of the insulin receptor such that insulin binding no longer activates insulin receptor signal transduction and glucose uptake. This lack of proper response in normally insulin sensitive cells such as hepatocytes, myocytes, and adipocytes is known as insulin resistance. The beta cells of the pancreas can eventually fail and then secreted insulin level from is no longer sufficient to trigger glucose uptake from normally insulin-sensitive cells. Beta-cell dysfunction and death are often seen in overt diabetic patients and animals. Chronic low-grade inflammation is seen in obese

mice and humans, and is proposed to have a crucial role in the development of metabolic disorders including T2D, fatty liver disease, and cardiovascular disease (3). Indeed, these diseases are often present in the same patient. While many metabolic factors contribute to insulin resistance, research is elucidating an important role for inflammatory cells and cytokines in metabolic diseases.

1.2 Insulin action, secretion by pancreas, and liver clearance mediated by CEACAM1:

Insulin normally controls glucose homeostasis by triggering its uptake into peripheral tissues and by suppressing gluconeogenesis in the liver and releasing stored lipid from adipose tissue (5). Binding of insulin to its receptor triggers tyrosine phosphorylation of insulin receptor's many intracellular substrates, but mainly the insulin receptor substrate (IRS) family of proteins (3). Insulin signaling mediates metabolism and growth through cascades of intracellular signaling pathways. Insulin action is regulated by the amount of circulating insulin that is in turn regulated by insulin secretion from the beta-cell and its clearance occurs mainly in the liver (6). An insulin resistant individual or animal can remain euglycemic as long as the pancreas compensates by increasing insulin production (7). However, as soon as insulin production wanes, mainly due to beta-cell exhaustion and death, overt diabetes develops quickly. Another main way that insulin resistance can develop is from a decrease in insulin clearance, leading to hyperinsulinemia. Insulin is mostly degraded in the liver and to a lower extent in kidney. Insulin undergoes degradation whereas the insulin receptor recycles back to the cell surface. CEACAM1 was identified as a substrate of insulin receptor tyrosine kinase in liver but not muscle or adipose (6). After years of research, a key role for CEACAM1 has

been elucidated in the mechanism of hepatic insulin clearance. Upon insulin binding insulin receptor (IR), intracellular IR tyrosine kinases are activated and phosphorylate other amino acid sites on IR. CEACAM1 tyrosine 488 phosphorylation is regulated by tyrosine 1316 in the beta-subunit of the IR (6). This triggers association with Shc, an ubiquitously expressed adaptor protein. Next, Shc and CEACAM1 tyrosine 513 trigger IR tyrosine 960 participate in the formation of the insulin-mediated receptor endocytosis complex (6). The entire complex is endocytosed in clathrin-coated vesicles, thus clearing insulin from the hepatic circulation. CEACAM1 serine 503 must be in its phosphorylated state to allow propagation of the signaling (6). The IR and CEACAM1 are eventually recycled to the cell surface. The two mouse stains used in the subsequent experiments have genetic alterations of CEACAM1 expression.

1.3 High fat and Western diets:

Diet plays an important role in the development of T2D impacting both glucose tolerance and insulin resistance. In Westernized countries, with the highest percentage of T2D cases, diets are often dominated by processed, high fat foods with an excess of simple carbohydrates such as sugar. Chronic ingestion of a poor quality diet, such as saturated versus unsaturated fats and simple sugars versus complex carbohydrates, can contribute to changes in metabolism. Diet can even have effects on gene expression. Indeed, HF feeding of WT mice for two months was able to reduce the level of hepatic CEACAM1 by about 50% with a slight further reduction in HF/HC fed group (Fig 1). Livers from obese humans are also being examined for this reduction in CEACAM1 level. To examine this hypothesis of diet-induced reductions of hepatic CEACAM1

playing a direct role in the development of insulin resistance, we investigated the effects of HF and HF/HC in mouse strains with altered CEACAM1 gene expression (described in detail below) and their wild type counterparts following two to four months of special diet feeding. Dietary compositions for the three experimental diets are shown in Table 1.

Figure 1. Liver CEACAM1 mRNA

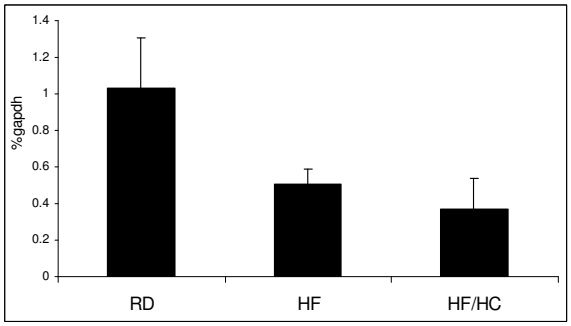

Table 1. Special diet composition.

Diet	% cal from carbohydrate	% cal from fat	%sucrose
Regular Diet	58	13.5	3.7
High Fat	35	45	17
Western Diet (HF/HC)	43	41	29

Figure 1: Reduction in murine liver CEACAM1 mRNA by HF and HF/HC diets.

A portion of liver, from individual mice in groups (n=3) of wild-type fed special diets for two months, was taken for purification of mRNA. mRNA was converted to cDNA using M-MLV reverse transcriptase for rt-PCR analysis. Liver CEACAM1 expression was analyzed from each liver in two separate experiments and expressed as an average. Gene expression is reported as the normalized % of glyceraldehyde-3 phosphate dehydrogenase (gapdh). Samples were tested in triplicate. A trend was identified wherein HF and HF/HC diets decreased CEACAM1 liver expression.

Diet imbalance leads to a gradual overload of the cells and organelles responsible for maintaining glucose homeostasis. Many of the inflammatory signaling pathways that inhibit insulin-receptor signaling and lead to metabolic imbalance are triggered directly or indirectly by nutrients, such as glucose and lipid (3). The negative effects of

glucotoxicity and lipotoxicity on the beta-cells of the pancreas help explain progressive beta-cell death that determines the progression of T2D. Glucotoxicity is a chronic elevation of blood glucose that impairs beta-cell function and insulin sensitivity (7). It is largely caused by increased oxidative stress from mitochondria due to excessive glucose metabolism (7). Chronic hyperglycemia can also trigger endoplasmic reticulum stress and apoptosis in many cell types (7). Lipotoxicity is a long-term elevation in circulating free fatty acids (FFA) which is found in concert with glucotoxicity (7). Chronic exposure to high FFA attenuates glucose-stimulated insulin secretion, induces apoptosis through the caspase pathway, and also induces reactive oxygen species (7). Elevated concentrations of certain saturated FFA are directly toxic to cells in culture.

1.4 Development and phenotyping of L-SACC (liver-specific serine to alanine Ceacam1) mice:

Due to the observed phenomena that high fat and Western diets lowered the expression of the CEACAM1 gene in the liver, the L-SACC strain was created as a mimic of this effect that is not dependent on diet. These mice (mixed genetic background C57Bl/6 x FVB) contain a stably transfected vector containing a point-mutation (ser to ala) of amino acid position 503 of the rat CEACAM1 gene targeted to the liver by the apolipoprotein A-1 enhancer and promoter (8). S503 is a key auto-phosphorylated amino acid that when mutated, blocks further signal transduction. Founder mice were confirmed to contain the transgene by southern blotting. Offspring were viable with normal liver, kidney, pancreas, and muscle development. Metabolic features of L-SACC mice have been investigated and described in detail in previous publications (6, 8-11). Extensive

metabolic phenotyping of L-SACC and WT mice fed regular diet chow confirmed the transgene functionality by inhibiting hepatic CEACAM1-facilitated insulin clearance and insulin receptor internalization (8). L-SACC mice developed glucose intolerance, secondary hepatic insulin resistance due to impaired insulin clearance (as opposed to a primary defect in insulin receptor expression) and obesity in addition to elevated levels of free fatty acids and triglycerides in plasma after two months of age (8, 11). L-SACC regular diet-fed mice showed a 200–500% increase in plasma insulin levels and impaired insulin clearance, measured as fasting molar C-peptide/insulin ratio, compared with age-matched wild type mice (8). The mechanism of insulin resistance in L-SACC mice was determined to be due to altered glucose and lipid metabolism in the liver, skeletal muscle, and adipose tissues (11). L-SACC mice fed regular diets develop insulin resistance but do not develop overt diabetes.

1.5 Development and phenotyping of CEACAM1 knock-out (null) mice:

Whole body CEACAM1 null mice were created by Beauchemin et al. on the C57Bl/6 background by eliminating the interior start ATG codon thereby removing the first two exons of the CEACAM1 gene and replacing with a neomycin resistance gene (12). Complete abrogation of CEACAM1 expression in homozygous progeny was confirmed by real time-PCR and Western blotting (12). CEACAM1 null ($Cc1^{-/-}$) mice were obtained from the Beauchemin group by the Najjar laboratory for usage at the University of Toledo Health Science Campus. Male $Cc1^{-/-}$ mice fed regular diet of different ages were analyzed by the Najjar group (13). Compared to wild type, they had increased visceral adipocity and slightly increased fasting serum insulin levels at two

months of age suggesting they clear exogenous insulin less efficiently. Older, six month old mice, display marked hepatic insulin resistance, a propensity towards hepatic gluconeogenesis rather than glycogen synthesis, increased lipogenesis, elevated serum FFA and triglyceride levels in parallel with increased visceral adipocity (13). Importantly, skeletal muscle glucose utilization and liver function was normal, as well as pancreas beta-cell mass and insulin secretion in response to glucose, and glucagon secreting alpha-cells being similar to wild type mice. These mice fed regular diets do not develop overt diabetes.

1.6 Inflammation and insulin resistance:

Adipose tissue is no longer considered an inert storage site of lipids as triglyceride, rather the adipose is now considered an active endocrine organ involved in homeostasis. Adipocyte derived hormones and adipocytokines are involved in a number of key processes such as glucose and lipid metabolism, inflammation, coagulation, blood pressure, and feeding behavior, thus affecting the entire individual (14). With a positive caloric balance, the adipose stores excess nutrient as intracellular triglyceride, stimulating adipocyte hypertrophy (increased size) and hyperplasia (increased numbers) (15). These changes can trigger adipocyte dysfunction including a change in adipocytokine secretion profile, and a release of free fatty acids and triglycerides (15). Increased circulating levels of FFA and triglycerides are associated with lipid accumulation in other tissues, such as liver, pancreas, skeletal muscle, and heart, contributing to insulin resistance, increased oxidative stress and inflammation in these tissues which collectively contribute to diabetes pathology (15). This viscous cycle of overnutrition, hyperglycemia,

hyperlipidemia, increased oxidative stress, reactive oxygen species, and other inflammatory mediators feeds forward contributing to insulin resistance development.

The link between inflammatory cytokines of the innate immune system and obesity is now firmly established (16-19). Therefore, obesity and type 2 diabetes are considered to be low-grade inflammatory diseases (reviewed in (16-23)). Although many signals are involved, it is not completely understood why hypertrophic, or obese, adipocytes begin to secrete increased levels of cytokines and chemokines (24). Interestingly, macrophages and adipocytes are closely related, share many genes and functions; both can be activated by LPS and secrete cytokines, and both are capable of phagocytosis (3).

Adipose tissue from obese humans and animals contains increased numbers of macrophages which are of a pro-inflammatory phenotype. Concurrently, resident adipose macrophages change polarization from a regulatory to an activated inflammatory phenotype (see figure 2) (1). Several hypotheses explain the mechanism of macrophage infiltration into adipose tissue. First, cellular stresses and inflammatory signals can trigger adipocyte apoptosis which would warrant macrophage infiltration to clear dead and dying adipocytes. Secondly, adipocyte hypertrophy or activation of adipocyte inflammatory pathways may cause overexpression of the chemokine MCP-1 with facilitates infiltration of circulating monocytes into adipose and subsequent differentiation into macrophages which also become pro-inflammatory (17, 25, 26). Macrophages are found in non-hypertrophic adipose tissue at a low basal level, however they have a different phenotype (M2) than those found in hypertrophic adipose (1). Macrophages mature based on the local tissue cytokine environment. M1 or “classically

activated" macrophages respond to inflammatory signals by secreting large amounts of pro-inflammatory cytokines such as tumor necrosis factor alpha (TNFα) and interleukins (IL) IL-1, IL-6, and IL-12 (27). M2 or "alternatively activated" macrophages are immunomodulatory and secrete mainly anti-inflammatory cytokines such as interleukin-10 (IL-10) (27).

Figure 2.

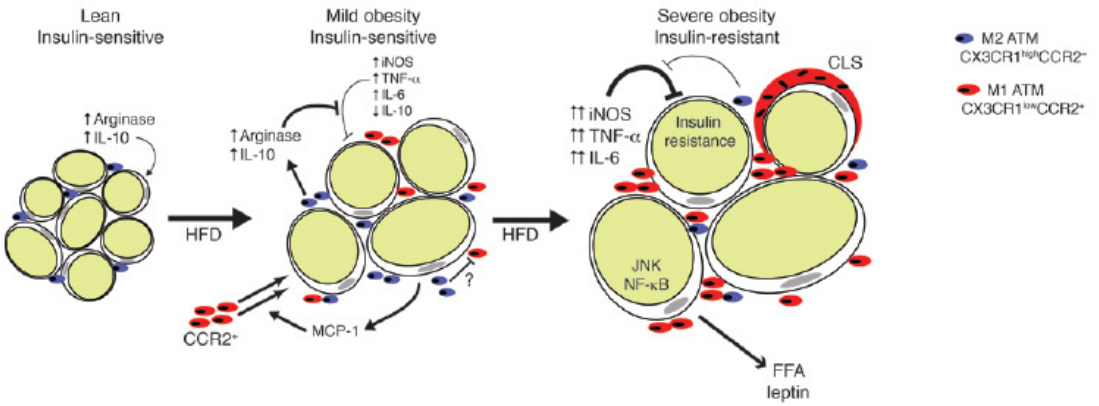

Figure 2: Proposed model for adipose tissue macrophage polarization and function in adipose tissue from lean to obese.

In lean, insulin-sensitive states, adipose tissue macrophages (ATMs) are polarized toward an M2 state with IL-10 and arginase expression. Early during high fat diet (HFD) treatment, adipocytes undergo hypertrophy, releasing chemokines that induce recruitment of M1-polarized ATMs with low IL-10 expression and increased iNOS and TNF-α production. In these early stages of mild obesity with retained insulin sensitivity, M2-polarized resident ATMs are able to partially protect adipocytes from these inflammatory factors and may block M1 polarization. With increased adiposity, M1-polarized ATMs form crownlike structures (CLS) and overwhelm the protective effects of M2 macrophages, leading to a dominant role for TNF-α and iNOS. These factors generate

insulin resistance in adipocytes, activate JNK and NF-κB, alter adipokine secretion, and lead to excess circulating levels of free fatty acids due to adipocyte lipolysis and impaired lipogenesis (1).

The local and systemic effects of cytokines are described in detail below. Adipocyte lipolysis may be stimulated by hypertrophy and/or inflammatory cytokines, releasing free fatty acids (FFA) into the micro-environment and circulation, contributing to the deleterious effects of lipotoxicity. Research has shown that endogenous molecules, including FFA, can activate the Toll-like receptors (TLR) (28, 29). Both adipocytes and macrophages express TLR on their cell surface and their close proximity enhances inflammatory interplay and paracrine effects. Antigen presenting cells isolated from adipose tissue of lean WT animals can be activated by free fatty acid treatment (30). A separation of the cell types contained within adipose tissue allows examination of the differential cytokine contributions in the adipose microenvironment. Lipid laden adipocytes float while stromal vascular cells (SVC) including endothelial cells, fibroblasts, pre-adipocytes, macrophages, and lymphocytes pellet during centrifugation (31). TNFα and IL-6 secreted by macrophages and adipocytes contribute to tissue insulin resistance by downregulating signaling molecules GLUT4 and IRS-1 (32). Adipocytes, endothelial cells, and adipose tissue macrophages are caught in a feed-forward cycle furthering inflammation and insulin resistance and contributing to the development of T2D.

Once macrophages and cytokines are implicated in disease pathology, the roles of TLR involvement need to be explored. Cell types involved in obesity, such as adipocytes

and macrophages (MΦs), are known to express TLR2 and TLR4 (29, 30, 33-35). Obese db/db mice have greater mRNA levels of TLR4 in epididymal fat pads, compared to db/+ littermates (34). Separation of whole, white adipose tissue into adipocyte and SVC fractions revealed that the increased TLR4 expression resided with the adipocytes (34). TLR4 mRNA expression is also increased in diet induced obese WT, ob/ob, and db/db mice in comparison to controls (29). Furthermore, the TLR4 was functional as determined by LPS stimulation and resultant IL-6 production (29). Creely et al. (33) showed that human adipocytes from patients across a range of BMI express TLR2 and TLR4 mRNA and protein, with higher expression in obese compared to lean subjects. In addition, ex vivo macrophages and dendritic cells derived from bone marrow stem cells were confirmed to display cell surface TLR2 and TLR4 on over 80% of the total cells (30). The hypothesis that nutritional free fatty acids can trigger TLR is discussed below in introduction section 1.8.

1.7 Cytokines, adipocytokines, and chemokines implicated in insulin resistance:

Below is a summary of the most common cytokines, adipocytokines, and chemokines linked with insulin resistance and T2D. Each is accompanied by key discoveries from research.

TNFα – TNFα is secreted in high levels by both M1 macrophages and adipocytes. TNFα was the first cytokine linked to obesity over 15 years ago by Hotamisligil et al (36). TNFα interferes with insulin stimulated IRS-1 phosphorylation of tyrosine by TNFα phosphorylation of serine residues (26, 37). Mice lacking TNFα or TNF receptors have improved insulin sensitivity in both dietary and genetic models of obesity (26, 37). Anti-

TNFα antibody treatment in mice improved insulin signaling and reversed liver steatosis (37). Weight loss in humans decreases circulating TNFα levels (26, 37).

IL-6 – IL-6 is a pro-inflammatory cytokine secreted by visceral fat and macrophages. Among the first cytokines implicated as a predictor of insulin resistance, circulating IL-6 levels are increased in obese and insulin resistant subjects (38). IL-6 concentrations decreases with weight loss in humans resulting in improved insulin sensitivity (26, 37). Mice treated with anti-IL-6 antibodies also improved insulin sensitivity (26, 37). Liver IL-6 in humans correlated with the degree of inflammation and fibrosis (37).

IL-1β – Macrophages are known to produce this strong pro-inflammatory cytokine. IL-1β reduces the expression of IRS-1 thus impairing insulin signaling (26, 37).

IL-10 – Produced and secreted primarily by T regulatory cells, signaling through the IL-10/IL-10R can potently inhibit pro-inflammatory cytokine production.

Inflammatory pathways IKK / NF-κβ and JNK– Activation of the Iκβ kinase (IKK) complex cleaves the inhibitory protein Iκβ from NF-κB dimmers in the cytoplasm, allowing translocation to the nucleus and activate inflammatory gene transcription on its nuclear response element. c-Jun N-terminal kinases (JNK) and other kinases have been investigated and implicated in obesity and insulin resistance (3, 26, 37). TLR, TNFα, FFA and oxidative stress can all activate these signaling pathways, leading to increased inflammation (see Fig 4).

Adipocytokines – Adipocytokines such as leptin and adiponectin differ from classical cytokines because they are produced solely by adipocytes.

Leptin – Leptin acts on the central nervous system to produce satiety and reduce food intake. Leptin improves glucose homeostasis improving insulin sensitivity in muscle

and liver, also inhibiting insulin release (26). However, levels in obesity are elevated implicating a state of leptin resistance. Leptin treatment in humans failed to correct hyperglycemia (26).

Adiponectin – Reduced levels of adiponectin are found in obese and insulin resistant individuals (26, 37). Adiponectin has anti-inflammatory properties on endothelial cells inhibiting TNFα and NF-κB (26, 37). Adiponectin infusion in mice improves insulin sensitivity. Disruption of both adiponectin receptors abolished beneficial actions and resulted in increased liver triglyceride content, inflammation and oxidative stress (26, 37).

Chemokine CCL2: monocyte chemotactic protein (MCP-1) – MCP-1 is secreted by adipocytes and acts mainly to attract blood monocytes from circulation. MCP-1 can stimulate expression of adhesion molecules, which allow monocytes to enter into the adipose tissue where they then receive further inflammatory signals and mature into inflammatory macrophages. Obese adipocytes have increased expression of MCP-1 and obese adipose has greater numbers of infiltrated macrophages (26). $CCL2^{-/-}$ mice had reduced adipose tissue macrophages and improved insulin sensitivity (26).

Signal transduction molecule SOCS: Originally identified as negative regulators of Jak/STAT signaling, these SH2-containing adaptor proteins, suppressor of cytokine signaling SOCS1 and SOCS3 are elevated in livers of obese diabetic *db*/*db* mice, both mRNA and protein levels are increased about 2–3-fold (39). Research has revealed that SOCS-1 and SOCS-3 bind to the sites of the insulin receptor which are important for the recognition of IRS proteins by suppressing tyrosine phosphorylation and contribute to ubiquitin-mediated degradation of IRS proteins thereby inhibiting insulin action (39-41).

SOCS3 also can bind the leptin receptor thus inhibiting normal receptor activation and leptin signal transduction (26, 37).

1.8 Free fatty acids as TLR2/1 and TLR4 ligands:

Well known TLR ligands such as LPS and Pam_3CSK_4 are fatty acid-containing molecules. Pam_3CSK_4 is a lipopeptide made up of six amino acids and three palmitate fatty acid chains. The main antigenic part of LPS is lipid A, a 1,4'-biphosphorylated glucosamine disaccharide with six fatty acids attached to the sugar moiety (Fig 3). The numbers below indicate the carbon chain length of the fatty acid. The crystal structure of the TLR2 / TLR1 complex bound to Pam_3CSK_4 was recently published (Fig 4)(2). The palmityl groups (lower horizontal section) interact tightly with the binding pockets of TLR2 (blue grid) and TLR1 (green grid). It is possible that fatty acids in circulation, especially in elevated concentrations seen in obese and diabetic patients, could bind TLR2 and TLR4 on macrophages and adipocytes and trigger the inflammatory NF-κB pathway.

Figure 3. Structure of Lipid A

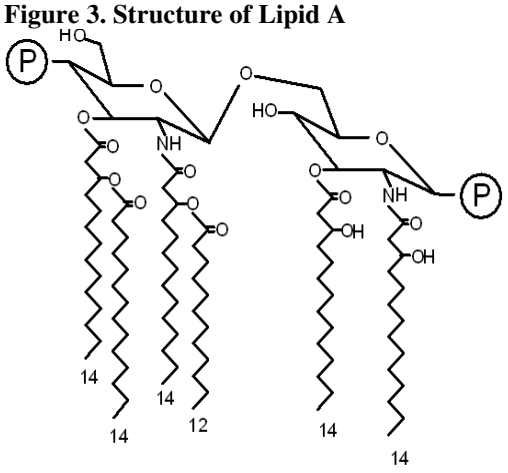

A common clinical finding in metabolic syndrome patients and animals is dyslipidemia. The hyperlipidemic state is indicative of lipid redistribution from adipose tissue

Figure 4. TLR2 / TLR1 binding pocket with Pam_3CSK_4 (2).

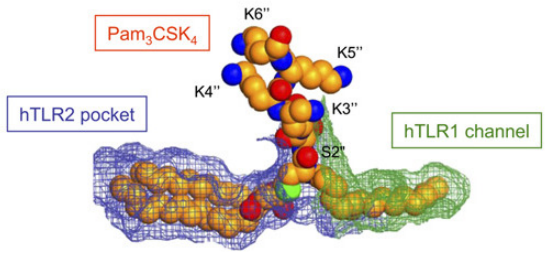

to muscles and liver (4). Many studies are investigating the possibility of free fatty acids (FFA) as TLR ligands. *In vitro* experiments using NF-κB luciferase reporter-transfected 293T cells showed that a mixture of the most abundant nutritional fatty acids palmitate and oleate can activate TLR4 (29). Positive results have been found using many of the medium chain (carbon length 12-18) saturated fatty acids for stimulating TLR4. Unsaturated FFA generally do not stimulate TLR and some have protective effects, capable of blocking LPS or FFA induced inflammatory changes (29). A mixture of saturated and unsaturated free fatty acids stimulate both TLR2 and TLR4 on dendritic cells (DC) and MΦs however, bone marrow-derived DC seem to have higher inflammatory capabilities compared to bone marrow derived macrophages by expression of cyclooxygenase 2 (COX-2), chemokine (C-C motif) receptor 2 (CCR2), IL-1 , IL-6, and TNFα expression (30). Therefore, palmitate and certain other saturated fatty acids can activate the TLR4 present on adipocytes, DC, and MΦs in a dose-dependent manner. Evidence from cell culture and animal tissue studies supports a role for signaling molecules NF-κB (33, 42), c-jun-N-Terminal kinase (JNK), IκBα (29) and IKKβ (30, 43) during TLR4-mediated inflammation. Corresponding increases in TNFα and IL-6 mRNA are seen in response to FFA stimulation and NF-κB activation (29, 42). TLR4 interference of any kind reduces FFA-induced signaling and inflammatory protein expression in mouse tissues, primary cells, and cell-lines. Studies using TLR4 deficient mice responses have proven extremely useful in understanding the role of TLR4 in obesity-related inflammation (29, 35, 43, 44). Importantly, mice strains with defective TLR4 signaling when fed a high fat diet, displayed increased feeding efficiency, increased metabolic rates, attenuated increases in serum and adipose tissue concentrations

of TNFα, IL-6, and serum FFA compared to control mice (35, 43, 44). Surprisingly, there was no significant difference between the TLR4-defective mouse and control strains for MΦ infiltration in adipose after a 16 week high fat diet (35) suggesting that TLR4 mutation does not affect MΦ infiltration. Studies reported increases in adipose and skeletal muscle insulin sensitivity. Therefore, inflammatory processes decrease and insulin sensitivity improves in diet-induced obesity and cells treated with free fatty acids when TLR4 is either not present or not fully functional. Refer to figures 3 and 7 for how FFA could interact with TLR. The definitive roles of TLR4 and TLR2 in insulin resistance and T2D are still being investigated.

1.9 Insulin resistance and nonalcoholic fatty liver disease:

Nonalcoholic fatty liver disease (NAFLD) and its more severe form nonalcoholic steatohepatitis (NASH) are very common in type 2 diabetes patients, with between 50 and 75% of subjects demonstrating fat in the liver by ultrasound (45). NAFLD is characterized by a dysregulation of lipid usage by the liver and fat deposits, while NASH is associated with fat, inflammation, and fibrosis and may progress to end-stage liver failure (37, 45). Metabolic syndrome is a good predictor of future development of NAFLD as obesity is the most common risk factor of NAFLD (45). The pathogenesis from insulin resistance to fatty liver remains unclear because many systems are involved; including intraabdominal fat, adipocytokines, oxidative stress, and other inflammatory mediators (45, 46).

1.10 Type 1 Diabetes and effects of diabetic hyperglycemia:

Type 1 diabetes differs from T2D in its etiology but long-term both diseases have the same detrimental effects and associated complications. Type 1 diabetes is due to an autoimmune destruction of the insulin producing beta cells of the pancreatic islets. With both diseases, the cells can no longer effectively use glucose resulting in hyperglycemia and hyperglycemia-related complications. Many diabetics, even those with good glucose control, maintain slightly elevated blood glucose levels. Uncontrolled diabetics can have blood glucose levels that frequently peak over 400 mg/dL. Diabetic individuals, both type 1 and type 2, are more susceptible to infection than non-diabetics (47). The presence of hyperglycemia has negative reversible and irreversible effects on cellular proteins (48). We have made an initial observation that bone marrow stem cells from type 1 diabetic mice differentiated in hyperglycemic conditions *ex vivo* have blunted responses to bacterial lipopolysaccharide (LPS) stimulus (49).

Hyperglycemia and its negative effects are implicated in many diabetic complications. Previous research from our lab has shown a dysregulation in TLR expression and responsiveness from bone-marrow derived macrophages isolated from type 1 diabetic NOD mice (49, 50). Analyses of diabetic NOD mice and genetic control NOR mice bone-marrow derived macrophage phenotype and responsiveness when precursors are matured and stimulated in euglycemic and hyperglycemic conditions will shed light on the detrimental effects of hyperglycemia on the cellular level. Of particular interest are the effects of TLR2 stimuli *Porphyromonas gingivalis* (*P. gingivalis*) LPS and *Escherichia coli* (*E. coli*) LPS on macrophage TLR2 expression, signal transduction molecules, nuclear translocation of inflammatory NF-κB dimers, and pro-inflammatory cytokine expression.

Chapter 2

Research Design and Methods

2.1 Mice:

For diet-induced metabolic syndrome experiments, L-SACC, L-SACC WT (C57BL/6J x FVB), $Cc1^{-/-}$, and C57BL/6J mouse strains were maintained in a specific pathogen free (SPF) room in filtered-top caging racks at the DLAR at the Health Science Campus. Mice within each experiment (including WT controls) were sex and age matched to within one to two months of age. At the onset of a feeding experiment, mice were identified using unique ear-punches and weighed. The night prior to the conclusion of an experiment, mice were weighed again and fasted overnight (16:00 to 10:00 the next morning). The morning of experiments, mice were given a lethal dose of sodium pentobarbital to immobilize mice prior to retro-orbital bleeding. Mice were sacrificed by cervical dislocation prior to tissue harvesting.

A sexual dimorphism of metabolic parameters has been observed from preliminary experiments using L-SACC and Ceacam1 knock-out mice. Males develop more severe insulin resistance and dyslipidemia than female littermates, in agreement with the protective effects of estrogen on the development of the metabolic syndrome (51). Several female-only experiments were performed for comparison; however the project focused on male mice for experiments.

For type 1 diabetes hyperglycemic effects on bone marrow-derived macrophages, NOD and NOR mouse strains were housed under barrier specific pathogen-free (SPF)

conditions in laminar flow caging at the University of Toledo Main Campus Department of Lab Animal Research (DLAR). All equipment, food, bedding, and caging entering the suite are autoclaved. All personnel before entering the suite wear personal protection equipment including gowns, hair bonnets, face masks, gloves, and booties over shoes. NOD/M2 mice starting at 12 weeks of age are tested every other day for diabetes development using Diastix (Bayer, Elkhart, IN, USA). NOD mice with two successive blood glucose levels >250 mg dl^{-1}, as measured with a TheraSense FreeStyle monitor (Abbott Laboratories, Chicago, IL, USA), were considered diabetic. The diabetic rate for the McInerney female NOD pool was 72% over the duration of experiments. Diabetic mice were used within 24–48 hours of becoming diabetic. NOR/Lt, a genetically related diabetes resistant control strain of mice (52) were purchased from The Jackson Laboratory (Bar Harbor, ME, USA) bred and maintained under the SPF conditions described above. For all NOD experiments, only female mice were used and NOR female mice were age-matched to the diabetic NOD mice.

The University of Toledo collective DLAR is under the supervision of a full-time veterinarian, Dr. Robinson, a part-time veterinarian, Dr. Cole, and staff. DLAR uses the ILAR publication, The Guide for the Care and Use of Laboratory Animals (National Research Council, National Academy Press, Washington, D.C., 1996), as a basis for operation. DLAR provides rooms, equipment and trained personnel for the maintenance of most common laboratory animal species. All procedures are approved by the Institutional Animal Care and Use Committee (IACUC) of the University of Toledo and animals are handled in accordance with the guidelines of the National Institutes of Health and the IACUC.

2.2 Special diets for metabolic syndrome experiments:

L-SACC, $Cc1^{-/-}$ mice and their respective genetic controls had free access to water and one of three diets; regular diet (Lab Diets #5001), high-fat diet or high-fat / high carbohydrate diet (Research Diets Inc, New Brunswick, NJ, USA #D12451 / D12079B). Special diet feeding began after mice were two months old. Individual feeding experiments were performed for two, three, and four month durations. A summary of diet composition is provided in table 1.

2.3 Anthropometric characterization and blood glucose levels:

At the conclusion of a feeding experiment, mice were weighed and fasted overnight (from 16:00-17:00 to 10:00-11:00 the following morning). Weight gain was calculated as the difference from starting fed mass to final fed mass. Mice were weighed again after overnight fast. Visceral adiposity was calculated as the percentage of peri-gonadal visceral white adipose tissue mass divided by final fasting mass. The entire liver was removed and weighed. Fasting blood glucose levels were measured from tail-snip blood with a TheraSense FreeStyle monitor and test strips (Abbott Laboratories, Chicago, IL, USA).

2.4 Adipose tissue separation:

Using whole adipose tissue, stromal vascular cells (SVC) and adipocyte fractions were isolated following a method modified from C. Lumeng of the University of Michigan (1). Visceral adipose tissue was removed and weighed, then up to 1 gram from each mouse was pooled together, finely minced, and suspended in PBS containing magnesium and calcium, 1.5% fatty acid and endotoxin free bovine serum albumin (BSA), 5 mM glucose, and 100 Units of penicillin and 100 μg streptomycin. The minced

tissue was centrifuged at 500 rcf for 5 minutes to pellet particulate matter and red blood cells (RBC). Collagenase (ThermoFisher Scientific, Pittsburg, PA, USA) was added to a final concentration of 1.0 mg/ml, and the tissue was digested in a shaking water bath (200 Hz) for 20-30 minutes at 37° Celsius. The slurry was strained through a 100 μm cell strainer (BD Biosciences, San Jose, CA, USA) and centrifuged at 500 rcf for 5 minutes to pellet SVC. RBC in the SVC fraction were lysed with erythrocyte lysing buffer (Lonza, Walkersville, MD, USA) for 5 min at room temperature. The floating adipocytes were removed and washed with PBS three times. Purified adipose fractions were lysed for mRNA collection and further analyzed by qPCR.

2.5 Magnetic separation of adipose tissue macrophages and T cells from SVC:

SVC pellets containing adipose tissue macrophages were labeled with mouse Fc blocking antibody (supplied in EasySep kit) at 10 μL/ml. SVC were then treated with anti-F4/80-PE antibody (eBioscience, San Diego, CA, USA) at a concentration of 2.0 μg/ml for magnetic separation of this cell population. The EasySep PE selection kit (Stemcell Technologies, Vancouver, BC, Canada) was used to isolate adipose tissue macrophages for further study. The negative selection cell populations were treated with anti-CD3-FITC and followed with EasySep FITC selection kit (Stemcell Technologies, Vancouver, BC, Canada) for isolation of T-cells. Manufacturer procedures and instructions for using EasySep FITC and PE selection kits were followed utilizing the EasySep Magnet (Stemcell Technologies, Vancouver, BC, Canada). Confirmation of separations were confirmed by FACS analysis of adipose separation total SVC, $F4/80^+$, and $CD3^+$ isolated populations using a BD FACScan and CELLquest software (BD Biosciences, San Jose, CA).

2.6 Flow cytometry:

In one experiment, negatively selected cells were harvested F4/80+ magnetic separation for further analysis. This population was plated overnight in a final concentration of 10 ng/ml of IL-2 and non-adherent cells were collected for FACS analysis the following morning. T cells were treated with 0.5 ug of Fc blocking antibody (BD Bioscience, San Diego, CA) for 5 minutes, primary antibody at a concentration of 1 μg per one million cells for 45 minutes, and washed with cold FACS buffer (3% horse serum, 0.5% sodium azide, PBS) three times. Primary antibodies used were anti-TCR-FITC and anti-CD4-PE from Biolegend (San Diego, CA, USA). This experiment was performed by Dr. Anthony Quinn (Department of Biological Sciences, The University of Toledo).

For type 1 diabetes experiments, BM-MΦ from diabetic NOD and age-matched NOR mice were differentiated in both low- and high-glucose complete media (described in 2.11). Cells were counted and plated to 10^6 cells per well in six-well tissue culture plates. Plated cells were stimulated with *Porphyromonas gingivalis (P. gingivalis)* LPS at 500 ng/ml for 24 hours. Cells were then harvested, blocked with a 1 : 60 dilution of Fc Block (eBioscience, San Diego, CA), and stained with a 1 : 60 dilution of biotin-conjugated anti-mouse TLR2 antibody (eBioscience) on ice for 1 hour. Cells were then washed three times with cold phosphate-buffered saline (PBS) and stained with a 1 : 400 dilution of streptavidin-phycoerythrin (eBioscience) on ice for 1 hour. Cells were again washed three times with cold PBS and analyzed by FACS. Geometric means of data histograms as calculated by BD CellQuest software (San Jose, CA) were used for comparison between conditions.

2.7 Tissue histology:

Tissue samples taken during dissection were fixed for histological analysis in Z-Fix zinc-formalin fixative (Anatech, Battle Creek, MI, USA) for 24 hours and changed to 70% ethanol. Post-fixation tissue processing, paraffin embedding, and sectioning (4 μm) including H&E staining was performed by the Clinical Pathology lab at The University of Toledo Medical Center. All photomicrograhs were captured using an Olympus (Center Valley, PA, USA) microscope, MediaCybernetics (Bethesda, MD, USA) Evolution MP digital camera, and ImagePro (MediaCybernetics, Bethesda, MD, USA) capture software and were further analyzed using Image J shareware (NIH, Bethesda, MD, USA).

2.8 RNA isolation and real time-PCR analysis:

Tissues were homogenized using sterile one-time-use generators and a Powergen 125 tissue homogenizer (Fisher Scientific, Pittsburg, PA, USA). Frozen tissue samples (30-50 mg by mass) previously stored at -80°C in protective buffer RNAlater (Qiagen, Valencia, CA, USA) were thawed and placed in 600 μl of cell lysis buffer RLT (Qiagen, Valencia, CA, USA) containing with 1% 2-mercaptoethanol followed by homogenization of greater than 15 seconds at high speed.

For type 1 diabetes experiments, bone marrow-derived macrophages were harvested from tissue culture wells in 350 μl buffer RLT. Messenger RNA (mRNA) was isolated and purified using RNeasy mini kit (Qiagen, Valencia, CA, USA) according to the manufacturer's protocol. M-MLV Reverse Transcriptase (ThermoFisher Scientific, Pittsburg, PA, USA) was used to make cDNA from the isolated mRNA which was then used in triplicate quantitative real time PCR reactions to measure the relative amount of

mRNAs. Amplification of product was monitored with the fluorescent DNA binding dye SYBR Green included in the Absolute QPCR SYBR Green Fluorescein Master Mix (ThermoFisher Scientific, Pittsburg, PA, USA) in combination with the CFX96 system or iCycler iQ system (Bio-Rad, Hercules, CA, USA) according to the manufacturer's instructions. Briefly, the cDNA was denatured at 95°C for 15 seconds, the primer was annealed at 60°C for 30 seconds, followed by cDNA extension at 72°C for 30 seconds. The denaturation to extension cycles were repeated 40 times followed by a standard melt curve program. Forward and reverse primers were designed using the Primer Express 1.5 software (Applied Biosystems, Foster City, CA, USA) or identified using PrimerBank, a public internet resource for PCR primers. Glyceraldehyde-3 phosphate dehydrogenase (gapdh) was used as an endogenous control. The delta delta Ct quantification method was employed. Mouse primers used are as follows:

Mouse Cytokine	Forward Primer	Reverse Primer
GAPDH	CCAGGTTGTCTCCTGCGACT	ATACCAGGAAATGAGCTTGACAAAGT
F4/80	CTTTGGCTATGGGCTTCCAGTC	CAAGGAGGACAGAGTTTATCGTG
CD68	CTTCCCACAGGCAGCACAG	AATGATGAGAGGCAGCAAGAGG
TNFα	CATCTTCTCAAAATTCGAGTGACAA	TGGGAGTAGACAAGGTACAACCC
IL-6	GGCCTTCCCTACTTCACAAG	ATTTCCACGATTTCCCAGAG
IL-10	GGTTGCCAAGCCTTATCGGA	ACCTGCTCCACTGCCTTGCT
TLR2	ACAATAGAGGGAGACGCCTTT	AGTGTCTGGTAAGGATTTCCCAT
CD3 (delta chain)	AGAGCAGCTGGCAAAGGTGGTGTC	CAGCCATGGTGCCCGAGTCTAGC
MCP-1	TTAAAAACCTGGATCGGAACCAA	GCATTAGCTTCAGATTTACGGGT
SOCS1	CTGCGGCTTCTATTGGGGAC	AAAAGGCAGTCGAAGGTCTCG
Adiponectin	AGCCGCTTATATGTATCGCTCA	TGCCGTCATAATGATTCTGTTGG

2.9 Adipose lipid fraction fatty acid analysis:

A fatty acid composition analysis by gas chromatography of lipid collected from mouse adipose tissue digestion was performed by POS Pilot Plant Corporation (Saskatoon, SK, Canada). The results provided fatty acid profile (% relative) and composition measurements of mg fatty acid per gram of oil.

2.10 Fatty acid treatment of RAWblue cells:

Fatty acids identified as being major components of adipose tissue deposits by gas chromatography, as described above, were purchased for further experimentation. Fatty acid stocks were prepared by dissolving fatty acids (NuCheck Prep, Inc., Elysian, MN) in 200 proof ethanol to a stock concentration of 100 mM fatty acid, as described previously (53). Briefly, lyophilized fatty acids were dissolved in 200 proof ethanol to prepare stock solutions at 100mM each. Stock solutions were diluted further to 50 to 100 μM for cell treatment in serum-free medium containing endotoxin-free, fatty acid–free bovine serum albumin (#A7030 Sigma-Aldrich, St. Louis, MO, USA) as a fatty acid carrier. The fatty acid to bovine serum albumin molar ratio for all experiments was 5:1. The final concentration of ethanol in the media is less than 0.1%. Equivalent amounts of fatty acid free BSA and ethanol were added to control plates. RAWblue cells (Invivogen, San Diego, CA, USA) were incubated for 24 hours with FFA in special DMEM (low glucose) media prepared with dialyzed FBS which contains no fatty acids (HyClone, part of Thermo Scientific, Waltham, MA, USA). Stimulation of RAWblue macrophages with TLR ligands (with the exception of TLR3 and 5) which induce signaling pathways leading to the activation of NF-κB or AP-1 trigger the production of secreted embryonic

alkaline phosphatase (SEAP) into cell culture. SEAP activity is detected by incubation of supernatant with QUANTI-Blue detection substrate (Invivogen, San Diego, CA, USA) and measured by absorbance optical density on a Molecular Devices SpectraMax Plus spectrophotometer.

2.11 Isolation and treatment of bone marrow-derived macrophages:

For type 1 diabetes experiments, mouse femurs and tibias were harvested from groups of four to seven mice and bone marrow was flushed from the bone. Marrow cells were suspended by pipetting up and down several times, isolated from connective tissues, and plated with macrophage colony-stimulating factor (M-CSF) (Calbiochem, San Diego, CA, USA) at a concentration of 1.0 ng/ml in complete medium low-glucose (100 mg/dl) DMEM (Mediatech, Manassas, VA, USA), 10% fetal bovine serum (FBS, Irvine Scientific, Santa Ana, CA, USA), 50 U/ml penicillin G, 50 g/ml streptomycin (Mediatech, Manassas, VA, USA), 2 mM L-glutamine (Mediatech, Manassas, VA, USA) and 5 x 10-5 M 2-mercaptoethanol (Bio-Rad, Hercules, CA, USA) initially for four days. On day four the media was changed to fresh complete media without M-CSF and cells were allowed to rest for an additional two days prior to removing from tissue culture wells and counting of mature macrophages. Method of differentiation into macrophages was modified from the procedure of Warren and Vogel (54). To test the influence of a hyperglycemic environment on differentiation, bone marrow-derived macrophages (BM-MΦ) were differentiated and matured as described above, in high-glucose (450 mg/dl) DMEM (Mediatech, Manassas, VA, USA) complete medium. Equal numbers of differentiated BM-MΦ were plated for stimulation with known TLR ligands *Escherichia coli* (*E. coli*) LPS (#L4391 strain 0111:B4, Sigma Aldrich, St, Louis, MO, USA) or *P.*

gingivalis LPS (gift of R. Darveau, University of Washington, Seattle, WA, USA or Ultrapure from Invivogen, San Diego, CA, USA) for 4 to 24 hours or left unstimulated.

2.12 ELISA:

For type 1 diabetes experiments, bone marrow-derived macrophages (BM-MΦ) were harvested from diabetic NOD and age-matched NOR mice, cultured and differentiated in both high and low glucose containing media and challenged with *E. coli* or *P. gingivalis* LPS or left untreated for type 1 diabetes hyperglycemia experiments. Supernatants from one million BM-MΦ each condition were collected and frozen after 24 hours LPS treatment or left untreated for 24 hours. Supernatants were analyzed for protein levels of TNFα using the Mouse TNFα ELISA Ready-SET-Go! kit (eBioscience, San Diego, CA, USA) following the manufacturer's protocol. Supernatants were tested in triplicate. Absorbance was read with a Molecular Devices (Sunnyvale, CA, USA) SpectraMax Plus microplate spectrophotometer at 450nm minus 550nm per manufacturer instructions. A standard curve was generated utilizing included TNFα standard to convert absorbance values to a corresponding TNFα protein concentration.

2.13 Western blot analysis of cytoplasmic and nuclear extracts:

For type 1 diabetes experiments, pools of BM-Φ were differentiated and matured in both high and low glucose containing media from diabetic NOD and age-matched NOR mice. BM-Φs were seeded in 6-well tissue culture plates and stimulated with P. gingivalis LPS at 500 ng ml^{-1} for 30 minutes. After stimulation, cells were washed and lysed to harvest protein as described previously (55). Total protein concentrations were measured using the Bradford assay and 40 μg of extracts were analyzed in a 13% SDS-PAGE gel. Protein bands were semi-dry electro-transferred to a poly-vinylidene

difluoride (PVDF) membrane. After blocking the membrane with 5% non-fat milk for 30 min and washing with Tris-buffered saline containing 0.2% Tween 20 (TBST), the membrane was incubated with anti-phospho-IkB-alpha (Ser32) (Cell Signaling Technology, Beverly, MA, USA), at a dilution of 1:1,000 overnight at 4°C. After washing the membrane with TBST, the secondary antibody horse-radish peroxidase (HRP) conjugated ImmunoPure goat anti-rabbit IgG (H + L) (Pierce Biotechnology, Rockford, IL, USA) was added at a dilution of 1:10,000 and incubated for 1 hour at room temperature. The membrane was again washed with TBST and incubated with SuperSignal West Pico Substrate (Pierce Biotechnology, Rockford, IL, USA) for 5 minutes while protected from light. The membrane was stripped with stripping buffer (2% SDS, 100 lM 2-mercaptoethanol, 62.5 mM Tris pH 6.7) and reprobed with anti-β-actin antibody (Sigma-Aldrich, St. Louis, MO, USA) at a dilution of 1:10,000 as described above. For detection, CL-X Film (Pierce Biotechnology, Rockford, IL, USA) was exposed to the membrane and developed using a Konica SRX-101 processor.

In a separate experiment, nuclear extracts (NE) were obtained from pools of BM-Φ cultured and differentiated in both high and low glucose containing media from diabetic NOD mice. BM-Φs were seeded at one million cells per well in six-well plates and stimulated with P. gingivalis LPS at 500 ng ml^{-1} for 30 minutes. NE were recovered using an Active Motif Nuclear Extraction Kit according to manufacturer protocol (Active Motif, Carlsbad, CA, USA). Total protein concentrations were measured using the Bradford assay and 5 μg of NE proteins were analyzed in a 13% SDS-PAGE gel. Protein bands were semi-dry electro-transferred to a PVDF membrane. The same procedure for Western blotting was used as described above. The primary antibody used was anti-p65

antibody (gift of Dr. Brian Ashburner, University of Toledo, Toledo, OH, USA) at a dilution of 1:5,000. The membrane was directly visualized using a Kodak Image Station 4000R Pro. The membrane was stripped and reprobed with anti-histone H1 (Santa Cruz Biotechnologies, Santa Cruz, CA, USA) at a dilution of 1:1,000 as described above.

2.14 Statistical analysis:

Statistical outliers were identified as being greater than three standard deviations away from the mean of included data points. Student's T-test, 1- and 2-way ANOVA, and Tukey and Bonferroni post-tests were performed by GraphPad Prism 5.0 (GraphPad Software, La Jolla, CA, USA).

Chapter 3

Diet-induced metabolic syndrome results

3.1 L-SACC and Cc1$^{-/-}$ mice have increased weight gain, visceral adiposity, and liver mass compared to wild type mice following special diet feeding:

The preliminary anthropometric analysis of L-SACC and Cc1$^{-/-}$ mice following special diet feeding of groups of male and female mice for two to four months revealed consistent trends in weight gain, visceral adiposity, and liver mass (Figs 5-7). Two month feeding experiments were performed on male L-SACC and Cc1$^{-/-}$ strains with respective WT controls. As expected, the majority of HF and HF/HC fed mice of all strains gained more weight than mice fed RD (Fig 5 A, B, C). In one experiment, all three diets showed a significant difference in weight gain between WT and Cc1$^{-/-}$ stains (Fig 5 C). Results for visceral adiposity of the two month male feedings mimicked the above described results for weight gain (Fig 5 D, E, F). However, strain differences in the aforementioned experiment for visceral adipocity were only seen between RD and HF diets and not between mice fed the HF/HC diet (Fig 5 F). The two month RD feeding caused an increase in visceral adiposity of L-SACC males over WT (Fig 5 D) but this was not repeated with the Cc1$^{-/-}$ strain. The liver mass of male L-SACC mice fed for two months was higher than WT in both the RD and HF feeding conditions, while only the L-SACC HF/HC livers were larger than the RD controls (Fig 5 G). Two separate experiments using Cc1$^{-/-}$ males fed for two months showed variable results in terms of liver mass (Fig 5 H, I). In one experiment, only the WT HF fed livers were larger than their RD controls

(Fig 5 H). However in a second experiment, both the Cc1$^{-/-}$ HF and HF/HC livers were enlarged compared to RD, and a strain difference in liver mass was seen only in mice fed the HF/HC diet (Fig 5 I).

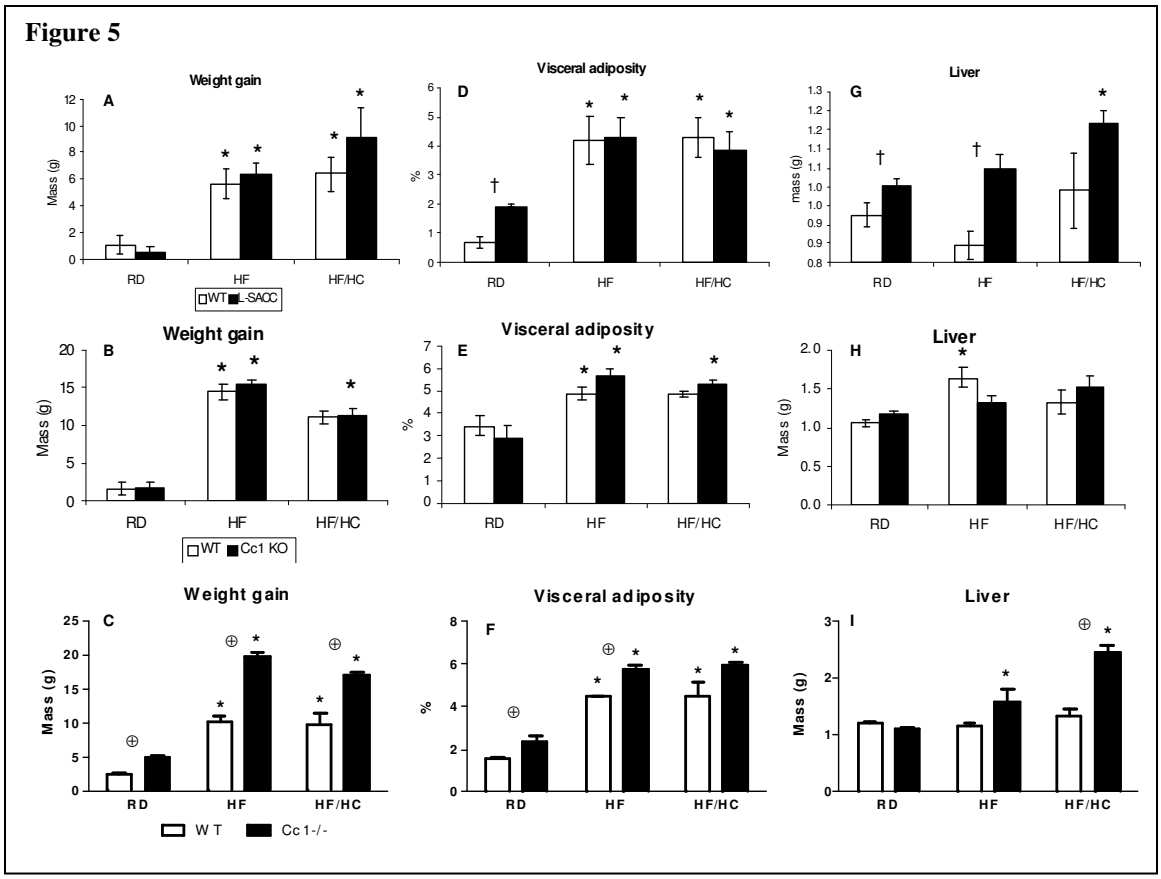

Figure 5: Anthropometric data from two month special diet fed L-SACC and Cc1$^{-/-}$ mice.

Groups of five to six male L-SACC, Cc1$^{-/-}$, and respective WT mice per diet were provided free access to specified diet and water for two months. Weight gain was calculated as the non-fasting change in body weight mass from diet start to end. Visceral adiposity was calculated as the percentage of peri-gonadal adipose tissue mass compared to diet end fasting body weight. Liver was excised and weighed after sacrifice. * indicates a student's T-test P value of less than 0.05 compared interstrain to RD. † or addition sign

enclosed in circle indicates a student's T-test P value of less than 0.05 intrastrain within the same diet condition.

Three month feeding experiments of groups of both female (Fig 6 A, E, I, B, F, J) and male (Fig 6 C, G, K, D, H, L) $Cc1^{-/-}$ mice were carried out. Female mice tended not to gain as much weight as their male counterparts (Fig 6 A and B females compared to C and D males) however the fattest females were more viscerally obese than males (Fig 6 E and F females compared to G and H males). Male special diet fed mice tended to have larger livers than females; liver mass of male mice was especially affected by the HF/HC diet (Fig K and L males compared to I and J females). Female WT and L-SACC mice fed the HF diet for three months gained more weight over the course of feeding than did RD fed mice, however a strain difference was seen only the L-SACC mice fed a HF/HC (Fig 6 A). Strain differences were seen in weight gain between WT and $Cc1^{-/-}$ females fed RD and HF but not HF/HC diet (Fig 6 B). In male experimental mice, both strains fed HF and HF/HC had increased weight gain over RD controls (Fig 6 C). Consistent strain differences between WT and $Cc1^{-/-}$ males fed HF and HF/HC diets were seen; in two separate experiments the $Cc1^{-/-}$ mice gained more weight over the three month feeding period than their WT controls (Fig 6 C, D). In one experiment, even the $Cc1^{-/-}$ males fed RD had statistically more weight gain than the WT mice (Fig 6 C).

Female L-SACC mice fed HF and HF/HC diets were more viscerally obese after three months than the RD controls (Fig 6 E). Strain differences of L-SACC mice having increased visceral adiposity over the WT were seen in both the RD and HF/HC feedings but not the HF fed group (Fig 6 E). Similar increases in visceral obesity were seen in an

experiment using female Cc1$^{-/-}$ mice. Both strains fed HF and HF/HC diets had statistically increased visceral adiposity, however there was no significance associated with the increase in L-SACC HF/HC over RD (Fig 6 F). Strain differences were again seen in two out of three feeding conditions, this experiment RD and HF but not HF/HC, whereas the HF/HC group was significant in the L-SACC female experiment (Fig 6 E vs. F). Similar trends in visceral adiposity were seen in three month male special diet fed mice. In two separate experiments, both strains (WT and Cc1$^{-/-}$) fed HF and HF/HC were more viscerally obese than the RD control mice (Fig 6 G and H). However, in one experiment male mice showed strain differences in both RD and HF diets, whereas mice in the other experiment did not show any statistically significant strain differences (Fig 6 G vs. H).

Changes in liver mass after three month special diet feeding were seen in female WT and L-SACC and in both female and male WT and Cc1$^{-/-}$ mice. Female L-SACC mice fed HF/HC and WT fed HF diets had larger livers than their RD controls (Fig 6 I). The strain difference of L-SACC mice having enlarged livers over WT was seen only in the HF/HC fed mice (Fig 6 I). In an experiment using female WT and Cc1$^{-/-}$ mice, only the HF/HC fed WT group was increased over RD (Fig 6 J). The strain difference was seen in liver mass, but this time the difference was seen in the HF fed mice and not the HF/HC fed mice (Fig 6 J compared to I). The male Cc1$^{-/-}$ mice fed HF and HF/HC diets for 3 months had larger livers than RD fed mice as well as a strain difference between males fed HF/HC diet (Fig 6 K). In a second separate experiment, both strains fed HF and HF/HC diets had enlarged liver mass over that of RD controls (Fig 6 L). The result of

$Cc1^{-/-}$ males fed HF/HC having larger livers than the WT mice on the same diet was repeated from the previous experiment (Fig 6 K, L).

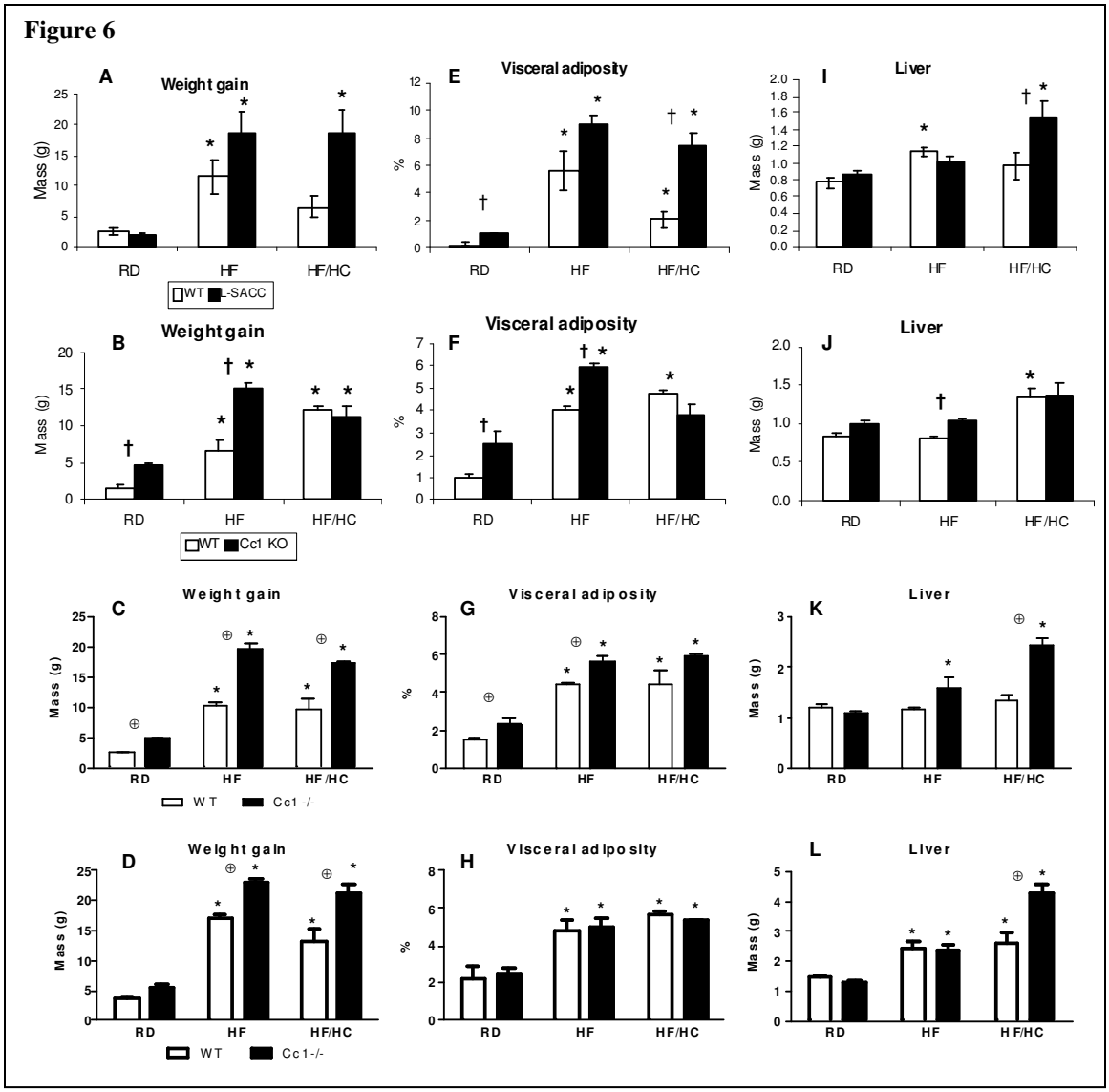

Figure 6: Anthropometric data from three month special diet fed L-SACC and $Cc1^{-/-}$ mice.

Groups of five to six L-SACC, $Cc1^{-/-}$, and respective WT mice per diet were provided free access to specified diet and water for three months. A, E, I, B, F, J represent female experiments while C, G, K, D, H, L are male experiments. Weight gain was calculated as the non-fasting change in body weight mass from diet start to end. Visceral adiposity was

calculated as the percentage of peri-gonadal adipose tissue mass compared to diet end fasting body weight. Liver was excised and weighed after sacrifice. * indicates a Student's T-test P value of less than 0.05 compared interstrain to RD. † or addition sign enclosed in circle indicates a student's T-test P value of less than 0.05 intrastrain within the same diet condition.

One experiment of four month special diet fed female L-SACC and WT mice was performed. Both strains of HF fed mice gained more weight than RD controls, but only the L-SACC females fed HF/HC gained more weight than RD (Fig 7 A). The strain difference of L-SACC mice gaining more weight than WT was seen in HF and HF/HC fed females (Fig 7 A). Both strains fed HF and HF/HC diets were more viscerally obese than RD fed controls. A strain difference of increased visceral adiposity of L-SACC mice compared to WT was seen in all three diet conditions (Fig 7 B). Only the L-SACC, and not WT, females had enlarged livers with HF and HF/HC diets compared to RD, and a strain difference in liver mass was seen in only the HF/HC feeding condition (Fig 7 C).

Figure 7

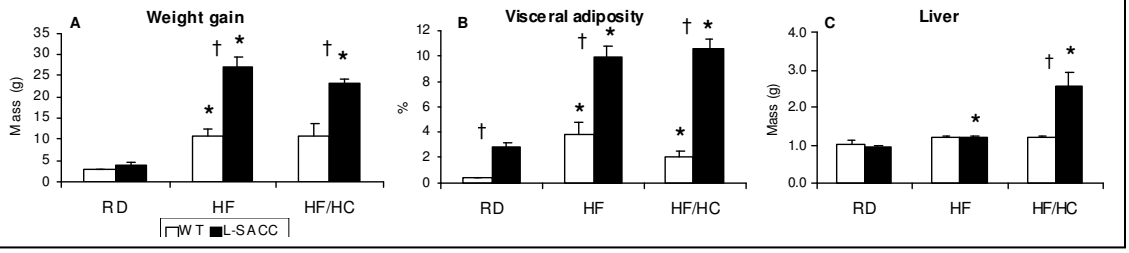

Figure 7: Anthropometric data from four month special diet fed L-SACC mice.

Groups of five to six WT (□) and L-SACC (■) female mice per diet were given free access to specified diet and water for four months. Weight gain was calculated as the non-fasting change in body mass from diet start to end. Visceral adiposity was calculated

as the percentage of peri-gonadal adipose tissue mass compared to diet end fasting body weight. Liver was excised and weighed after sacrifice. * indicates a student's T-test P value of less than 0.05 compared interstrain to RD. † indicates a Student's T-test P value of less than 0.05 intrastrain within the same diet condition.

To summarize the anthropometric results, L-SACC and $Cc1^{-/-}$ mice fed HF or Western diets gained more weight and were more viscerally obese than WT mice fed the same diet or when compared intrastrain to mice which had been fed RD. Interestingly, the HF/HC diet did not exacerbate weight gain and visceral adiposity compared to HF results. The livers of L-SACC and $Cc1^{-/-}$ mice were enlarged when fed the HF diet compared to RD, however the largest livers by far were seen when these mice were fed HF/HC diet. The WT mice weight gain, visceral adiposity, and liver mass were affected by the special diets, but not as consistently or to as great an extent as the experimental strains.

Liver mass and appearance depended greatly on the final body weight and visceral adiposity of the mouse. The most obese mice had enlarged, pale colored, speckled livers by visual inspection (Fig 8). When liver masses were plotted against visceral adiposity percentages, a trend was observed. Mice with visceral adiposity lower than 5.0% formed a trend-line of liver weight at approximately 1.2 grams (Fig 9). The data points falling on the left of the trend-line corresponded to both strains of RD fed mice. The WT HF fed mice remained on the far right of the trend-line. The WT HF/HC mice by far had the most variability in placement, some points falling on the trend-line

Figure 8. Large fat-speckled mouse liver.

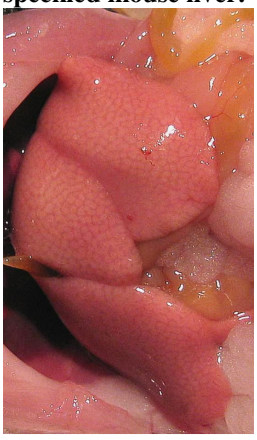

and others scattered among the Cc1$^{-/-}$ HF and HF/HC data points. Above 5.0% visceral adiposity, the liver masses were variable but all greater than the ~1.2g trend-line liver mass. A similar trend was seen in two and three month durations of male WT and Cc1$^{-/-}$ diet experiments but with varying values of adiposity and trend-line liver mass.

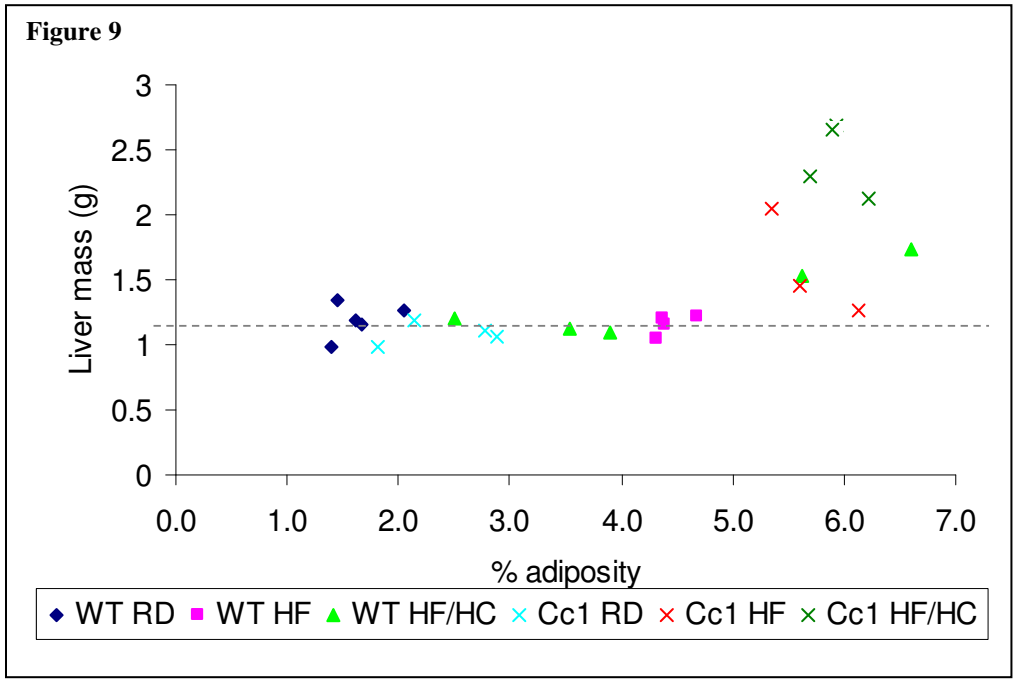

Figure 9: Comparison of visceral adiposity to liver mass of WT and Cc1$^{-/-}$ male mice.

Individual mouse anthropometric data of male two month experiment visceral adiposity and liver mass were plotted to reveal a trend-line of the experimental groupings: WT RD, WT HF, Cc1$^{-/-}$ RD, and some WT HF/HC mice that fell around the 1.2 gram liver mass. The HF/HC fed mice and Cc1$^{-/-}$ HF had with the largest livers corresponding to visceral adiposity percentages above 5.0 and fell far above the trend-line of the other conditions. Data is representative of four separate experiments using male WT and Cc1$^{-/-}$ mice fed special diets for two to three months.

3.2 HF and HF/HC diets cause liver steatosis and leukocyte infiltration which is worsened in L-SACC and Cc1$^{-/-}$ strains:

Poor diets, such as high fat or Western diet, can cause pathological liver changes in humans and animals. The L-SACC and Cc1$^{-/-}$ mouse strains have been purposed as l models to examine non-alcoholic steatohepatitis (NASH), a common form of liver injury associated with metabolic syndrome and type 2 diabetes (10). Special diet feeding of HF and HF/HC exacerbated several features of NASH, such as fatty deposits, leukocytic infiltration, and hepatocyte ballooning, seen in L-SACC and Cc1$^{-/-}$ mice (Fig 10). Both durations of special diet feeding and sex played roles in the extent of liver damage. Figure 10 shows representative photomicrographs of liver H&E histology from one mouse per diet condition of groupings of 5-6 mice. Male L-SACC develop mild steatosis and few loci of inflammation after two months of HF and HF/HC feeding (Fig 10 A) compared to minimal steatosis in control WT livers. Both female and male Cc1$^{-/-}$ mice after three month HF and HF/HC diets develop moderate to severe steatosis with associated inflammation (Fig 10 B-female, C-male). Hepatocyte ballooning, a pathologic cell injury / degeneration, can be seen in HF/HC fed male WT and Cc1$^{-/-}$ livers (Fig 10 C). Female L-SACC mice fed special diets for four months also show signs of moderate steatosis, inflammation, and minimal hepatocyte ballooning. While L-SACC and Cc1$^{-/-}$ strains have more severe liver pathology, WT livers are not protected from the effects of HF and HF/HC diets. The level of damage seen in WT HF/HC livers is often similar to damage after HF diet in the L-SACC and Cc1$^{-/-}$ mice. The most severe liver pathology was seen in the male Cc1$^{-/-}$ mice fed HF/HC diet for three months (Fig 10 C) but the females in this same condition also had severe pathology (Fig 10 B).

Figure 10

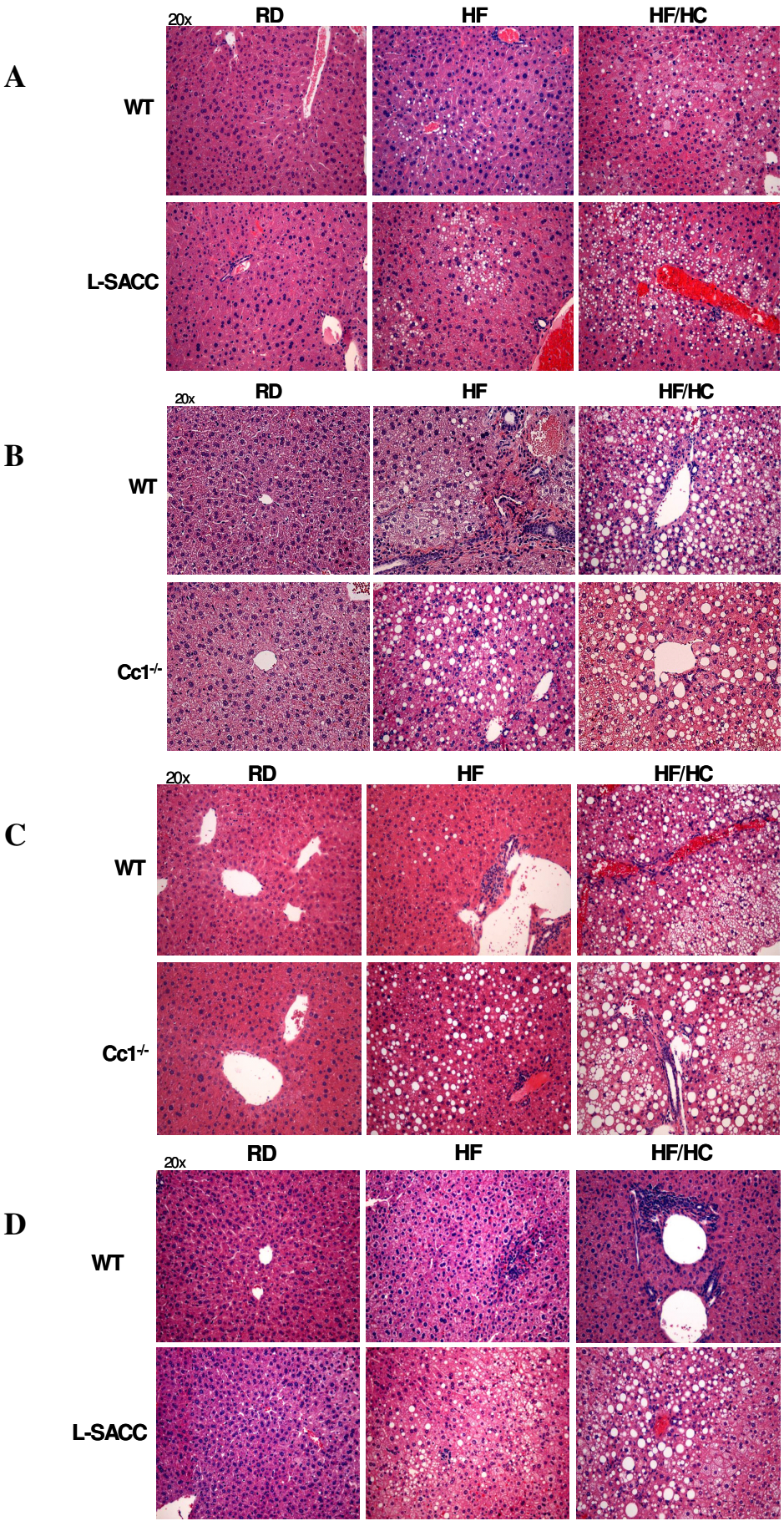
A
20x
RD
HF
HF/HC
WT
L-SACC
B
20x
RD
HF
HF/HC
WT
Cc1-/-
C
20x
RD
HF
HF/HC
WT
Cc1-/-
D
20x
RD
HF
HF/HC
WT
L-SACC

Figure 10: Histological analysis of special diet fed L-SACC and Cc1$^{-/-}$ livers.

A portion of liver tissue was excised from the visceral abdominal cavity of sacrificed L-SACC, Cc1$^{-/-}$, and WT mice following two, three, and four month special diet feeding. The liver was fixed in Z-fix, processed, and embedded in paraffin wax. Four micrometer sections were cut using a microtome and stained with hematoxylin and eosin. Photomicrographs were captured using an Olympus microscope, MediaCybernetics Evolution MP digital camera, and ImagePro software and were optimized for appearance using ImageJ shareware. All photomicrographs were taken with a 20x objective lens. (A) Male WT and L-SACC fed special diets for two months. (B) Female WT and Cc1$^{-/-}$ fed special diets for three months. (C) Male WT and Cc1$^{-/-}$ fed special diets for three months. (D) Female WT and L-SACC fed special diets for four months.

3.3 HF and HF/HC diets induce adipose tissue leukocyte infiltration:

In many models of obesity, leukocytes associated with inflammation such as macrophages and T cells are known to accumulate in adipose tissue (1, 31). The function of adipose tissue macrophages and T cells is currently under much investigation, in lean adipose these leukocytes are of a more regulatory phenotype (56). In obese adipose these leukocytes change to produce pro-inflammatory mediators and influence the function of other resident adipose cells (1, 57). Hematoxylin and eosin staining of adipose showed an increase in leukocytes in adipose of L-SACC, Cc1$^{-/-}$, and even WT mice when fed HF and HF/HC diets for variable durations (Figs 11 and 12). Crown-like structures (CLS) which are thought to be macrophages surrounding dead or dying adipocytes were seen

more frequently in the transgenic and knock-out mice which had been on the HF or HF/HC diets.

Leukocytes and CLS were seen in special diet fed female and male WT and $Cc1^{-/-}$ mice fed for three months. The difference in severity of infiltration between female and male mice is seen easily in figure 11 (female top set compared to male bottom set). The male adipose samples of both WT and $Cc1^{-/-}$ had more CLS than corresponding female tissues. CLS were seen more prevalently in the adipose tissue of female $Cc1^{-/-}$ HF and HF/HC compared to WT adipose from mice on the same diet (Fig 11 top set of six). The male HF and HF/HC fed WT and $Cc1^{-/-}$ mice all show examples of CLS (Fig 11 bottom set of six). Adipocyte size of $Cc1^{-/-}$ and WT female and male mice fed HF and HF/HC diets mice appeared larger than adipocytes from RD controls. One limitation of H&E histology is that although leukocytes can be seen in each diet condition, no information can be gained about identity or phenotype of these cells without further investigation. The HF/HC diet consistently showed examples of an anomalous type of adipocytes shown in the inset of the $Cc1^{-/-}$ HF/HC condition of figure 11. These areas interspersed among mature adipocytes showed multiple small adipocytes of an immature nature with centrally located nuclei and multiple lipid droplets inside cells. Mature adipocytes have one large lipid droplet occupying ~95% of the cytoplasmic area, thus forcing the nucleus to the edge of the cell right along the membrane and often times the nucleus of individual adipocytes is not visible in paraffin histology sections.

Figure 11

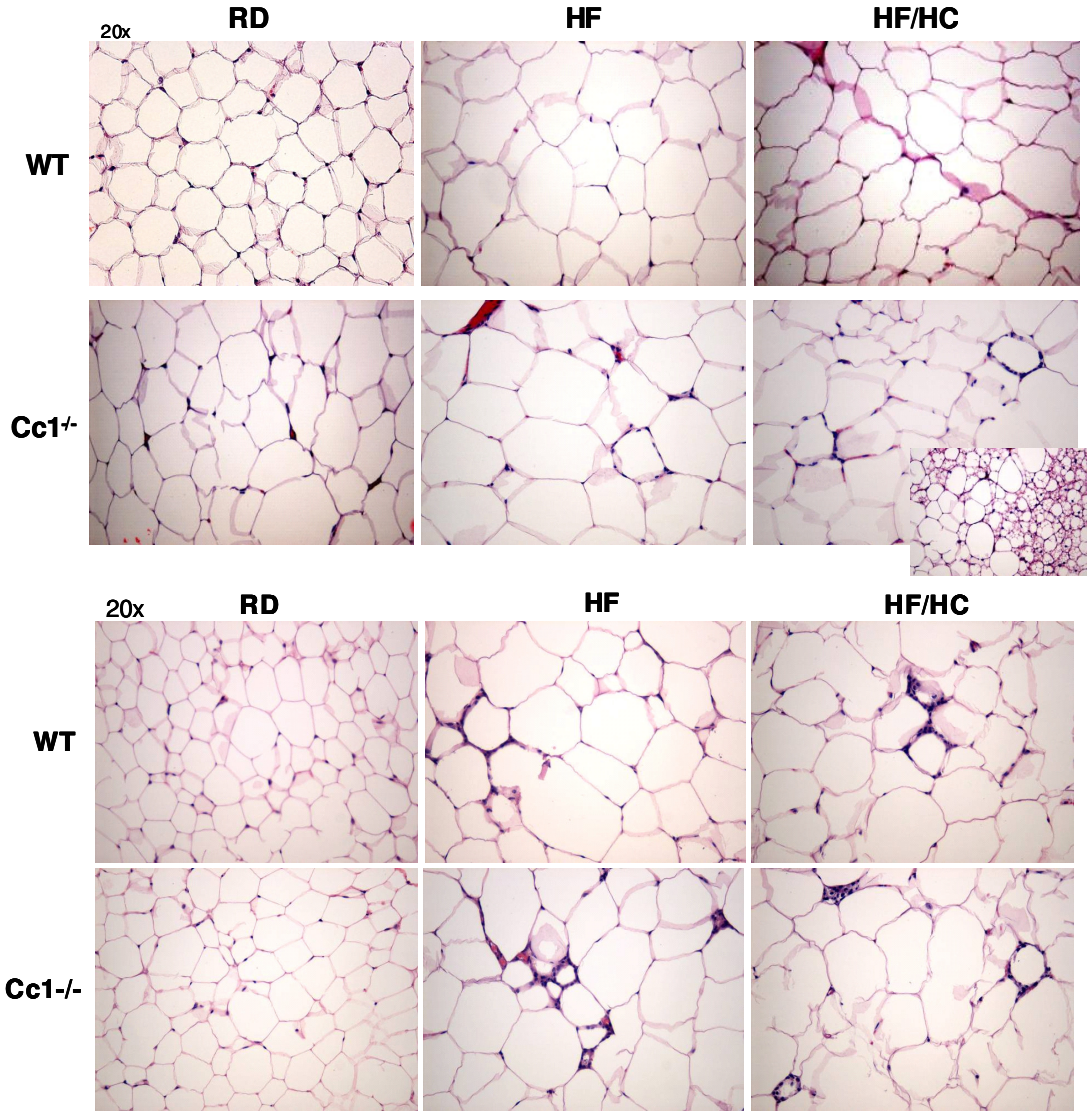

Figure 11: Histological analysis of WT and Cc1$^{-/-}$ adipose tissue following three month special diet feeding.

A portion of adipose tissue was excised from the visceral abdominal cavity of sacrificed female (top set of six photomicrographs) and male (bottom set) mice following three month special diet feeding. The adipose was fixed in Z-fix, processed, and embedded in paraffin wax. Four micrometer sections were cut using a microtome and stained with hematoxylin and eosin. Photomicrographs were captured using an Olympus microscope, MediaCybernetics Evolution MP digital camera, and ImagePro software and were

optimized for appearance using ImageJ shareware. All photomicrographs were taken with a 20x objective lens. Evidence of leukocytes, dark blue staining small cells, is seen in female top set $Cc1^{-/-}$ HF and HF/HC and male bottom set WT and $Cc1^{-/-}$ HF and HF/HC photomicrographs. Top $Cc1^{-/-}$ HF/HC inset is an example of anomalous immature small adipocytes.

Leukocytes were seen especially well in four month diet fed female L-SACC HF and HF/HC photomicrographs below as dark blue staining small cells (Fig 12). A typical CLS is seen in the L-SACC HF diet condition. The WT HF/HC inset is another example of anomalous immature adipocytes. The L-SACC HF/HC inset shows an extreme focus of leukocytes. The WT RD mice in this experiment did not have enough excess adipose to allow sampling for histology indicated by N/A.

Figure 12

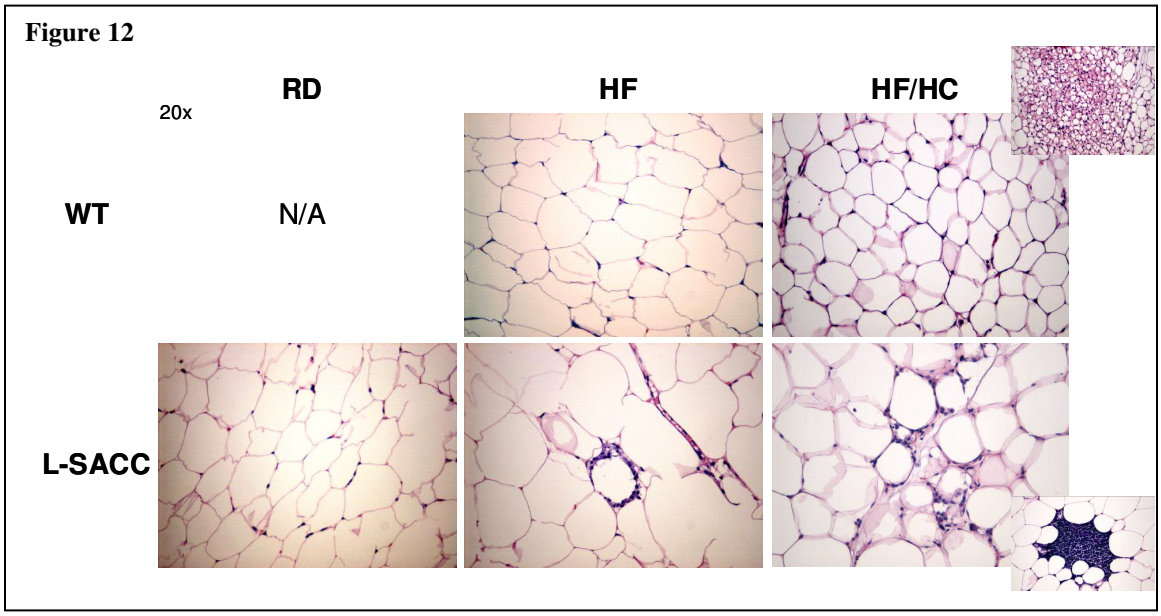

Figure 12: Histological analysis of WT and L-SACC adipose tissue following four month special diet feeding.

A portion of adipose tissue was excised from the visceral abdominal cavity of sacrificed female mice that had been on special diets for four months. The adipose was fixed in Z-fix, processed, and embedded in paraffin wax. Four micrometer sections were cut using a microtome and stained with hematoxylin and eosin. Photomicrographs were captured using an Olympus microscope, MediaCybernetics Evolution MP digital camera, and ImagePro software and were optimized for appearance using ImageJ shareware. All photomicrographs were taken with a 20x objective lens. Evidence of infiltrated leukocytes, dark blue staining small cells, is seen in L-SACC HF and HF/HC photomicrographs. N/A: Adipose was not available for harvest from WT RD as these animals were lean with very little visceral adipose. WT HF/HC inset is an example of the anomalous immature small adipocytes. L-SACC HF/HC inset is an extreme focus of leukocyte infiltration.

3.4 rt-PCR analysis of dysregulated macrophage marker, cytokine, and chemokine expression in adipose tissue:

Adipose tissue is considered to be an active endocrine organ, able to sense changes in metabolism or energy storage and respond by producing and secreting bioactive molecules such as adipocytokines, cytokines, chemokines, and changing expression of signaling and/or adhesion molecules which have wide-reaching effects. Various experimental methods have been used to quantitative levels of immune cell markers, cytokines, chemokines, and signal transduction molecules from adipose tissues which have been implicated in the development of metabolic syndrome and insulin resistance. We have used quantitative rt-PCR analysis of samples of whole adipose tissue

for analysis of messenger RNA (mRNA). Increased levels of mRNA indicate upregulation of gene transcription. Two different macrophage markers were used in the following experiments. F4/80 is a transmembrane protein expressed on the majority of mature macrophages and is a very common marker used to identify macrophages. CD68, or macrosialin, is a transmembrane protein which is a member of the lysosomal-associated membrane protein (LAMP) family expressed on macrophages, Langerhans cells, and a subpopulation of dendritic cells and is associated with phagocytosis. An experiment of three month special diet fed $Cc1^{-/-}$ and WT male visceral adipose deposits found trends of increased mRNA expression of the chemokine CCL2 (also known as monocyte chemotactic protein-1 {MCP-1}) and macrophage marker CD68 in $Cc1^{-/-}$ mice fed HF and HF/HC compared to RD-fed adipose (Fig 13). However, mRNA expression levels of TLR2, IL-6, and IL-10 were not significantly altered by strain or diet. TNFα mRNA was significantly elevated in the adipose of HF/HC-fed $Cc1^{-/-}$ compared to the RD mice. Levels of the T cell marker CD3 were also elevated in the $Cc1^{-/-}$ mice compared to WT especially in HF and HF/HC feeding conditions; however there was no statistical significance associated with this finding.

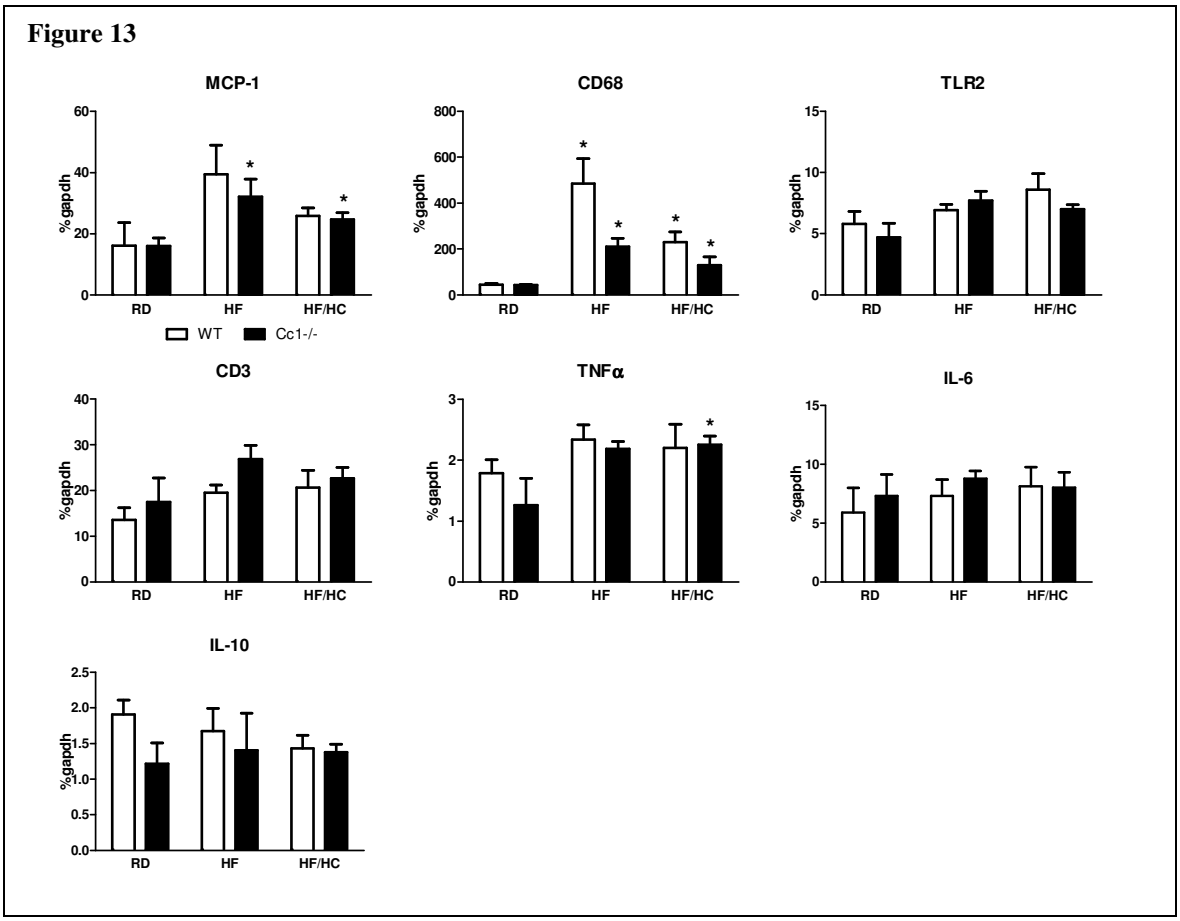

Figure 13: Real-time PCR analysis of cellular markers and cytokines from three month special diet fed Cc1$^{-/-}$ male adipose tissue.

Sections of visceral peri-gonadal adipose tissue were harvested from three month special diet fed male WT and Cc1$^{-/-}$ mice and homogenized using single-use sterile generators. mRNA was purified from homogenates and converted to cDNA for rt-PCR analysis. Gene expression reported was normalized to gapdh. Samples were tested in triplicate. * indicates a Students T-test P value of less that 0.05 compared intrastrain to RD feeding condition.

We repeated the analysis in an experiment of two month special diet fed Cc1$^{-/-}$ and WT male mice which was preformed later to investigate if result trends would be repeatable with this shorter feeding duration. We found increased mRNA levels of the

macrophage marker F4/80 in HF and HF/HC $Cc1^{-/-}$ mouse adipose tissue and increased MCP-1 in HF fed $Cc1^{-/-}$ adipose (Fig 14). This experiment also revealed strain differences in F4/80 expression between WT and $Cc1^{-/-}$ in both HF and HF/HC diets. Contrary to the previous experiment, levels of MCP-1 mRNA in HF/HC $Cc1^{-/-}$ adipose were significantly lower than levels found in WT adipose from the same diet, but the adipose from HF fed $Cc1^{-/-}$ mice had increased MCP-1 mRNA compared to WT. No significant differences based on strain or diet were seen with expression of CD3 or TLR2. Surprisingly, the expression of IL-6 in HF/HC fed $Cc1^{-/-}$ mice was significantly lower than the WT mice on the same diet (Fig 14). Correspondingly and equally unexpected, the regulatory cytokine IL-10 was increased in $Cc1^{-/-}$ mice over WT in both HF and HF/HC feeding conditions. IL-10 production can limit the expression of inflammatory cytokines such as IL-6 and TNFα by cells in the same microenvironment. Also the adipose from $Cc1^{-/-}$ HF fed mice IL-10 mRNA was statistically increased above the RD feeding condition, whereas the $Cc1^{-/-}$ HF/HC adipose level of IL-10 was elevated compared to RD but not reaching statistical significance (Fig 14). TNFα mRNA levels were not affected by strain or diet. Interestingly, expression level of the signaling molecule SOCS1, which like TNFα has direct and indirect effects on IRS-1 and IRS-2 and is able to blunt insulin action, was elevated only in WT HF/HC adipose (Fig 14).

Figure 14

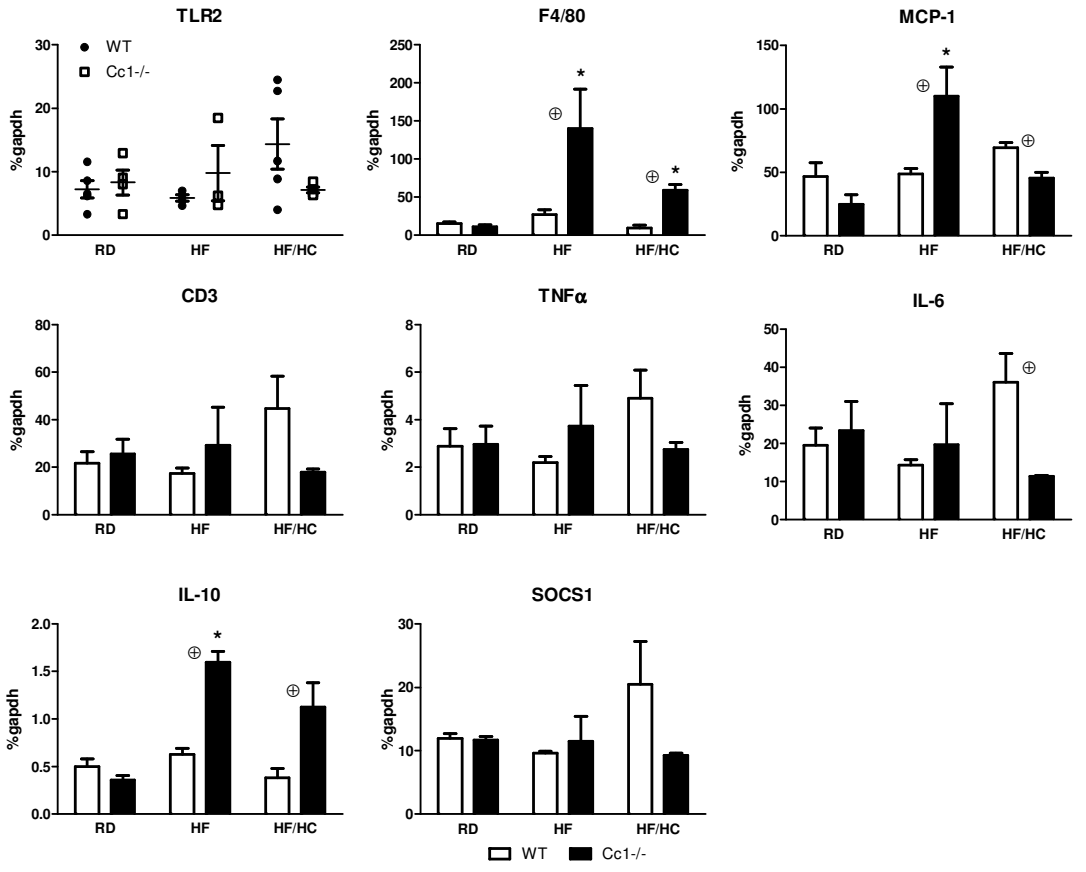

Figure 14: Real-time PCR analysis of cellular markers and cytokines from two month special diet fed Cc1$^{-/-}$ male adipose tissue.

Sections of visceral peri-gonadal adipose tissue were harvested from two month special diet fed male WT and Cc1$^{-/-}$ mice and homogenized using single-use sterile generators. mRNA was purified from homogenates and converted to cDNA for rt-PCR analysis. Samples were run in triplicate. * indicates a Student's T-test P value of less that 0.05 compared intrastrain to RD feeding condition. Plus symbol surrounded by circle indicates a P value of less than 0.05 compared interstrain of the same diet condition.

3.5 Adipose tissue separation into distinct cellular fractions shows differential cytokine contribution:

The observation that immune cells such as macrophages and T cells infiltrate the adipose tissue of obese animals suggests that in order to get a clear idea of cytokine contributions from each individual cell type, the distinct cell populations must be separated prior to analysis. It is known that classically activated or M1 macrophages and T helper 1 or T helper 17 cells have a great capacity to secrete inflammatory cytokines that can activate other cell types and contribute to insulin resistance. Adipocytes express certain TLR and have a capacity to produce and secrete chemokines and chemokines such as MCP-1 which can lead to monocytic cell infiltration, and adipocytokines, among which are some of the classical inflammatory cytokines such as TNFα. The full potential of adipocytes to secrete cytokines and other factors is unknown. Enzymatic digestion of adipose with collagenase followed by centrifugation and washes is the most commonly used technique to isolate immune cells into a stromal vascular cell (SVC) fraction away from adipocytes. An initial observation was made that adipocytes and stromal vascular cells had differential cellular mRNA expression of the cytokines IL-6, a pro-inflammatory mediator, and IL-10, a classic regulatory molecule (Fig 15). If the mRNA level of IL-6 expressed by WT RD SVC represents basal, then the HF/HC feeding reduces IL-6 mRNA from SVC in both strains of mice (Fig 15). Surprisingly, IL-10 mRNA originated mainly from the adipocytes and was inversely related to IL-6 expression. IL-10 mRNA was significantly increased in both WT and L-SACC adipocytes following HF and HF/HC diets (Fig 15). Also, the L-SACC HF/HC was

significantly higher than the WT adipocytes from the same diet. Signaling through the IL-10/IL-10R can potently inhibit pro-inflammatory cytokine production and secretion.

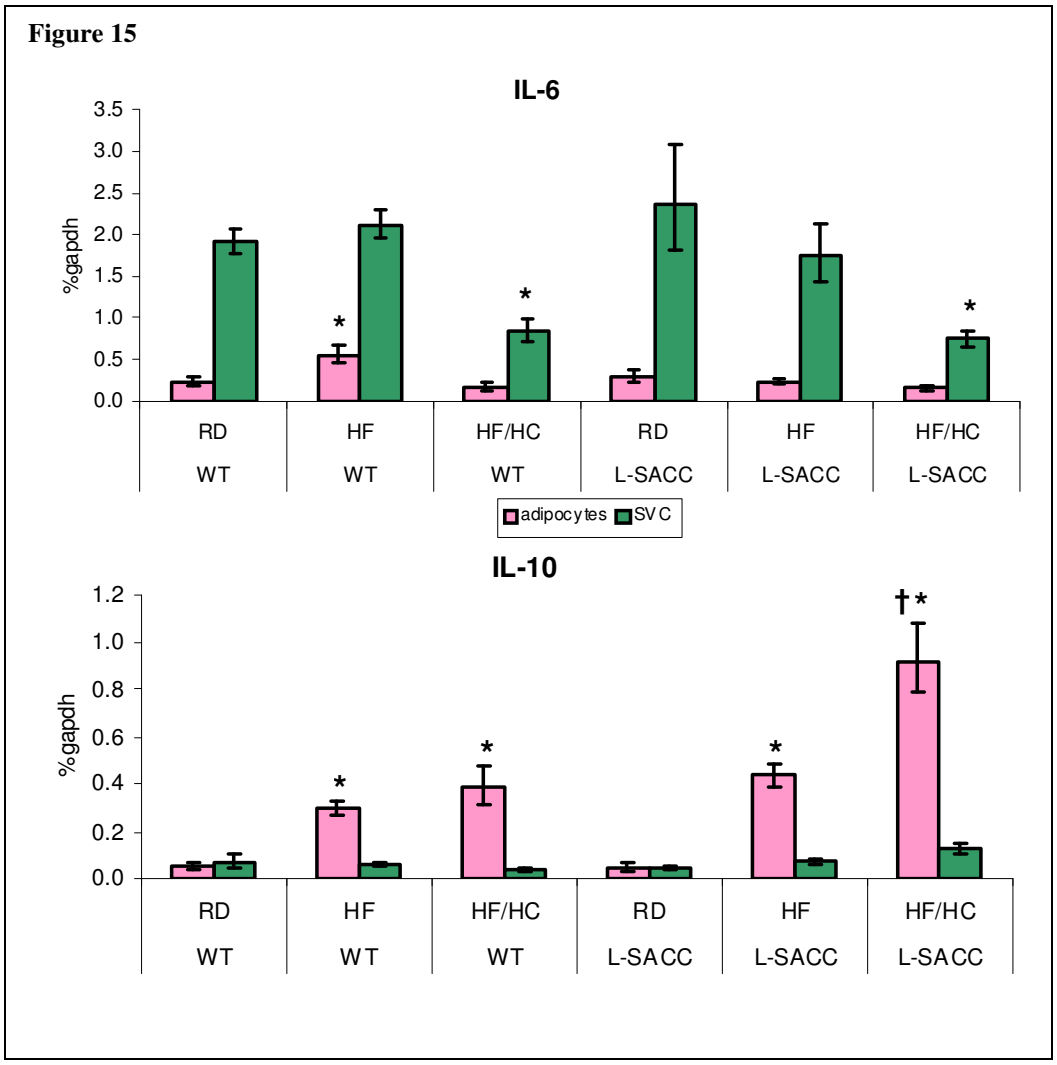

Figure 15: Differential expression of IL-6 and IL-10 cytokine from separated adipocytes and stromal vascular cell populations.

Up to one gram of visceral adipose was harvested from groups of two month special diet fed WT and L-SACC male mice. Adipose was collagenase digested, separated into floating adipocyte and pelleted SVCs, and lysed with buffer RLT. mRNA was harvested,

purified, and converted to cDNA for rt-PCR analysis. Samples were tested in triplicate. * indicates Students T-test P value less than 0.05 compared interstrain to RD, † indicates P value less than 0.05 compared interstrain to same diet.

To confirm a pure separation of adipocytes from SVC, both populations of cells were analyzed for expression of adipocyte adiponectin and macrophage marker F4/80 mRNA after two months of HF feeding. Adiponectin is an adipocytokine expressed only by adipocytes. Adiponectin mRNA expression is very high in both WT and $Cc1^{-/-}$ floating cell fractions (Fig 16). F4/80 is expressed by mature macrophages as well as on a subset of dendritic cells. However, rt-PCR analyses of multiple adipose separations of experimental strains (one example shown in figure 16) have shown that the separated floating fractions consistently have higher expression of F4/80 compared to the SVCs (Fig 16). Based on this result, the separated floating cell fractions contain both adipocytes and macrophages. One important point is that the $Cc1^{-/-}$ adipose cell fractions did have consistently higher expression of F4/80 (Fig 16). This result is consistent with the findings of figure 12. To test the possibility of adipocytes expressing macrophage markers, mRNA was obtained from the pre-adipocyte cell line 3T3-L1, in both the pre-adipocyte and matured adipocyte forms from Dr. David Kennedy (Lerner Research Institute, The Cleveland Clinic). Each of the cell types had been stimulated or left unstimulated. These four samples were tested for expression of F4/80, CD68, and CD11b (or Mac-1, another typical macrophage marker) and normalized to gapdh. Consistent with the findings of Khazen et al. (59) on adipocytes, all four samples had low expression of CD68 (average 1.0% gapdh) and very little expression of CD11b and F4/80 (average

0.004% and 0.01% gapdh respectively). This confirms that F4/80 should be used for further identification of macrophages in adipose tissue or the adipocyte cell fraction. In future experiments, purifying these contaminating macrophages from adipocytes could be attempted using a modified method of magnetic bead separation using an antibody specific for F4/80.

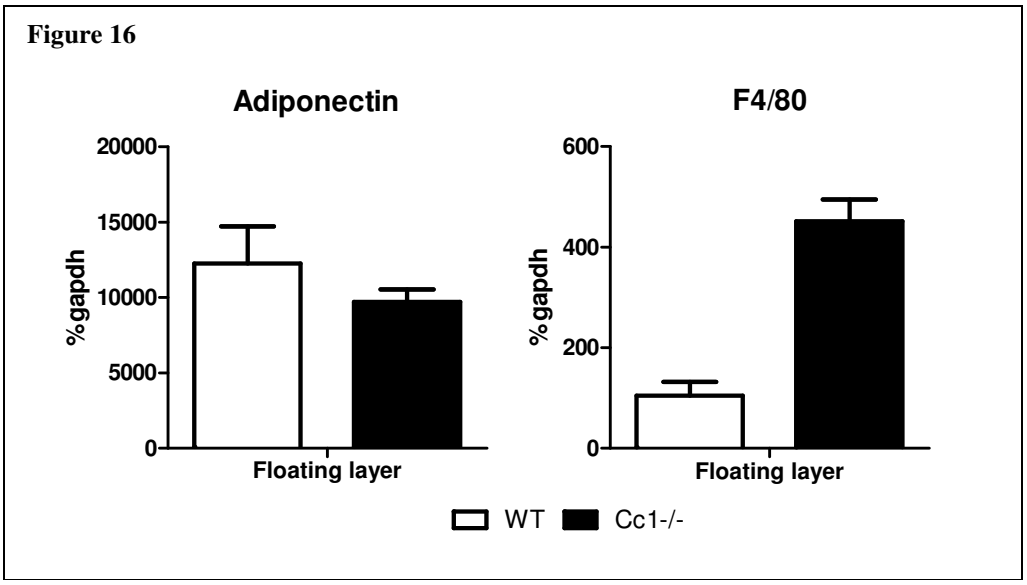

Figure 16: Purity analysis of separated adipose floating cell fraction by rt-PCR for adiponectin and macrophage marker F4/80.

Equal amounts of adipose were harvested from WT (□) and $Cc1^{-/-}$ (■) mice fed high fat diet for 2 months. Pooled adipose was collagenase digested, separated into floating adipocyte and pelleted SVCs, and lysed with buffer RLT. mRNA was harvested from the floating layer, purified, and converted to cDNA for rt-PCR analysis of adipocyte and macrophage markers. Samples were tested in triplicate. The floating layer of cells consistently expressed macrophage marker F4/80.

Several steps to improve the purity of adipose cell fractions after separation have been taken. First the digestion time was increased to at least 30 minutes to attempt to obtain a single cell suspension and release any macrophages trapped among adipocytes. Second, the SVC fraction was purified further by magnetic bead separation using an antibody specific to F4/80 to obtain pure macrophage populations for further study. Population purity before and after sorting purity by FACS analysis is shown in figure 17. Lastly, the floating adipocytes were put briefly in tissue-culture to allow settling and adherence of any contaminating macrophages, fibroblasts, or endothelial cells to tissue-culture plastic (results shown in Fig 18).

Figure 17

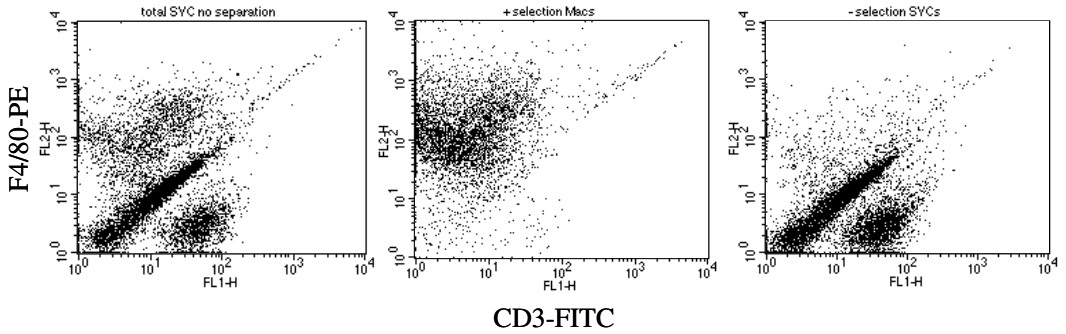

Figure 17: Magnetic separation of F4/80$^+$ macrophages from stromal vascular cell population.

F4/80$^+$ macrophages were separated from SVCs from a murine adipose digestion by a magnetic bead technique using anti-F4/80$^+$ antibody following manufacturer's instructions. FACS confirmed the purity of positively selected macrophages. FL2 axis is F4/80-PE and FL1 axis is CD3-FITC. Left is FACS dot-plot of the total SVC population prior to magnetic separation, middle is dot-plot after anti-F4/80$^+$ magnetic separation, right is dot-plot of negative selection cells remaining after isolating F4/80$^+$ cells.

In an experiment using only HF fed WT and Cc1-/- mouse adipose tissue, different populations of purified adipocytes were obtained and analyzed for the expression of different macrophage markers. The first population of adipocytes was obtained after centrifugation and wash steps of whole digested adipose. The second population was harvested from the floating cells after allowing adipocyte layer to settle in tissue culture for 2 hours with the goal of macrophages attaching to the plastic. The last population was harvested from the top floating cells after allowing overnight settling in tissue culture. However in a previous experiment it was discovered that stimulating purified adipose tissue macrophages with LPS or no stimulation (control) in overnight culture severely decreased the mRNA expression of TNFα, TLR2, MCP-1, and IL-10 (data not shown). Quantitative rt-PCR was used to examine cytokine, chemokine, and cellular marker expression of each of these populations of adipocytes. Tissue culture of adipocytes for 2 hours down-regulated the expression of all cytokines analyzed (Fig 18) and overnight culture further depressed mRNA expression of TNFα and other markers (data shown for overnight culture of TNFα). Levels of TNFα and IL-10 mRNA were increased over WT but no differences were seen in TLR2 or IL-6 expression (Fig 18). Thus, we decided for future experiments to not continue with culturing for any length of time but rather to determine cell marker and cytokine levels directly *ex vivo* after thorough washing of the adipocyte fraction.

Figure 18

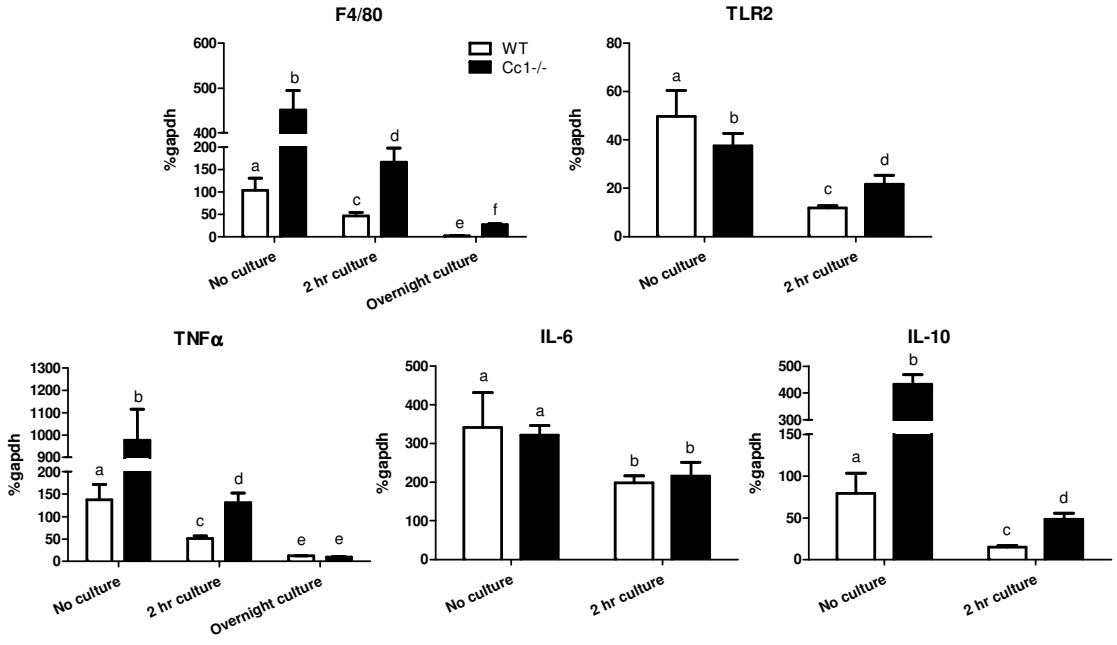

Figure 18: Cell marker and cytokine expression from adipocytes before and after tissue culture.

Equal amounts of adipose were harvested from WT (□) and $Cc1^{-/-}$ (■) mice fed high fat diet for 2 months. Adipose was separated into adipocyte and SVC fractions after collagenase digestion. Adipocytes were either lysed directly after washing, or plated for tissue culture for 2 hours or overnight in attempts to further purify adipocytes. Overnight samples were not tested for TLR2, IL-6 or IL-10 mRNA due to the small size and therefore volume of this sample. mRNA was harvested from each group and converted to cDNA for rt-PCR analysis. Samples were run in triplicate. Bars with different superscript letters indicate a significant difference by Students T-test (P value of less that 0.05).

Also from the same experiment of HF-only fed WT and Cc1-/- mice, magnetically separated F4/80^{+} adipose tissue macrophages (ATM) and the negatively selected cells consisting hypothetically of endothelial cells, fibroblasts, and any other immune cells which could be infiltrating adipose tissue were analyzed by q-PCR. No significant differences were seen in expression of TLR2 mRNA. A trend emerged that all cell populations from the Cc1$^{-/-}$ mice had elevated levels of TNFα and IL-10 mRNA (Fig 19). Another inflammatory cytokine, IL-6, appears mainly to be upregulated in the Cc1$^{-/-}$ fibroblast, endothelial, and other immune cell population.

Figure 19

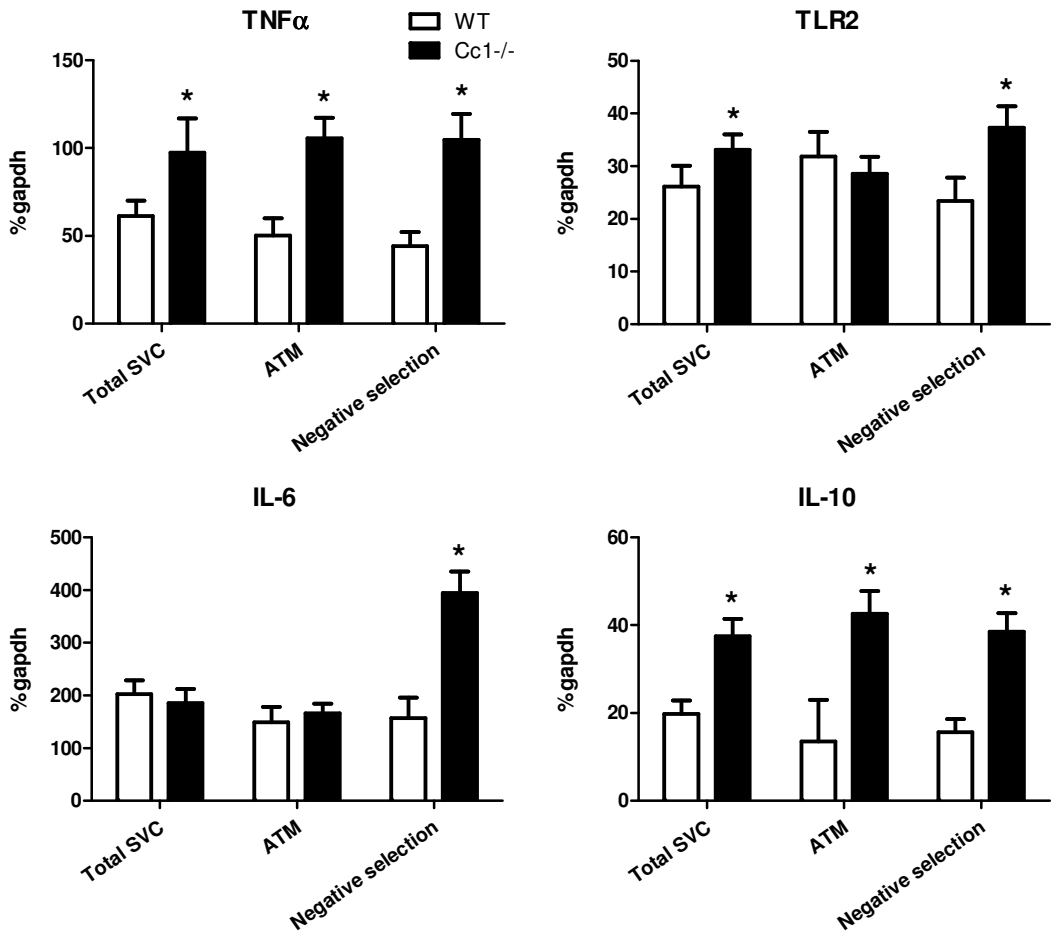

Figure 19: TLR2 and cytokine expression from stromal vascular cells before and after adipose tissue macrophage purification.

Visceral adipose was harvested from groups of two month HF diet fed WT and $Cc1^{-/-}$ male mice (WT n=11, $Cc1^{-/-}$ n=7). Equal amounts of adipose were collagenase digested, separated into floating adipocyte and pelleted SVCs. SVC were stained with F4/80 antibody and magnetically purified adipose tissue macrophages (ATM) were obtained. The F4/80 depleted flow-through was stained with CD3 antibody to further isolate T cells. Final negative flow-through hypothetically contains fibroblasts, endothelial cells, and other immune cells. Each population of cells was lysed and mRNA was harvested, converted to cDNA for rt-PCR analysis. Samples were tested in triplicate. * indicates Students T-test P value of less than 0.05 compared interstrain (WT vs. $Cc1^{-/-}$).

An experiment was performed using pooled adipose from five male WT and $Cc1^{-/-}$ mice following three month special diets (n=5 each group). After collagenase digestion, the negative selection cells following macrophage depletion of SVC was stimulated for T cell survival overnight with IL-2. In this morning, non-adherent cells were stained using antibodies specific for T cell receptor (TCR) and CD4 and analyzed by FACS. As shown in figure 20, the HF and HF/HC diets increased the percentages of $CD4^+$ T cells in WT animals. The $Cc1^{-/-}$ RD T cell sample was lost during the magnetic separation and wash steps. Comparing between strains shows that $Cc1^{-/-}$ adipose had slightly higher percentages of T cells (TCR positive). This experiment needs to be repeated to attain statistical significance between diets or strains of mice. In a separate experiment of WT and $Cc1^{-/-}$ mice fed HF diet only for two months, T cells were magnetically separated

from adipose tissue and harvested for rt-PCR analysis. No differences were seen in classic T helper 1 cytokines IFNγ or IL-12 mRNA between the strains, however T cells isolated from $Cc1^{-/-}$ adipose has elevated expression of IL-10 and IL-17 mRNA (normalized to gapdh) compared to WT adipose T cells (%gapdh IL-10 mRNA: 9.90 ± 1.5 WT vs. 22.02 ± 3.6 $Cc1^{-/-}$, IL-17 mRNA: 0.97 ± 0.05 WT vs. 1.51 ± 0.44 $Cc1^{-/-}$).

Figure 20

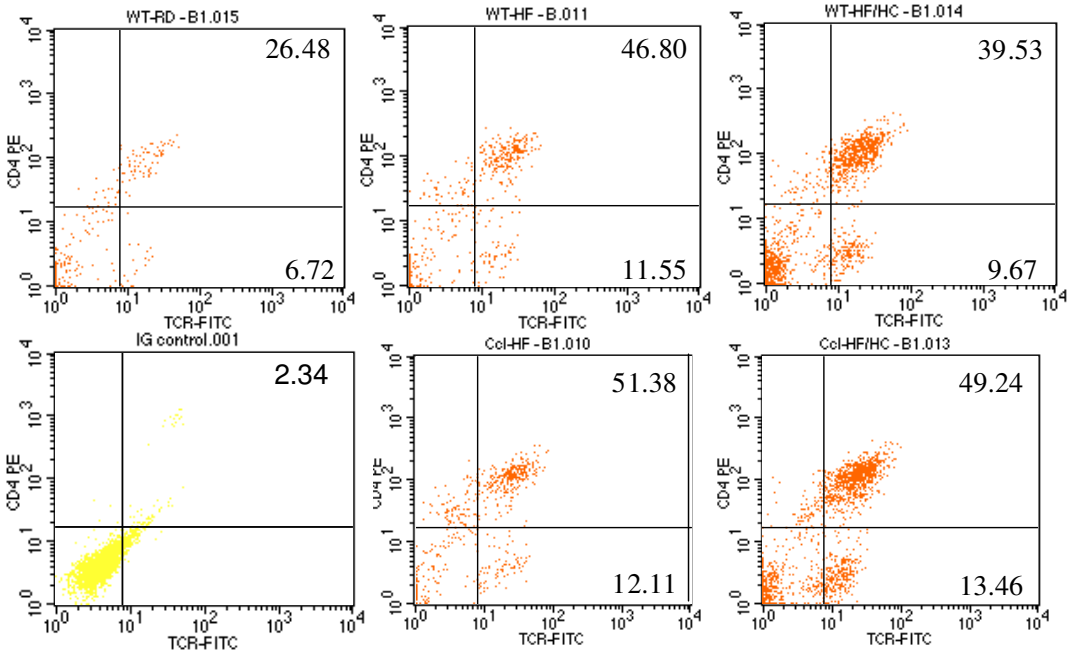

Figure 20: FACS analysis of T cells from the stromal vascular cell population from male WT and $Cc1^{-/-}$ mice fed special diets for 3 months.

Up to one gram of visceral adipose was harvested from groups of three month special diet fed WT and $Cc1^{-/-}$ male mice (group n=5). Adipose was collagenase digested, separated into floating adipocyte and pelleted SVCs. F4/80 negative cells were put into tissue culture overnight with IL-2 at a final concentration of 10 ng/ml. The following morning, non-adherent cells were stained with antibodies specific for the T cell receptor (TCR-FITC) and CD4 (CD4-PE) and analyzed by flow cytometry. Initial forward scatter and

side scatter dot plots were gated on lymphocytes. Numbers represent the % of gated cells in each quadrant. $Cc1^{-/-}$ RD cells were not collected due to experimental loss of this population. Negative control isotype staining shown bottom left (yellow). The HF and HF/HC diets increased the percentage of T cells infiltrating the adipose with obesity, also the $Cc1^{-/-}$ mice fed HF/HC had a greater percentage of infiltrating T cells than the WT.

3.6 Pancreatic abnormalities of HF and HF/HC fed $Cc1^{-/-}$ mice including immune cell infiltration and lipid deposits:

The beta cells of the islets of Langerhans in the pancreas are the only cells of the body which produce and secrete insulin. In the development of type 1 diabetes, these cells become the target of an auto-immune attack. Pancreatic insulitis, an infiltration of the islets with macrophages and T cells, occurs prior to overt diabetes onset. Very few investigations of animal models of the metabolic syndrome have focused on the pancreas for evidence of insulitis or other abnormalities. This disease mainly has an etiology of liver, adipose and skeletal muscle disturbances of glucose utilization and storage. We examined special diet fed L-SACC and $Cc1^{-/-}$ mice along with their WT controls and found histological evidence of pancreatic islet infiltration and lipid deposits. Instances of leukocytic infiltration were seen in each diet condition except for WT RD, WT HF, and L-SACC HF (Fig 21). Surprisingly, even on a RD, the $Cc1^{-/-}$ mice did show some evidence of islet infiltration. The severity of infiltration ranged from no islet involvement, to peri-insulitis, to complete islet infiltration. However, infiltration was also observed in exocrine pancreas nearby islets (Fig 21). The number of affected islets within one specimen was few in contrast to Type 1 diabetes in which all islets become infiltrated.

This suggests that either the infiltration is just beginning at these time points or that only a few areas of the pancreas will be affected.

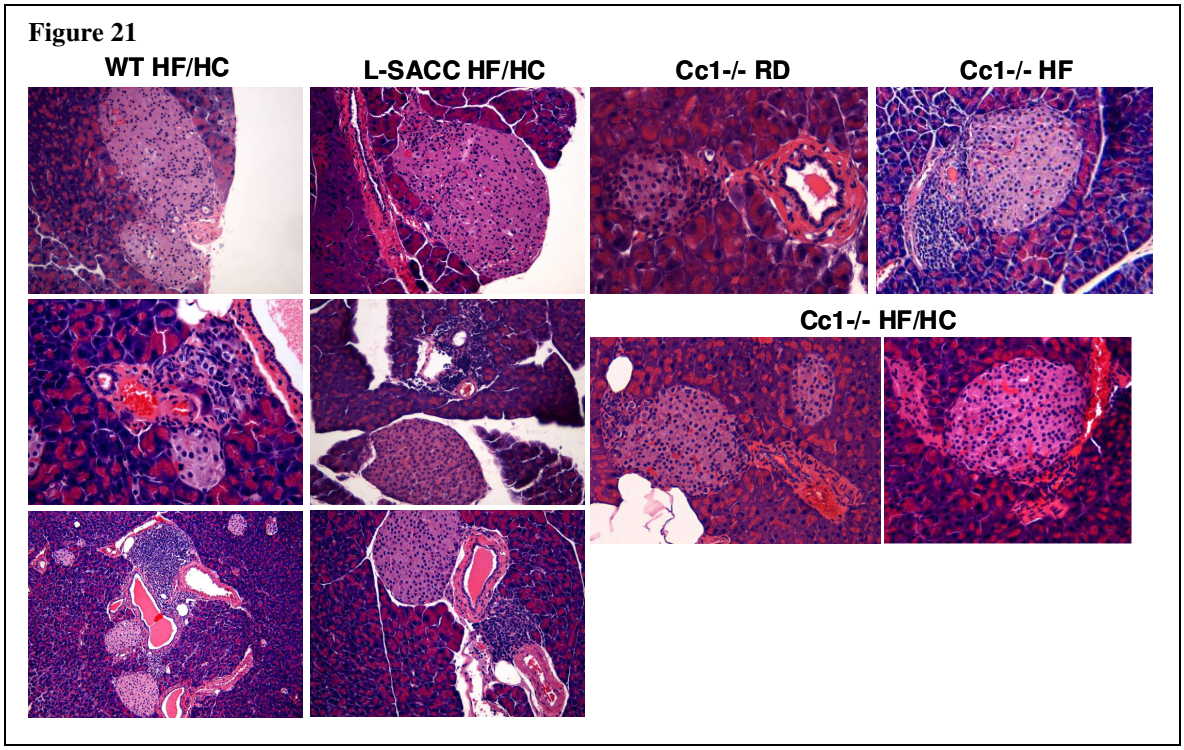

Figure 21: Pancreatic insulitis associated with diet-induced insulin resistance.

A small portion of pancreas was taken from sacrificed male and female L-SACC, $Cc1^{-/-}$, and their respective WT control mice that had been on special diets for 2 to 4 months. The pancreas was fixed in Z-fix, processed, and embedded in paraffin wax. Four micrometer sections were cut using a microtome and stained with hematoxylin and eosin. Photomicrographs were captured using an Olympus microscope, MediaCybernetics Evolution MP digital camera, and ImagePro software and were optimized for appearance using ImageJ shareware. Photomicrographs were taken with either a 10x or 20x objective lens. Evidence of infiltrated leukocytes is seen in varying degrees of severity; from mild peri-insulitis to infiltration of entire islets seen as dark blue foci.

To confirm macrophage and/or T cell involvement in the leukocytic infiltration, pancreata from an experiment of WT and $Cc1^{-/-}$ males fed over 3 months were harvested, mRNA isolated, and was converted to cDNA for real-time PCR analysis. Expression levels of the macrophage marker CD68 were elevated in the pancreata from WT mice fed HF and both WT and $Cc1^{-/-}$ fed the HF/HC diet (Fig 22). However, none of these increases were statistically significant. Levels of TLR2, commonly found on macrophages and other antigen presenting cells which can infiltrate the islets of Langerhans, were unchanged by strain or diet in this experiment. T cells, as measured by CD3 mRNA expression, appeared to be involved in the infiltration of the pancreata from the WT HF/HC fed mice. However, the $Cc1^{-/-}$ special diet mice had reduced levels of CD3 mRNA from pancreata, with a significant reduction of the HF feeding condition compared to the level seen in the RD fed mice (Fig 22). Future experiments should investigate phenotype of T-cells found in the pancreas.

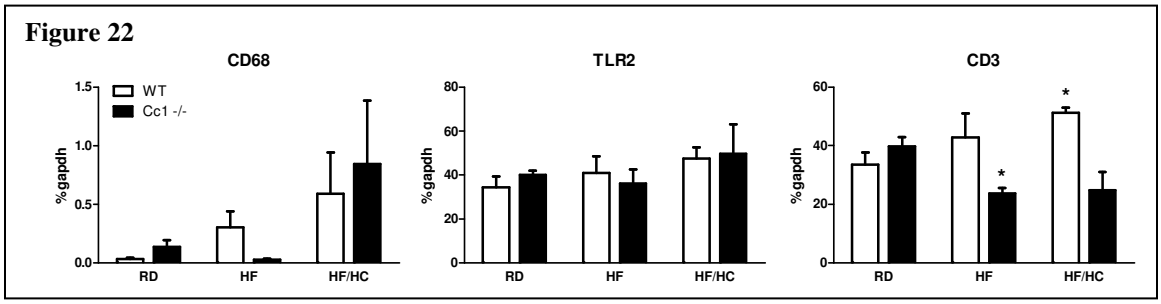

Figure 22: Real-time PCR analysis of infiltration markers in pancreata isolated from male $Cc1^{-/-}$ fed special diets for 3 months.

Sections of pancreas were harvested from three month special diet fed male WT and $Cc1^{-/-}$ mice and homogenized using single-use sterile generators. mRNA was purified from homogenates and converted to cDNA for rt-PCR analysis. Samples were run in triplicate.

* indicates a Student's T-test P value of less that 0.05 compared intrastrain to RD feeding condition.

A histological tissue abnormality found with metabolic syndrome and T2D patients and animals is lipid deposits in tissues such as liver and skeletal muscle. This is due to an increased level of circulating lipids (dyslipidemia) and triglycerides caused by a dysfunction in liver homeostasis and contributed to by poor diet. This excess lipid accumulates in adipose tissue; making the visceral adipocytes larger and increasing the number of cells, but with further metabolic dysfunction, lipid deposits in the liver, skeletal muscle, and pancreas. A histological analysis of L-SACC, $Cc1^{-/-}$, and WT mice at varying durations of diet showed many examples of lipid droplets and adipocyte-like cells forming in the pancreas (Fig 23). Instances of lipid deposits in pancreas tissue were seen in each diet condition except for WT RD, L-SACC RD and L-SACC HF. Surprisingly, even on fed RD, the $Cc1^{-/-}$ mice did show multiple instances of adipocytes forming in the pancreas. Lipids, at certain concentrations, can be toxic to beta cells and cause dysregulation (60). The lack of L-SACC examples is due to the fact that the pancreas was not examined for histology in several early experiments.

Figure 23

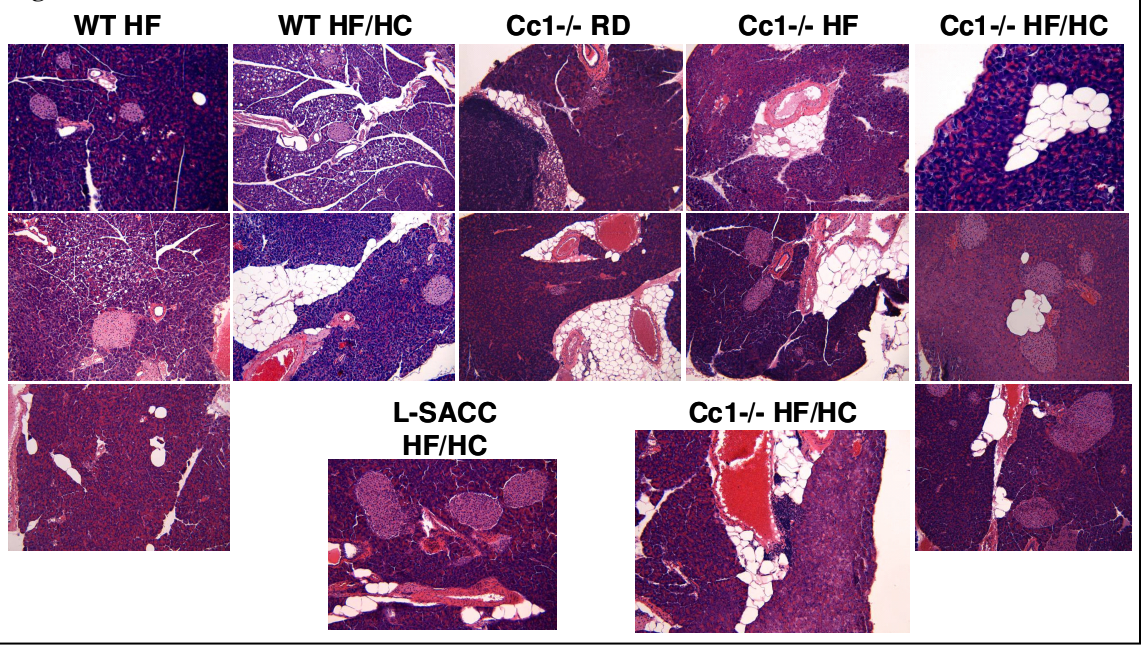

Figure 23: Anomalous lipid deposits in the pancreata of special diet fed L-SACC and Cc1$^{-/-}$ mice.

A small portion of pancreas was taken from sacrificed male and female L-SACC, Cc1$^{-/-}$, and their respective WT control mice that had been on special diets for two, three, or four months. The pancreas was fixed in Z-fix, processed, and embedded in paraffin wax. Four micrometer sections were cut using a microtome and stained with hematoxylin and eosin. Photomicrographs were captured using an Olympus microscope, MediaCybernetics Evolution MP digital camera, and ImagePro software and were optimized for appearance using ImageJ shareware. Photomicrographs were taken with either a 10x or 20x objective lens. Lipids can be seen in each image as small white circular droplets or as distinct groupings of adipocytes forming within the pancreas.

3.7 You are what you eat; adipose tissue from mice fed HF and HF/HC diets had greater saturated fat content than RD-fed mice.

A fatty acid composition analysis by gas chromatography of lipid collected from mouse adipose tissue enzymatic digestion was performed by an independent provider. The results provided fatty acid profile (% relative) of each of the feeding conditions - RD, HF, HF/HC. Pie charts summarize the most prevalent FFA from the digested adipose tissue of mice fed for three months as oleic acid, linoleic acid, palmitic acid, palmitoleic acid, and myristic acid (Fig 24). Only slight changes in FFA composition was seen between lipid from RD and HF fed mice. Most notably there are changes in the distribution of unsaturated fatty acids; increased oleic acid while linoleic and palmitoleic acids were slightly decreased. However compared to both RD and HF, the oil composition of the HF/HC sample had elevated levels of the saturated fatty acids palmitate and myristate, as well as increased unsaturated palmitoleic acid. The level of unsaturated linoleic acid was decreased while oleic acid levels were equivalent to the HF sample.

Figure 24

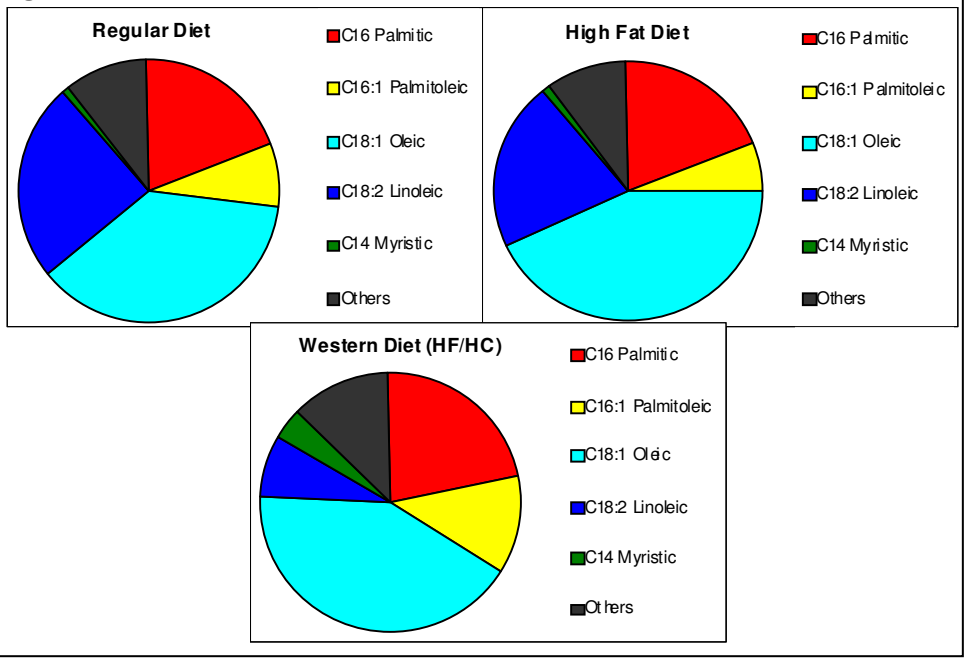

Figure 24: Gas chromatography fatty acid composition analysis of adipose lipid.

Lipid was collected during adipose tissue separation as the top floating layer and sent for free fatty acid analysis by gas chromatography. Results are shown as a pie chart of the five most prevalent fatty acids. Analysis performed by POS Pilot Corporation in Canada. FFA composition is similar between RD and HF feedings while HF/HC increased the proportion of saturated palmitic and myristic acids. Unsaturated palmitoleic acid also increased while the amount of unsaturated linoleic acid decreased with HF/HC feeding.

3.8 Fatty acid stimulation of TLR on RAWblue reporter macrophage line.

The fatty acids identified as being most prevalent in adipose tissue of RD, HF, and HF/HC fed mice were used for stimulation of reporter macrophage line RAWblue cells. These macrophages have high expression of all TLR except TLR3 and 5 and are stably transfected with an enzyme, secreted embroyonic alkaline phosphatase. The presence of TLR agonists which leads to signal transduction of NF-κB and/or AP-1 induces the secretion of SEAP. Supernatants containing SEAP are analyzed for color change by incubation with a substrate of SEAP and quantified by spectrophotometry.

Figure 25

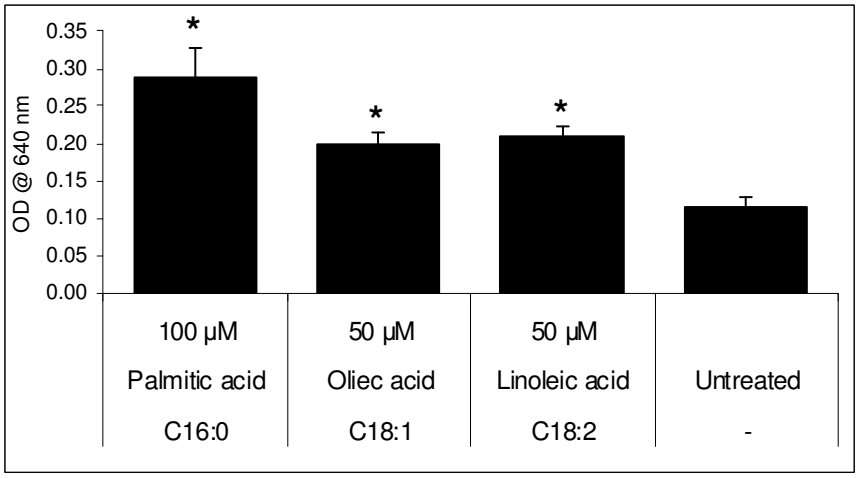

Figure 25: Stimulatory effect of free fatty acids on TLRs of RAWblue macrophage reporter line.

RAWblue macrophages were incubated in the presence of free fatty acids at varying concentrations for 24 hours in triplicate. Supernatants were collected and analyzed for SEAP activity by spectrophotometry. Optical density readings and standard error (n=3) are reported only for conditions which resulted in TLR stimulation. Fatty acid carbon chain length and number of points of unsaturation are shown below FA identity.

Chapter 4

Type 1 diabetes hyperglycemia results: refer to introduction 1.10

4.1 Hyperglycemic effects on inflammatory responses of Type 1 diabetic macrophages.

Prolonged elevated blood glucose levels have a negative effect on newly differentiated macrophages from the bone marrow. Hyperglycemia-altered macrophages are the very cells that then migrate into hypertrophic adipose tissue and/or liver and may play a role in disease progression or pathogenesis. Determining the mechanism of dysregulation could reveal a new pharmacological target for the prevention of chronic infection in both T1D and T2D. This could possibly reduce the incidence and severity of hyperglycemia related complications such as macrovascular disease, neuropathy, nephropathy, and retinopathy.

Previous research revealed that basal level gene expression profiles of diabetic NOD BM-Φ differ in response to their glucose environment (50). To further investigate this phenomenon and the effect of hyperglycemia on the ability of BM-Φ to respond to a TLR2 ligand, bone marrow stem cells harvested from diabetic NOD and NOR mice were differentiated into BM-Φ using M-CSF in high or low glucose conditions and stimulated with the TLR2 ligand *P. gingivalis* LPS. TLR2 mRNA expression detected by quantitative RT-PCR was significantly up-regulated in NOR BM-Φ differentiated and stimulated in both the high and low glucose conditions, while only the low glucose condition BM-Φ from diabetic NOD mice showed up-regulated TLR2 expression upon

stimulation (Fig 26). BM-Φ generated from diabetic NOD mice in the high glucose condition showed no significant change in TLR2 expression upon stimulation with *P. ginigivalis* LPS (Fig 26, NOD-diab. High). These hyperglycemic BM-Φ (differentiated and stimulated) derived from diabetic NOD mice appear to be unable to respond via up-regulation of TLR2 receptor, as is seen in the low glucose condition.

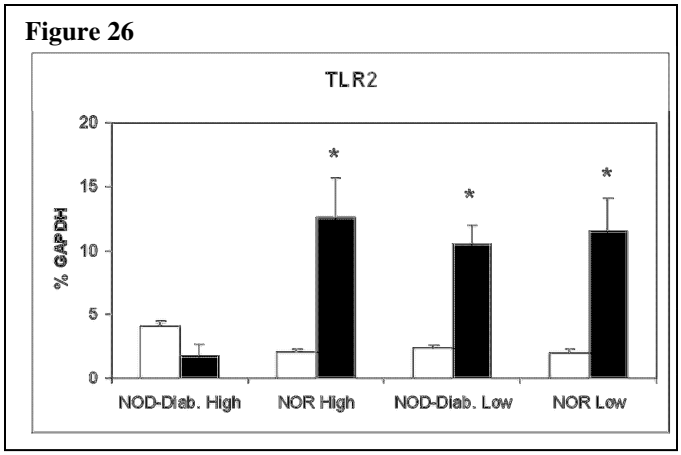

Figure 26: Real time PCR analysis of TLR2 expression from type 1 diabetic macrophages.

BM-Φ from pools of 4 diabetic female NOD and 4 age-matched female NOR mice were differentiated in either low glucose DMEM (100 mg/dl) or high glucose DMEM (450 mg/dl) to mimic a hyperglycemic environment. Both differentiation and stimulation occurred in low or high glucose media. BM-Φ were either left unstimulated (□) or stimulated with *P. gingivalis* LPS at 500 ng/ml for 4 hours (■). RNA was isolated, converted to cDNA, and quantitated by real-time PCR analysis using TLR2 specific primers. Results expressed as %GAPDH are the mean and SD of triplicate samples for each glucose condition. These results are representative of three separate experiments. The asterisk (*) indicates significant differences (Student's T-test P value <0.05) between high glucose stimulated NOD diabetic BM-Φ and the three remaining conditions when stimulated.

An examination of cell surface expression of TLR2 parallels the observation made for TLR2 mRNA expression. Hyperglycemic diabetic NOD BM-Φ stimulated with *P. gingivalis* LPS had approximately 20% less cell surface expression of TLR2 (Fig 27A) as compared to normoglycemic NOD BM-Φ. Control NOR mice exhibited the same level of cell surface expression of TLR2 following stimulation with *P. gingivalis* LPS in both the high and low glucose conditions (Fig 27B). TLR2 cell surface expression was equivalent for all treatment conditions except for hyperglycemic diabetic NOD BM-Φ as they expressed distinctly less TLR2 (20% less than the average geometric means of the other conditions) on the cell surface (Fig 27C shown as overlay).

Figure 27

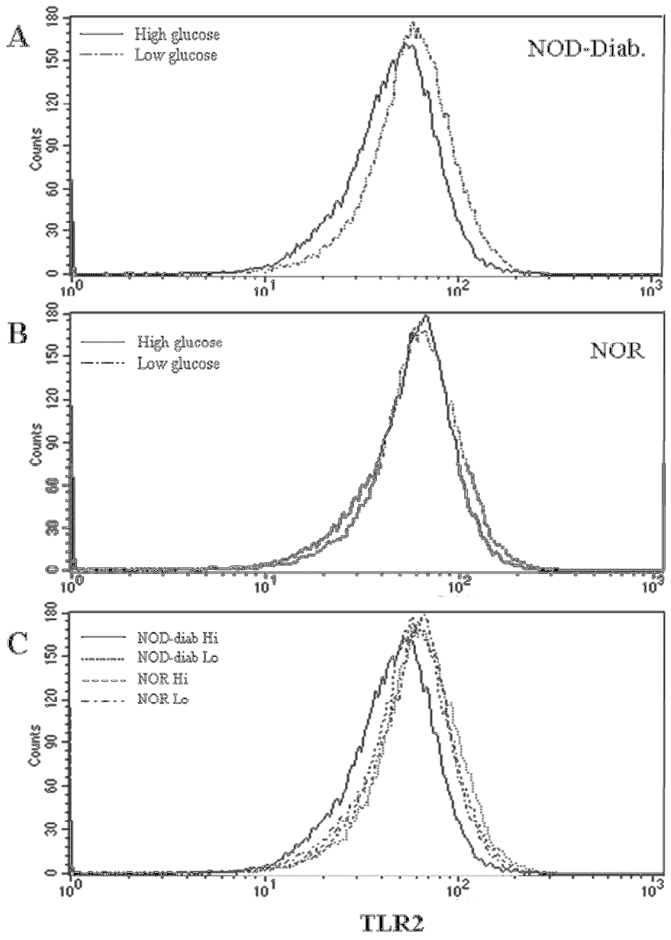

Figure 27: Flow cytometry analysis of TLR2 on cell surface.

BM-Φ from pools of 4 diabetic female NOD and 5 age-matched female NOR mice were cultured and differentiated in either low or high glucose media. Cells were analyzed for surface TLR2 by flow cytometry using a biotinylated-TLR2 antibody followed by secondary staining with SA-PE. A and B represent NOD diabetics and NOR strains respectively, while C is a combined overlay.

TLR2 signals through the MyD88-dependent pathway, eventually activating the IκB kinase (IKK) complex to phosphorylate the inhibitor of NF-κB (IκB), releasing NF-κB dimers to translocate into the nucleus where they activate gene transcription. The low level of TLR2 expression in diabetic NOD BM-Φ generated in a high glucose condition should correspond with a lack of TLR2 signal transduction. Therefore, BM-Φ were differentiated in both glucose conditions and cell lysates were analyzed via Western blot

to determine their ability to phosphorylate IκB-α in response to *P. gingivalis* LPS stimulation. Normoglycemic diabetic NOD and both normoglycemic and hyperglycemic NOR BM-Φ can effectively phosphorylate IκB-α (Fig 28A). However, hyperglycemic diabetic NOD BM-Φ display diminished phosphorylated IκB-α at 30 minutes post-stimulation with *P. gingivalis* LPS (Fig 28A, High glucose NOD-Diab (+) vs. NOD-Diab Low glucose (+) or High glucose NOD-Diab (+) vs. NOR High glucose (+) or NOR Low glucose (+) conditions). These results suggest that diabetic NOD BM-Φ effectively phosphorylate IκB-α when differentiated and stimulated under normoglycemic conditions, but are defective when differentiated and stimulated under hyperglycemic conditions.

Translocation and binding to DNA of certain NF-κB dimers to the nucleus induces gene transcription and expression of proinflammatory molecules such as TNFα. Isolated nuclear extracts of BM-Φ derived in low and high glucose conditions both show the presence of the p65 (RelA) subunit of NF-κB in the nucleus following stimulation (Fig 28B). However, the increase in p65 from unstimulated to post-stimulation is far more robust in the low glucose condition. Histone H1 levels confirmed approximate equal amounts of protein in each lane. An ELISA was performed to determine the amount of TNFα protein produced in response to *P. gingivalis* LPS stimulation. BM-Φ generated from both NOR and diabetic NOD mice in both high and low glucose conditions produce significant amounts of TNFα in response to *P. gingivalis* LPS compared to untreated control cells (Fig 28C). However, it is evident that the smallest increase in TNFα production following stimulation is seen in the hyperglycemic diabetic NOD supernatants. In the hyperglycemic condition, BM-Φ generated from diabetic NOD

experience a significant seven fold reduction in the production of TNFα compared to the same cells when generated in a normoglycemic condition. BM-Φ from both strains of mice in the low glucose condition produce elevated amounts of TNFα compared to those BM-Φ stimulated in the high glucose environment (Fig 28C, intrastrain low glucose compared to high glucose, closed boxes). TNFα production from NOR BM-Φ was less affected by the high glucose condition. The results indicate that BM-Φ generated from diabetic NOD mice are poignantly affected by the hyperglycemic condition as evidenced by a reduction or non-activation in response to *P. gingivalis* LPS stimulated TLR2 signal transduction events and TNFα protein production.

Figure 28

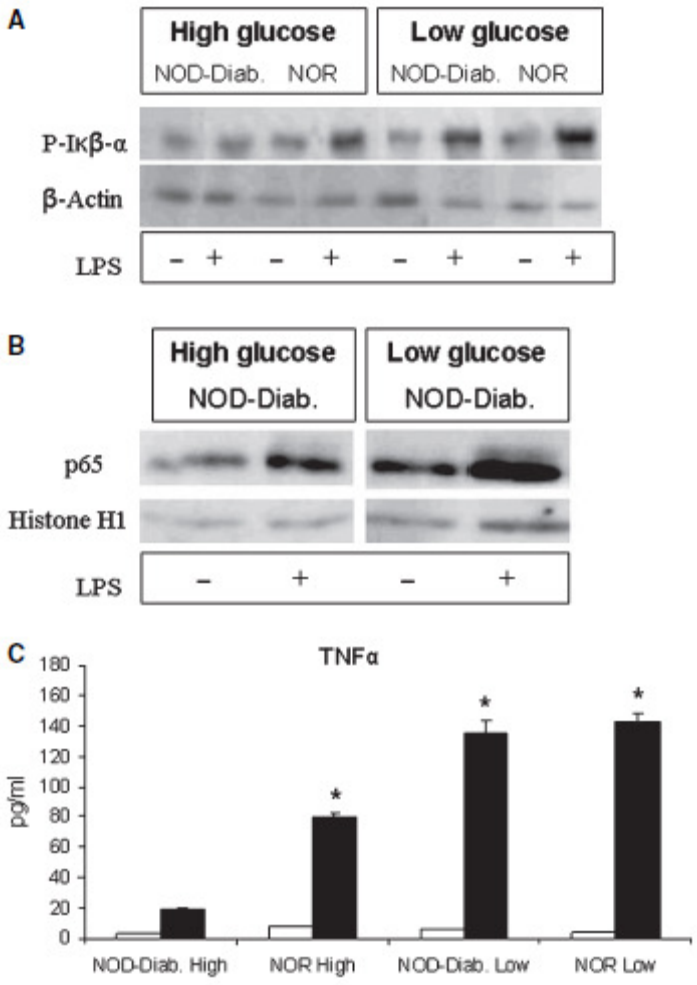

Figure 28: Signal transduction investigation.

A. BM-Φ from pools of 4 diabetic female NOD and 5 age-matched female NOR mice were cultured and differentiated in either low or high glucose media. Cells were left unstimulated (-) or stimulated with *P. gingivalis* LPS at 500

ng/ml for 30 minutes (+). Phosphorylated IκB-alpha (P-IκB-α), and β-Actin were detected by standard Western Blot procedure using specific antibodies. Results are representative of two separate experiments. **B.** BM-Φ either left unstimulated (-) or stimulated with *P. gingivalis* LPS at 500 ng/ml for 30 minutes (+). Nuclear extract p65 and histone H1 was detected by Western blot using specific antibodies. **C.** BM-Φ supernatants were analyzed for TNFα protein by ELISA. BM-Φ were left either unstimulated (□) or stimulated with *P. gingivalis* LPS at 500 ng/ml for 24 hours (■). TNFα standards were utilized to convert absorbance to protein concentration (pg/ml). Results are the mean and SD of triplicate samples. The asterisk (*) indicates significant differences (Student's T-test P value <0.05) between high glucose stimulated NOD diabetic BM-Φ and the three remaining conditions when stimulated.

Further experiments using both *P. gingivalis* LPS and *E. coli* LPS as stimuli provide evidence, at the mRNA level, for the dysfunctional responsiveness of the hyperglycemic diabetic NOD BM-Φ. As analyzed by quantitative rt-PCR, significantly depressed levels of TNFα mRNA were generated by hyperglycemic diabetic NOD BM-Φ in response to both LPS stimulations (Fig 29). These results further indicate a stunting in the ability of hyperglycemic diabetic NOD BM-Φ to respond to a bacterial stimulus. Using the methods and findings described here from type 1 diabetic mice, we can continue the investigation using bone marrow-derived macrophages from CEACAM1 knock-out and WT mice fed RD, HF, and HF/HC Western diets to compare effects of hyperglycemia in T2D to those seen in T1D (49, 50).

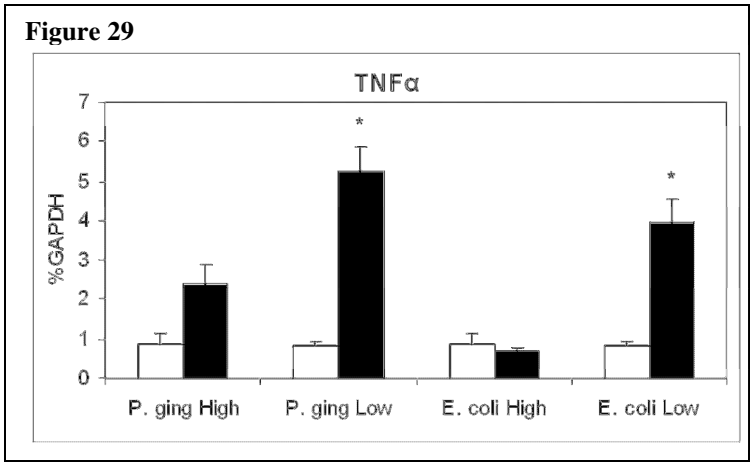

Figure 29: Real time PCR analysis of BM-MΦ stimulation in hyperglycemic and normoglycemic conditions with two strains of LPS.

BM-Φ from pools of 4 diabetic NOD were differentiated in low or high glucose containing media. BM-Φ were either left unstimulated (□) or stimulated with *P. gingivalis* LPS at 500 ng/ml or *E.coli* LPS at 100 ng/ml as indicated on the graph for 4 hours (■). RNA was isolated, converted to cDNA, and quantified by real-time PCR analysis using TNFα specific primers. Results expressed as %GAPDH are the mean and SD of triplicate samples for each glucose condition. The asterisk (*) indicates significant differences (Student's T-test P value <0.05) between low and high glucose conditions within the same bacterial stimulation.

Chapter 5

Discussion

5.1 Diet-induced metabolic syndrome inflammation

Anthropometric results from male WT and $Cc1^{-/-}$ feeding experiments of two and three month duration were mostly consistent while results from male and female L-SACC mice were less consistent. The genetic background of the L-SACC mice is mixed C57Bl6 and FVB while the background of the knockout line is C57Bl6. The C57Bl6 mice are used as a model of diet induced obesity while the FVB are resistant to developing visceral obesity and insulin resistance (61, 62). Furthermore, the dominant-negative transgenic L-SACC strain still has expression of the endogenous CEACAM1 molecule in organs and tissues other than the liver. Therefore, the whole body knockout of CEACAM1 ($Cc1^{-/-}$) may be more reliable than the liver specific dominant-negative CEACAM1 construct of the L-SACC transgenic line for the inflammation experiments described.

To summarize the most consistent anthropometric results, high fat and Western (high fat/high carbohydrate) diets increased both WT and $Cc1^{-/-}$ groups' weight gain and visceral adiposity over that of mice fed regular diet. In addition, three out of the four feeding experiments showed some strain difference between the WT and $Cc1^{-/-}$, usually there was an increase in weight gain and visceral adiposity of the $Cc1^{-/-}$ fed special diets over the WT mice fed special diets. A further common finding was that the Western diet lead to increased liver mass in the male $Cc1^{-/-}$ over RD and over WT mice also fed

Western diet. Published work already indicates that L-SACC males can be used as a model to study fatty liver diseases such as non-alcoholic steatohepatitis (NASH) (10).

One of the most interesting findings is the relationship discovered between visceral adiposity and liver mass. It appears that poor diet leads to enlarged liver once the mouse gets beyond a certain threshold of visceral adiposity. As figure 9 shows, mice fed high fat or Western diets developed abnormally large livers once they were greater than 5.0% viscerally obese. This suggests that one way to predict risk of fatty liver disease in humans is to measure viscerally adiposity. Accumulation of intra-abdominal fat is positively correlated with cardiovascular disease risk (63) and liver fat and hepatic insulin resistance in both men and women (45). A recent publication showed a relationship between visceral fat, serum adipokines, and liver steatosis in humans (64). We also examined livers by histology from diet-induced obese L-SACC, $Cc1^{-/-}$, and WT mice. NASH is differentiated from more simple non-alcoholic fatty liver disease (NAFLD) benign fat deposits by liver biopsy in patients. Features of NASH include macrovesicular fatty changes of hepatocytes with displacement of the nucleus to the edge of the cell, ballooning degeneration of hepatocytes, mixed lobular inflammation, and fibrosis (65). Figure 10 shows representative photomicrographs of liver sections from male and female WT, L-SACC, and $Cc1^{-/-}$ mice fed regular, high fat, or Western diets. Evidence of fatty deposits between and within hepatocytes, foci of inflammation, and hepatocyte ballooning can be seen mainly in male $Cc1^{-/-}$ mice fed HF or Western diet. Female mice of both experimental strains, L-SACC males, and WT mice show varying degrees of NAFLD signs but this does not necessarily indicate severe pathology. Future work would enlist the collaboration of a pathologist to score the photomicrographs for disease. Work

beyond this dissertation that could be useful for a more precise diagnosis of the special diet fed mice are histological staining to visualize fibrosis, immunological staining for local inflammatory cytokines and macrophages, and serum analysis of liver function such as alanine aminotransferase (ALT), aspartate aminotransferase (AST), and albumin.

Adipose tissue morphology and inflammation were also examined by histology. The major findings were increased adipocyte size and increased crown-like structures (CLS) and leukocytic presence associated with high fat and Western diet feeding of WT, L-SACC, and $Cc1^{-/-}$ mice. The transgenic and knock-out strains tended to have more CLS and leukocytes when compared to WT controls (figures 11 and 12). The anomalous areas we described as immature or preadipocyte-like cells closely resemble brown adipose tissue (BAT) (Figure 30). We have not been able to find literature describing the ability of white adipose tissue (WAT) to change into BAT, nor are BAT tissue deposits found in the same areas as WAT in mice. Therefore we can not find any explanation for small areas of BAT within the visceral WAT, if indeed it is BAT. Again, future work would require the collaboration of a pathologist to specifically identify cells in these areas within the WAT.

Figure 30. Comparison of anomalous WAT to BAT.

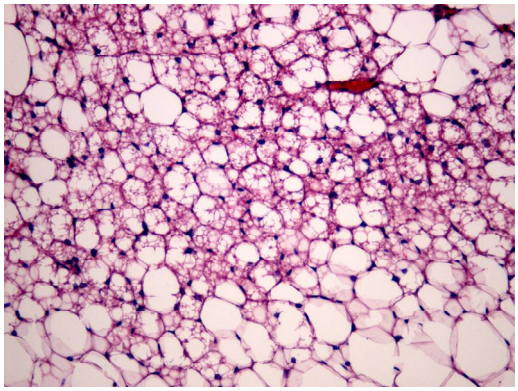

Anamolous area of white adipose tissue isolated from a female Cc1$^{-/-}$ fed HF/HC for 3 months

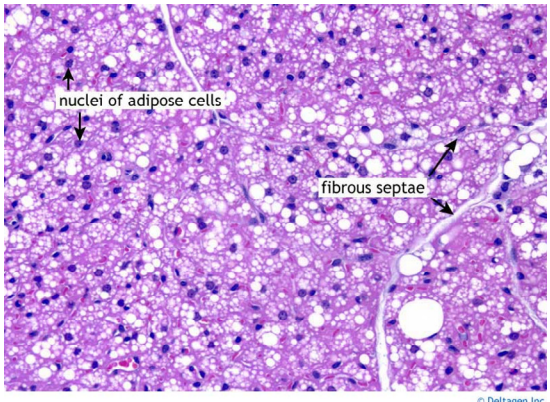

Brown Adipose Tissue

Figure courtesy of Deltagen Incorporated 2000-2006.

Quantitative real-time PCR was utilized to get more information about adipose tissue obtained from special diet fed WT and Cc1$^{-/-}$ strains. A profile of cellular and cytokine changes has been well-documented using other models of obesity. Obese animals have increased adipose pro-inflammatory genes and proteins such as TNFα, IL-1, IL-6, MCP-1 often associated with inflammatory macrophages (14, 66). These elevations in inflammatory cytokines are being linked with adipose tissue dysfunction and insulin resistance by interactions of inflammatory signal transduction pathways, including those associated with TLR signaling and with insulin receptor signaling (66-68). Macrophages gained the attention of researchers first as cells which could be responsible for inflammation in adipose due to several key studies on adipose resident macrophages and diet-induced changes in macrophage phenotype from regulatory to inflammatory types (1, 57, 69, 70). T cells have more recently been implicated in obese adipose dysfunction, particularly a change in T cell phenotype found in lean adipose tissue as regulatory to the inflammatory T helper 1 (Th1) subset found in obese adipose tissue (56, 71). Similar patterns of elevated immune cells and inflammatory cytokines are emerging in human studies of obesity (72). Inflammation also actives oxidative stress and reactive oxygen

species are highly implicated in obesity-related changes of insulin sensitivity and mitochondrial dysfunction which affects liver and skeletal muscle usage of glucose (68). Our findings diverge from the ones described above; the lack of significant changes in IL-6 mRNA from HF and HF/HC fed mice is contradictory to findings in obese humans and other strains of mice such as ob/ob and db/db, in which obese states are associated with elevated circulating levels of IL-6. However, elevated IL-6 in the aforementioned mouse models of obesity could depend on duration of diet and age of mice at analysis. Our results showed one experiment in which IL-6 mRNA was significantly elevated, that was the $Cc1^{-/-}$ SVC negative selection cell population purified from macrophages and T cells of a two month HF diet. This result suggests that endothelial cells and fibroblasts are major producers of IL-6. The most consistent finding from rt-PCR analysis of separated adipocytes, SVC, and further isolated macrophages has been that L-SACC and $Cc1^{-/-}$ mice have elevated expression of both inflammatory TNFα and regulatory IL-10 mRNA compared with WT mice (figures 15, 18, 19). The elevations in $Cc1^{-/-}$ TNFα and IL-10 mRNA are most pronounced in the HF and HF/HC diet conditions. Interestingly, another group has found increases in adipose tissue alternatively activated M2 macrophages in association with upregulated adipocyte IL-10 expression after high fat diet feeding (73). IL-10 and TNFα are opposite in function and are usually not seen elevated together. Elevated IL-10, being an immuno-regulatory cytokine mainly produced by T regulatory cells could be keeping the inflammation of the special diet-fed $Cc1^{-/-}$ mice under control. However the elevated levels of TNFα mRNA in $Cc1^{-/-}$ adipose suggest that the balance is tenuous. One explanation is suggested from studies of obese human adipose tissue. Findings of Zeyda et al. (72) suggest a blurring of the normal function of M1 and M2

macrophages found in obese subcutaneous adipose tissue. Adipose tissue macrophages were found to be M2-like, producing high amounts of IL-10 and IL-1 receptor antagonist, however the same macrophages were found to secrete high levels of inflammatory cytokines TNFα, IL-1β, and the chemokine MCP-1 into culture supernatant both unstimulated and stimulated by three different methods (72).

The purity of the adipocyte fraction form separated adipose tissue is questionable as seen in figure 16. One possibility is that macrophages, which very highly phagocytic, are becoming buoyant after phagocytosing adipocytes or lipids in the microenvironment and floating to the adipocyte layer during separation. A recent paper showed that while CD68 and CD14 mRNA was found in human and rodent adipocytes, F4/80 mRNA was exclusively in macrophages (59). To test this finding, mRNA was obtained from the pre-adipocyte cell line 3T3-L1, in both the pre-adipocyte and matured adipocyte forms from Dr. David Kennedy (Lerner Research Institute, The Cleveland Clinic). Each of the cell types had been stimulated or left unstimulated. These four samples were tested for expression of macrophage markers F4/80, CD68, and CD11b and normalized to GAPDH. Consistent with the findings of Khazen et al.(59) on adipocytes, all four samples had low expression of CD68 and very little expression of CD11b and F4/80. This confirms that F4/80 is the most appropriate marker to identify macrophages in adipose tissue or the adipocyte cell fraction.

It is important to note how many more significant differences were found when cell populations were attempted to be purified from whole adipose tissue. rt-PCR analysis of whole adipose tissue mostly revealed statistical significances in macrophage markers and MCP-1, the chemokine which draws monocytes into tissue which then differentiate

into macrophages (Figure 13 and 14). One significant difference of TNFα mRNA was revealed in $Cc1^{-/-}$ adipose tissue of HF/HC fed mice compared to RD fed mice (Figure 13). Elevated IL-10 mRNA emerged as significantly different in adipose from HF fed $Cc1^{-/-}$ mice compared to RD, and the strain difference was seen for the first time between WT and $Cc1^{-/-}$ mice fed HF and HF/HC diets (Figure 14). Far more interesting differences emerged once the adipose was separated into different cell populations. First, IL-6 mRNA was found to be from the SVC population, further experiments implicate endothelial cells and fibroblasts as the main producers. IL-10 mRNA was elevated in several different populations, adipocytes from HF and HF/HC fed WT and L-SACC mice (Figure 15), $Cc1^{-/-}$ adipocytes from HF fed mice (Figure 18), and $Cc1^{-/-}$ isolated populations of adipose tissue macrophages (ATM), negatively selected cells (endothelial cells and fibroblasts), and total SVCs prior to separation (Figure 19). Significant differences in TNFα mRNA were also revealed in separated populations of HF fed $Cc1^{-/-}$ adipocytes (Figure 18) and SVCs, ATM, and negative selection cells (Figure 19). Also there is some evidence of an increased percentage of $CD4^+$ T-cells in HF and HF/HC diets compared to RD in both WT and $Cc1^{-/-}$ mice along with higher percentages of $CD4^+$ T-cells in $Cc1^{-/-}$ adipose compared to WT (Figure 20).

It is known that pancreatic beta cell dysfunction and death precede the development of type 2 diabetes. It is known that beta cells compensate by increasing in size and insulin production, during stressors such as obesity, insulin resistance, and pregnancy and that only some individuals progress onward to the development of overt diabetes (60, 74). The key role of the pancreas to maintain glucose homeostasis and the breakdown of this control is implicated in both type 1 and type 2 diabetes, thus bringing

the etiology of these two different diseases closer together. The mechanisms of beta cell death have not been investigated as much as other organs; liver, adipose, and skeletal muscle, involved in the development of insulin resistance and type 2 diabetes. In type 1 diabetes, the beta cells are destroyed by an autoimmune attack by macrophages, T and B cells. In figure 21, leukocytic infiltration is shown in the pancreatic islets of WT, L-SACC, and $Cc1^{-/-}$ mice mainly after HF and HF/HC feeding. This suggests another commonality between type 1 and type 2 diabetes which has not been thoroughly investigated. The rt-PCR results in figure 22 are not particularly helpful in determining the role of diet or strain on inflammation in the pancreas. Results point to a trend in increased macrophages in WT HF fed mice and both WT and $Cc1^{-/-}$ fed a HF/HC diet. However there were no implications that TLR2 (highly expressed on macrophages) is affected. T cells are implicated in the HF/HC feeding of only the WT mice; somewhat surprisingly the expression of CD3 mRNA was decreased by HF and HF/HC feeding of $Cc1^{-/-}$ mice. Importantly, T cell phenotype was not investigated and before conclusions are drawn, the identity of these T cells needs to be examined. There are differences in contributions to inflammation from T helper 1, T helper 2, T regulatory, and T helper 17 subsets of T cells. Interesting future studies using the model diet-induced $Cc1^{-/-}$ insulin resistance could include immunohistochemical analysis of cell type infiltrating islets, isolation, purification, and identification of these cells, investigation of phenotype, and attempts to identify epitopes if T cells are implicated.

Elevated serum levels of free fatty acids and triglycerides are associated with disease. Previous research has shown that saturated fatty acids can be ligands to TLR2 and/or TLR4 stimulating the upregulation of inflammatory cytokines (29, 30, 33-35, 42,

43). Fatty acids can also contribute to lipotoxicity effects in organs, the beta cells of the islets of Langerhans are one well documented cell type that suffers from lipotoxicity (60). High fat and high fat / high carbohydrate diets may increase the size of individual adipocytes in adipose tissue. The larger the adipocytes become, the more fragile they are. Burst adipocytes release their intracellular stores of FFA into the local microenvironment of the adipocytes and immune cells potentially triggering TLR on cell surfaces. Metabolic factors from the liver can also stimulate a re-distribution of lipid from adipose and lead to elevated serum lipids, as well as lipid deposits in other organs such as the liver, skeletal muscle, and pancreas (75, 76). Figure 23 shows many instances where lipid droplets or adipocytes were found within pancreas tissue of HF and HF/HC fed WT and $Cc1^{-/-}$ mice and surprisingly even RD fed $Cc1^{-/-}$ mice. The presence of lipid and adipose near pancreatic islets is worrisome in light of findings of glucotoxicity and lipotoxicity and related oxidative stress causing apoptosis of beta cells (60).

We have shown changes in free fatty acid composition in adipose lipids mainly from RD and HF to HF/HC fed mice in figure 24. In HF/HC fed mice, levels of the saturated fatty acids palmitate and myristate were elevated, along with increased unsaturated palmitoleic acid, while the level of unsaturated linoleic acid was decreased. Future work in the laboratory could examine affects of each of these fatty acids on adipocytes, immune cells, and beta cells. We did study the potential of these fatty acids to stimulate TLR on the RAWblue reporter macrophage line. In figure 25 we found that only addition of palmitic, oleic, and linoleic acids to overnight culture could activate the TLR on these macrophages. Tangent to the work presented here, further investigation

would determine which TLR were activated and other signal transduction events taking place to understand the mechanism of FFA stimulation of TLR.

Overall, the work reported here on high fat and Western diet induced obesity and metabolic syndrome in mice with altered CEACAM1 expression showed an increase in weight, visceral adiposity, and fatty liver disease. Macrophage attracting chemokine MCP-1 is increased as well as macrophage marker F4/80 in adipose tissue by rt-PCR analysis. Adipose tissue purification of macrophages and T cells from vascular stromal cells indicates that cytokines TNFα and IL-10 are being expressed concurrently and that IL-6 is most likely being made by fibroblast or endothelial cells by rt-PCR analysis. There is a question as to the kinetics of inflammatory cell infiltration in adipose during progression to obesity. We have so far performed two, three, and four month experiments and found evidence of inflammatory cell involvement. Further feeding experiments focusing on one month or shorter feeding durations will be beneficial in understanding kinetics and the key players involved in the development of obesity and insulin resistance. If the relationship between mouse and human lifespan is linear, one month to a mouse would approximate just over 3 years of human lifetime. The two, three, and four month mouse feeding experiments described here are more translatable to long-term human obesity and type 2 diabetes.

5.2 Type 1 diabetes and hyperglycemic effects

It is known that hyperglycemia can alter homoeostasis of multiple body systems, including gene expression (77-82), but it is not yet fully understood how diabetic hyperglycemia contributes to dysregulated innate immune responses that contribute to the

development of chronic infections which are often seen in diabetic individuals. To investigate the effects of chronic hyperglycemia on macrophages, BM-Φ were derived from diabetic NOD mice and the NOR genetic control strain under normoglycemic and hyperglycemic conditions and stimulated with *P. gingivalis* or *E. coli* LPS.

We have found that a hyperglycemic condition, comparable to that found systemically in uncontrolled diabetes, is able to stunt BM-Φ TLR2 receptor expression, NF-κB signal transduction, and TNFα cytokine production in response to *P. ginigivalis* and *E. coli* LPS. The presence of hyperglycemia does not interfere with LPS binding to TLR2 as evidenced by the ability of diabetes-resistant NOR derived BM-Φ to effectively respond to stimulation. This suggests that the diabetic NOD mouse has an inherent defect that does not allow BM-Φ compensation to hyperglycemia.

Use of primary bone marrow stem cells, differentiated into macrophages in a hyperglycemic environment, may provide insight into the *in vivo* characteristics of macrophages in long-term diabetic individuals, as macrophages are replenished from common myeloid progenitor cells which are exposed to a hyperglycemic bloodstream once leaving the bone marrow. Furthermore, differentiated macrophages are highly affected by their microenvironment because they retain the plasticity to respond to stimuli (83, 84). For example, macrophages become classically activated and are capable of microbiocidal activity in response to IFNγ and TNFα whereas, the presence of IL-4 leads to wound healing macrophages, and exposure to IL-10 leads to a regulatory macrophage phenotype (84). Therefore, it is reasonable to assume a microenvironment of hyperglycemia could have an effect on macrophage differentiation and the ability to respond to infection. Prolonged exposure to a diabetic milieu leading to immune

defectiveness could be associated with the risk of infection. Similarly, chronic hyperglycemia (six months) in streptozotocin-induced diabetes in BALB/c mice led to decreased B and T lymphocyte cell proliferation in primary immune responses to both T cell dependent and independent antigens indicating that pathological levels of high glucose could result in the immunosuppressive state observed in diabetic mice (85).

We have seen previously that bone marrow stem cells obtained from diabetic NOD mice and differentiated in high glucose media had increased basal levels of TLR2, TLR4, and TNFα (50). Similarly, Dasu et al. incubated THP-1 monocytic cells in high glucose and found induced expression of TLR2, TLR4, and activation of NF-κB with involvement of protein kinase C (86). Furthermore, diabetic patients in a hyperglycemic crisis have elevated plasma levels of pro-inflammatory cytokines in the absence of an infection (87). Even studies investigating the effects of acute hyperglycemia have found increased plasma levels of multiple pro-inflammatory cytokines which have metabolic effects contributing to maintaining elevated glucose levels (88). These results suggest that a hyperglycemic environment has a stimulatory effect on the innate immune system. An important question is how hyperglycemia stimulated immune cells respond to further bacterial stimulation. In a study by Wasmuth et al. hyperglycemia in patients admitted to the intensive care unit was associated with increased serum levels of inflammatory cytokines including TNFα (89). However, *ex vivo* stimulation of whole blood from the same hyperglycemic patients with LPS led to significantly decreased levels of TNFα compared to normoglycemic patients. These results appear to be paradoxical; the innate immune system is activated by high levels of glucose, however, secondary stimulation with a bacterial ligand leads to hyporesponsiveness. Medvedev et al. have shown that

pretreatment of cells with LPS causes tolerance to endotoxin (loss of responsiveness) upon restimulation with LPS (90). Lastly, clinical studies of glycemic control in diabetic patients provide evidence that patients with adequate metabolic control, determined by fasting glucose and glycated hemoglobin, produce more TNFα from stimulated mononuclear cells compared to patients with inadequate metabolic control (91). The results reported in chapter 4 indicate that culturing BM-Φ in high glucose media may function as a primary TLR stimulus and that subsequent restimulation with a bacterial ligand can induce tolerance and loss of responsiveness.

Clinically, the cause of diabetes may be less important than the detrimental disease complications of chronic exposure to hyperglycemia which also implicates poorly controlled type 2 diabetic patients (92). The well described adverse effects of hyperglycemia on insulin target tissues and particularly pancreatic islet beta cells have been termed "glucotoxicity". Chronic hyperglycemia induces multiple shortcomings in beta cells including the loss of glucose-stimulated insulin gene transcription and secretion, and is linked to beta cell apoptosis and necrosis (93, 94). The observations reported in chapter four may represent a type of glucotoxicity of the macrophage resulting in impaired immune responses. In future studies, we are planning on repeating these experiments using bone marrow-derived macrophages from $Cc1^{-/-}$ mice after high fat and Western diet feeding to promote type 2 diabetes development. Results similar to ones found with the type 1 diabetes model NOD mice would argue that any form of diabetes with uncontrolled hyperglycemia has severe negative effects on macrophages.

Chapter 6

References

1. Lumeng CN, Bodzin JL, and Saltiel AR. 2007. Obesity induces a phenotypic switch in adipose tissue macrophage polarization. *The Journal of Clinical Investigation* 117:175.
2. Jin MS, Kim SE, Heo JY, Lee ME, Kim HM, Paik SG, Lee H, and Lee JO. 2007. Crystal structure of the TLR1-TLR2 heterodimer induced by binding of a tri-acylated lipopeptide. *Cell* 130:1071.
3. Hotamisligil GS, and Erbay E. 2008. Nutrient sensing and inflammation in metabolic diseases. *Nature Reviews Immunology* 8:923.
4. Hotamisligil GS. 2006. Inflammation and metabolic disorders. *Nature* 444:860.
5. Muoio DM, and Newgard CB. 2008. Molecular and metabolic mechanisms of insulin resistance and beta-cell failure in type 2 diabetes. *Nature Reviews Molecular Cell Biology* 9:193.
6. Najjar S. 2002. Regulation of insulin action by CEACAM1. *Trends in Endocrinology & Metabolism* 13:240.
7. Lencioni C, Lupi R, and Prato S. 2008. Beta-cell failure in type 2 diabetes mellitus. *Current diabetes reports* 8:179.

8. Poy MN, Yang Y, Rezaei K, Fernstrom MA, Lee AD, Kido Y, Erickson SK, and Najjar SM. 2002. CEACAM1 regulates insulin clearance in liver. *Nature Genetics* 30:270.

9. Dai T, Abou-Rjaily G, Al-Share Q, Yang Y, Fernstrom M, DeAngelis A, Lee A, Sweetman L, Amato A, Pasquali M, et al. 2004. Interaction between altered insulin and lipid metabolism in CEACAM1-inactive transgenic mice. *The Journal of Biological Chemistry* 279:45155.

10. Lee SJ, Heinrich G, Fedorova L, Share QY, Ledford KJ, Fernstrom MA, McInerney MF, Erickson SK, Gatto-Weis C, and Najjar SM. 2008. Development of nonalcoholic steatohepatitis in insulin-resistant Liver-specific S503A carcinoembryonic antigen-related cell adhesion molecule 1 mutant mice. *Gastroenterology* 135:2084.

11. Park S, Cho Y, Kim H, Hong E, Higashimori T, Lee S, Goldberg I, Shulman G, Najjar S, and Kim J. 2006. Mechanism of glucose intolerance in mice with dominant negative mutation of CEACAM1. *American Journal of Physiology - Endocrinology and Metabolism* 291:E517.

12. Leung N, Turbide C, Olson M, Marcus V, Jothy S, and Beauchemin N. 2006. Deletion of the carcinoembryonic antigen-related cell adhesion molecule 1 (Ceacam1) gene contributes to colon tumor progression in a murine model of carcinogenesis. *Oncogene* 25:5527.

13. DeAngelis A, Heinrich G, Dai T, Bowman T, Patel P, Lee S, Hong E, Jung D, Assmann A, Kulkarni R, et al. 2008. Carcinoembryonic antigen-related cell adhesion molecule 1 - a link between insulin and lipid metabolism. *Diabetes* 57:2296.

14. Hajer G, van Haeften T, and Visseren F. 2008. Adipose tissue dysfunction in obesity, diabetes, and vascular diseases. *European Heart Journal* 29:2959.

15. de Ferranti S, and Mozaffarian D. 2008. The perfect storm: obesity, adipocyte dysfunction, and metabolic consequences. *Clinical Chemistry* 54:945.

16. Bastard J, Maachi M, Lagathu C, Kim M, Caron M, Vidal H, Capeau J, and Feve B. 2006. Recent advances in the relationship between obesity, inflammation, and insulin resistance. *European Cytokine Network* 17:4.

17. Cancello R, and Clement K. 2006. Is obesity an inflammatory illness? Role of low-grade inflammation and macrophage infiltration in human white adipose tissue. *British Journal of Obstetrics and Gynaecology* 113:1141.

18. Fernandez-Real JM, and Pickup JC. 2008. Innate immunity, insulin resistance and type 2 diabetes. *Trends in Endocrinology and Metabolism* 19:10.

19. Pickup JC. 2004. Inflammation and activated innate immunity in the pathogenesis of type 2 diabetes. *Diabetes Care* 27:813.

20. Alexandraki K, Piperi C, Kalofoutis C, Singh J, Alaveras A, and Kalofoutis A. 2006. Inflammatory process in type 2 diabetes: The role of cytokines. *Annals of the New York Academy of Sciences* 1084:89.

21. Jellinger PS. 2007. Metabolic consequences of hyperglycemia and insulin resistance. *Clinical Cornerstone* 8 Suppl 7:S30.

22. Kolb H, and Mandrup-Poulsen T. 2005. An immune origin of type 2 diabetes? *Diabetologia* 48:1038.

23. Shoelson SE, Lee J, and Goldfine AB. 2006. Inflammation and insulin resistance. *The Journal of Clinical Investigation* 116:1793.

24. Tataranni PA, and Ortega E. 2005. A burning question: does an adipokine-induced activation of the immune system mediate the effect of overnutrition on type 2 diabetes? *Diabetes* 54:917.

25. Wellen K, and Hotamisligil G. 2003. Obesity-induced inflammatory changes in adipose tissue. *The Journal of Clinical Investigation* 112:1785.

26. Tilg H, and Moschen A. 2008. Inflammatory mechanisms in the regulation of insulin resistance. *Molecular Medicine* 14:222.

27. Benoit M, Desnues B, and Mege J. 2008. Macrophage polarization in bacterial infections. *The Journal of Immunology* 181:3733.

28. Senn J. 2006. Toll-like receptor-2 is essential for the development of palmitate-induced insulin resistance in myotubes. *The Journal of Biological Chemistry* 281:26865.

29. Shi H, Kokoeva MV, Inouye K, Tzameli I, Yin H, and Flier JS. 2006. TLR4 links innate immunity and fatty acid-induced insulin resistance. *The Journal of Clinical Investigation* 116:3015.

30. Nguyen MTA, Favelyukis S, Nguyen A-K, Reichart D, Scott PA, Jenn A, Liu-Bryan R, Glass CK, Neels JG, and Olefsky JM. 2007. A subpopulation of macrophages infiltrates hypertrophic adipose tissue and is activated by free fatty acids via Toll-like receptors 2 and 4 and JNK-dependent pathways. *The Journal of Biological Chemistry* 282:35279.

31. Weisberg SP, McCann D, Desai M, Rosenbaum M, Leibel RL, and Ferrante AWJ. 2003. Obesity is associated with macrophage accumulation in adipose tissue. *The Journal of Clinical Investigation* 112:1796.

32. Lumeng CN, Deyoung SM, and Saltiel AR. 2007. Macrophages block insulin action in adipocytes by altering expression of signaling and glucose transport proteins. *American Journal of Physiology, Endocrinology and Metabolism* 292:E166.

33. Creely S, McTernan P, Kusminski C, Fisher M, Da Silva N, Khanolkar M, Evans M, Harte A, and Kumar S. 2007. Lipopolysaccharide activates an innate immune system response in human adipose tissue in obesity and type 2 diabetes. *American Journal of Physiology, Endocrinology and Metabolism* 292:E740.

34. Song MJ, Kim KH, Yoon JM, and Kim JB. 2006. Activation of toll-like receptor 4 is associated with insulin resistance in adipocytes. *Biochemical and Biophysical Research Communications* 346:739.

35. Suganami T, Mieda T, Itoh M, Shimoda Y, Kamei Y, and Ogawa Y. 2007. Attenuation of obesity-induced adipose tissue inflammation in C3H/HeJ mice carrying a Toll-like receptor 4 mutation. *Biochemical and Biophysical Research Communications* 354:45.

36. Hotamisligil GS, Shargill NS, and Spiegelman BM. 1993. Adipose expression of tumor necrosis factor-alpha: direct role in obesity-linked insulin resistance. *Science* 259:87.

37. Tilg H, and Moschen A. 2008. Insulin resistance, inflammation, and non-alcoholic fatty liver disease. *Trends in Endocrinology & Metabolism* 19:371.

38. Pickup JC, Mattock MB, Chusney GD, and Burt D. 1997. NIDDM as a disease of the innate immune system: association of acute-phase reactants and interleukin-6 with metabolic syndrome X. *Diabetologia* 40:1286.

39. Ueki K, Kadowaki T, and Kahn C. 2005. Role of suppressors of cytokine signaling SOCS-1 and SOCS-3 in hepatic steatosis and the metabolic syndrome. *Hepatology Research* 33:185.

40. Rui L, Yuan M, Frantz D, Shoelson S, and White M. 2002. SOCS-1 and SOCS-3 block insulin signaling by ubiquitin-mediated degradation of IRS1 and IRS2. *Journal of Biological Chemistry* 277:42394.

41. Ueki K, Kondo T, and Kahn C. 2004. Suppressor of cytokine signaling 1 (SOCS-1) and SOCS-3 cause insulin resistance through inhibition of tyrosine phosphorylation of insulin receptor substrate proteins by discrete mechanisms. *Molecular and Cellular Biology* 24:5434.

42. Suganami T, Tanimoto-Koyama K, Nishida J, Itoh M, Yuan X, Mizuarai S, Kotani H, Yamaoka S, Miyake K, Aoe S, et al. 2007. Role of the toll-like receptor 4/NF-kappaB pathway in saturated fatty acid-induced inflammatory changes in the interaction between adipocytes and macrophages. *Arteriosclerosis, Thrombosis, and Vascular Biology* 27:84.

43. Tsukumo DML, Carvalho-Filho MA, Carvalheira JBC, Prada PO, Hirabara SM, Schenka AA, Araujo EP, Vassallo J, Curi R, Velloso LA, and Saad MJA. 2007. Loss-of-function mutation in Toll-like receptor 4 prevents diet-induced obesity and insulin resistance. *Diabetes* 56:1986.

44. Poggi M, Bastelica D, Gual P, Iglesias MA, Gremeaux T, Knauf C, Peiretti F, Verdier M, Juhan-Vague I, Tanti JF, et al. 2007. C3H/HeJ mice carrying a toll-like receptor 4 mutation are protected against the development of insulin resistance in white adipose tissue in response to a high-fat diet. *Diabetologia* 50:1267.

45. Utzschneider KM, and Kahn SE. 2006. The role of insulin resistance in nonalcoholic fatty liver disease. *The Journal of Clinical Endocrinology and Metabolism* 91:4753.

46. Malaguarnera M, Di Rosa M, Nicoletti F, and Malaguarnera L. 2009. Molecular mechanisms involved in NAFLD progression. *Journal of Molecular Medicine* 87:679.

47. Moutschen M, Scheen A, and Lefebvre P. 1992. Impaired immune responses in diabetes mellitus: analysis of the factors and mechanisms involved. Relevance to the increased susceptibility of diabetic patients to specific infections. *Diabète & métabolisme* 18:187.

48. Brownlee M, Vlassara H, and Cerami A. 1984. Nonenzymatic glycosylation and the pathogenesis of diabetic complications. *Annals of internal medicine* 101:527.

49. Morran MP, Alexander LA, Slotterbeck BD, and McInerney MF. 2009. Dysfunctional innate immune responsiveness to Porphyromonas gingivalis lipopolysaccharide in diabetes. *Oral microbiology and immunology* 24:331.

50. Mohammad MK, Morran MP, Slotterbeck B, Leaman DW, Sun Y, Grafenstein Hv, Hong S-C, and McInerney MF. 2006. Dysregulated Toll-like receptor expression and signaling in bone marrow-derived macrophages at the onset of diabetes in the non-obese diabetic mouse. *International Immunology* 18:1101.

51. McCarthy JJ. 2007. Gene by sex interaction in the etiology of coronary heart disease and the preceding metabolic syndrome. *Nutrition, Metabolism and Cardiovascular Diseases* 17:153.

52. Prochazka M, Serreze D, Frankel W, and Leiter E. 1992. NOR/Lt mice: MHC-matched diabetes-resistant control strain for NOD mice. *Diabetes* 41:98.

53. Chen W, Jump DB, Grant MB, Esselman WJ, and Busik JV. 2003. Dyslipidemia, but not hyperglycemia, induces inflammatory adhesion molecules in human retinal vascular endothelial cells. *Investigative Ophthalmology & Visual Science* 44:5016.

54. Warren M, and Vogel S. 1985. Bone marrow-derived macrophages: development and regulation of differentiation markers by colony-stimulating factor and interferons. *The Journal of Immunology* 134:982.

55. Yi A, and Krieg A. 1998. Rapid induction of mitogen-activated protein kinases by immune stimulatory CpG DNA. Am Assoc Immnol. 4493.

56. Feuerer M, Herrero L, Cipolletta D, Naaz A, Wong J, Nayer A, Lee J, Goldfine AB, Benoist C, Shoelson S, and Mathis D. 2009. Lean, but not obese, fat is enriched for a unique population of regulatory T cells that affect metabolic parameters. *Nature Medicine* 15:930.

57. Lumeng CN, Deyoung SM, Bodzin JL, and Saltiel AR. 2007. Increased inflammatory properties of adipose tissue macrophages recruited during diet-induced obesity. *Diabetes* 56:16.

58. Kunisch E, Fuhrmann R, Roth A, Winter R, Lungershausen W, and Kinne RW. 2004. Macrophage specificity of three anti-CD68 monoclonal antibodies (KP1, EBM11, and PGM1) widely used for immunohistochemistry and flow cytometry. *Ann Rheum Dis* 63:774.

59. Khazen W, M'Bika J, Tomkiewicz C, Benelli C, Chany C, Achour A, and Forest C. 2005. Expression of macrophage-selective markers in human and rodent adipocytes. *FEBS letters* 579:5631.

60. Chang-Chen KJ, Mullur R, and Bernal-Mizrachi E. 2008. Beta-cell failure as a complication of diabetes. *Reviews in Endocrine and Metabolic Disorders* 9:329.

61. Hu CC, Qing K, and Chen Y. 2004. Diet-induced changes in stearoyl-CoA desaturase 1 expression in obesity-prone and -resistant mice. *Obesity* 12:1264.

62. Le Lay S, Boucher J, Rey A, Castan-Laurell I, Krief S, Ferr P, Valet P, and Dugail I. 2001. Decreased resistin expression in mice with different sensitivities to a high-fat diet. *Biochemical and Biophysical Research Communications* 289:564.

63. Stevens J. 1995. Obesity, fat patterning and cardiovascular risk. *Advances in Experimental Medicine & Biology* 369:21.

64. Gonzalez-Reimers E, Castellano-Higuera A, Aleman-Valls R, Alvarez A, H., de la Vega-Prieto MJ, Abreu G, P., Lopez-Prieto J, Santolaria-Fernandez F, and Valladares-Parrilla F. 2009. Relation between body fat and liver fat accumulation and cytokine pattern in non-alcoholic patients with chronic HCV infection. *Annals of Nutrition & Metabolism* 55:351.

65. Wieckowska A, and Feldstein AE. 2008. Diagnosis of nonalcoholic fatty liver disease: invasive versus noninvasive. *Seminars in Liver Disease* 28:386.

66. Gutierrez D, Puglisi M, and Hasty A. 2009. Impact of increased adipose tissue mass on inflammation, insulin resistance, and dyslipidemia. *Current diabetes reports* 9:26.

67. Fève B, and Bastard J. 2009. The role of interleukins in insulin resistance and type 2 diabetes mellitus. *Nature Reviews Endocrinology* 5:305.

68. Karalis KP, Giannogonas P, Kodela E, Koutmani Y, Zoumakis M, and Teli T. 2009. Mechanisms of obesity and related pathology: linking immune responses to metabolic stress. *FEBS Journal* 276:5747.

69. Bourlier V, and Bouloumie A. 2009. Role of macrophage tissue infiltration in obesity and insulin resistance. *Diabetes and Metabolism* 35:251.

70. Odegaard J, and Chawla A. 2008. Mechanisms of macrophage activation in obesity-induced insulin resistance. *Nature Clinical Practice Endocrinology & Metabolism* 4:619.

71. Winer S, Chan Y, Paltser G, Truong D, Tsui H, Bahrami J, Dorfman R, Wang Y, Zielenski J, Mastronardi F, et al. 2009. Normalization of obesity-associated insulin resistance through immunotherapy. *Nature Medicine* 15:921.

72. Zeyda M, Farmer D, Todoric J, Aszmann O, Speiser M, Györi G, Zlabinger G, and Stulnig T. 2007. Human adipose tissue macrophages are of an anti-inflammatory phenotype but capable of excessive pro-inflammatory mediator production. *International Journal of Obesity* 31:1420.

73. Fujisaka S, Usui I, Bukhari A, Ikutani M, Oya T, Kanatani Y, Tsuneyama K, Nagai Y, Takatsu K, and Urakaze M. 2009. Regulatory mechanisms for adipose tissue M1 and M2 macrophages in diet-induced obese mice. *Diabetes* 58:2574.

74. Karaca M, Magnan C, and Kargar C. 2009. Functional pancreatic beta-cell mass: Involvement in type 2 diabetes and therapeutic intervention. *Diabetes and Metabolism* 35:77.

75. Bluher M. 2009. Adipose tissue dysfunction in obesity. *Experimental and Clinical Endocrinology & Diabetes* 117:241.

76. Goossens GH. 2008. The role of adipose tissue dysfunction in the pathogenesis of obesity-related insulin resistance. *Physiology & Behavior* 94:206.

77. Graves D, and Kayal R. 2008. Diabetic complications and dysregulated innate immunity. *Frontiers in bioscience: a journal and virtual library* 13:1227.

78. Mealey B. 2006. Periodontal disease and diabetes: A two-way street. *The Journal of the American Dental Association* 137:26S.

79. Naito M. 2008. Macrophage differentiation and function in health and disease. *Pathology International* 58:143.

80. Nassar H, Kantarci A, and Van Dyke T. 2007. Diabetic periodontitis: a model for activated innate immunity and impaired resolution of inflammation. *Periodontology 2000* 43:233.

81. Palmeira C, Rolo A, Berthiaume J, Bjork J, and Wallace K. 2007. Hyperglycemia decreases mitochondrial function: The regulatory role of mitochondrial biogenesis. *Toxicology and Applied Pharmacology* 225:214.

82. Ryan M, Carnu O, and Kamer A. 2003. The influence of diabetes on the periodontal tissues. *The Journal of the American Dental Association* 134:34S.

83. Martinez F, Sica A, Mantovani A, and Locati M. 2008. Macrophage activation and polarization. *Frontiers in bioscience: a journal and virtual library* 13:453.

84. Mosser D, and Edwards J. 2008. Exploring the full spectrum of macrophage activation. *Nature Reviews Immunology* 8:958.

85. Rubinstein R, Genaro A, Motta A, Cremaschi G, and Wald M. 2008. Impaired immune responses in streptozotocin-induced type I diabetes in mice. Involvement of high glucose. *Clinical Experimental Immunology* 154:235.

86. Dasu M, Devaraj S, Zhao L, Hwang D, and Jialal I. 2008. High glucose induces toll-like receptor expression in human monocytes: mechanism of activation. *Diabetes* 57:3090.

87. Stentz F, Umpierrez G, Cuervo R, and Kitabchi A. 2004. Proinflammatory cytokines, markers of cardiovascular risks, oxidative stress, and lipid peroxidation in patients with hyperglycemic crises. *Diabetes* 53:2079.

88. Turina M, Fry D, and Polk Jr H. 2005. Acute hyperglycemia and the innate immune system: clinical, cellular, and molecular aspects. *Critical care medicine* 33:1624.

89. Wasmuth H, Kunz D, Graf J, Stanzel S, Purucker E, Koch A, Gartung C, Heintz B, Gressner A, and Matern S. 2004. Hyperglycemia at admission to the intensive care unit is associated with elevated serum concentrations of interleukin-6 and reduced ex vivo secretion of tumor necrosis factor-alpha. *Critical care medicine* 32:1109.

90. Medvedev A, Kopydlowski K, and Vogel S. 2000. Inhibition of lipopolysaccharide-induced signal transduction in endotoxin-tolerized mouse macrophages: dysregulation of cytokine, chemokine, and toll-like receptor 2 and 4 gene expression. *The Journal of Immunology* 164:5564.

91. Foss-Freitas M, Foss N, Donadi E, and Foss M. 2006. In vitro TNF-alpha and IL-6 production by adherent peripheral blood mononuclear cells obtained from type 1 and type 2 diabetic patients evaluated according to the metabolic control. *Annals of the New York Academy of Sciences* 1079:177.

92. Lalla E. 2007. Periodontal infections and diabetes mellitus: when will the puzzle be complete? *Journal of clinical periodontology* 34:913.

93. Brownlee M. 2003. A radical explanation for glucose-induced cell dysfunction. *Journal of Clinical Investigation* 112:1788.

94. Stumvoll M, Goldstein B, and van Haeften T. 2005. Type 2 diabetes: principles of pathogenesis and therapy. *The Lancet* 365:1333.